الأية

بسم الله الرحمن الرحيم

(اللَّهُ لَا إِلَهَ إِلَّا هُوَ الْحَيُّ الْقَيُّومُ لَا تَأْخُذُهُ سِنَةٌ وَلَا نَوْمٌ لَهُ مَا فِي السَّمَوَاتِ وَمَا فِي الْأَرْضِ مَنْ ذَا الَّذِي يَشْفَعُ عِنْدَهُ إِلَّا بِإِذْنِهِ يَعْلَمُ مَا بَيْنَ أَيْدِيهِمْ وَمَا خَلْفَهُمْ وَلَا يُحِيطُونَ بِشَيْءٍ مِنْ عِلْمِهِ إِلَّا بِمَا شَاءَ وَسِعَ كُرْسِيُّهُ السَّمَاوَاتِ وَالْأَرْضَ وَلَا يَئُودُهُ حِفْظُهُمَا وَهُوَ الْعَلِيُّ الْعَظِيمُ).

(سورة البقرة الاية 255)

I

Dedication

- To the Soul of my dear and beloved mother and Sister Hanan.

- To my father, brothers, sisters.

- To my wife Reem and my Kids.

- To my friends.

- And to my colleagues.

Acknowledgement

I would like to thank *Prof. Mohammed Elfadil Mohammed*,   my Supervisor for his kind advice, true guidance, great help and valuable critics: I'm very grateful to *Dr, Asma Ibrahim, my co-supervisor* for her full advice, encouragement and great help.

I would like also to thank *Dr, Mohammed Mohamed Omer*, Dean of college of Medical Radiological Sciences (SUST) for his help and good advice. My thanks to *Dr. Ahmed Mustafa Abo Kunna.* My great thanks to *Mr, Abd Elrahman Hassan* for his close support and also *Mr, Sulaiman Mohammed Elhassan* for his help and support.

I'm continuous very full thanks to *my brother Mohammed Abd Elwahab* for his encouragement and support .Thanks are also extended to Mr. *Osman Mohammed Osman, Dr. Aymen Elsaed and Mr. Abd Elrahman Salah Eldin.*

المستخلص

هذه الدراسة وصفية وأجريت خلال سبتمبر 2013م إلي مايو 2016م أجريت فى (مستشفيات ابن سيناء ، الرباط وكلية علوم الأشعة الطبية) ولاية الخرطوم بجمهورية السودان. الدراسة ناقشت تقييم توصيف أمراض الكبد الإنتشارية باستخدام الموجات فوق الصوتية والتحليل النسيجى. هنالك (200) مريض اختيروا عشوائيا ولكن جميعهم لديهم أعمار اكبر من 20 سنة ، لديهم كبد طبيعية، التهاب الكبد الوبائى (ب)، التهاب الكبد الوبائى (س) أو تليف الكبد وجميعهم محولين بواسطة الطبيب. كل مريض لديه نوع اخر من أمراض الكبد أستبعد من هذه الدراسة. كل هؤلاء المرضى تم فحصهم بالموجات فوق الصوتية باستخدام ماسحات هوندا، أيوكوب وجنرال اليكتريك بطاقة مقدارها 3.5 ميقا هرتز. اجري المسح عن طريق البطن لكل المرضى وتم تقييم شكل الكبد ، اذا كان طبيعيا أوغير طبيعى؛ وتقييم المظهر، الحافة اليسرى للكبد، قياس حجم الكبد، الفص الأيمن، الفص ذو الذيل، حجم الوريد البوابى ووجود سائل فى البطن وأخيرا قياس حجم الطحال. البيانات تم جمعها بواسطة ورقة تجميع البيانات التى تم تحليلها باستخدام الجداول الاحصائية، التحليل الخطى، التحليل التمييزى والتحليل النسيجى. الدراسة وجدت أن الكبد الطبيعية يمكن التعرف عليها بدقة (83.3 %)، بينما التعرف على تليف الكبد بدقة (98.3%)، لالتهاب الكبد الفيروسى(ب) دقة التشخيص (91.7%) حيث أن (8.3%) من الحالات أظهرت ملامح شبيهة للكبد الطبيعية، هذا يحدث خاصة فى المراحل الأولى للمرض. ولالتهاب الكبد الفيروسى(س) الدقة (45%) حيث أن (55%) من الحالات أظهرت ملامح شبيهة للكبد الطبيعية. الدراسة عرضت أن علامات الموجات فوق الصوتية فى حالة تليف الكبد غالبا هي تغيير شكل الكبد 52 مريض(87%) من 60 مريض لديهم تليف الكبد، تغير المظهر (زيادة المظهر ومظهر حبيبى) 55 مريض (95%) (تغير الشكل أو تغير المظهر) وزيادة نسبة الفص ذو الذيل/ الفص الأيمن، وجود سائل فى البطن وتضخم الطحال. الدراسة وجدت أن المسح بالموجات فوق الصوتية لوحده غير موثوق ودقيق فى تشخيص التهاب الكبد الوبائى (س) ولكنه موثوق ودقيق فى التمييز بين الكبد السليمة والكبد المريضة. بالاضافة لذلك الدراسة وجدت أن مشاركة المسح بالموجات فوق الصوتية مع التحليل النسيجى يزيد دقة التمييز بين أمراض الكبد الإنتشارية.

ABSTRACT

This is a descriptive study which was carried out during the period from September-2013 to May 2016 in (Ibn Sena, Ribat and college of Medical Radiologic Sciences) Khartoum- Sudan. This study discusses the depiction of diffuse liver diseases using ultrasonography and texture analysis. A total of "200" patients were selected randomly; all patients have ages above 20 years, they include: patient with normal liver, hepatitis B, hepatitis C and liver cirrhosis; all referred by physician. Any patient with other liver disorder was excluded from this study. All patients were examined by ultrasound scanning using 'Honda' Eucup and General Electric scanners with 3,5MHz probe. Trans abdominal Scanning were performed for all patients to evaluate liver shape; i.e. if it is normal or abnormal; also evaluate liver texture, left edge of the liver, the liver span measure, right lobe size, caudate lobe size, portal vein diameter, presence of ascites and spleen size. Data was collected using master data collection sheet where it was analyzed using crosstabulation, linear regression, discriminant analysis and pattern recognition. The results of this study shows that the normal liver can be identified by an accuracy of (83.3%) while the sensitivity of diagnosing liver cirrhosis was 98.3%, for hepatitis type B the sensitivity was 91.7% where 8.3% of the cases showed measures similar to the normal liver; this occurs specially in early stage. But for hepatitis type C the sensitivity was 45% where 55% of the cases showed measures similar to the normal liver. Study shows that; the U/S findings of the liver cirrhosis mostly changes shape 52 patients (87%) out of 60 cases with liver cirrhosis, changed texture (hyper echoic and nodular) 55 patients (95%), (Abnormal shape or abnormal texture and increased the C/R ratio, presence of ascites and splenomegaly). Study revealed that the ultrasound scanning

alone is not reliable and accurate in diagnosis of hepatitis C, but reliable and accurate in differentiate between normal liver and disorder liver. In addition to that the study concluded that: Computer aided texture analysis is very Combination of ultrasound scanning with texture analysis increased the accuracy of diffuse liver classification. Study recommended that: If there is a prediction of liver disorder by U/S scanning, the patient images must be analyze using IDL program, then the histopathology will be done for confirmation only, if it is not available, no need of it for giving the patient treatment, because the accuracy of U/S and texture analysis tools together is very high.

List of contents

List of Tables

List of Figures

List of Abbreviations

ALT	Alanine aminotransaminase
ANN	Artificial Neural Network
AST	Aspartate aminotransaminase
CC	Cranio-caudal
CL	Caudate lobe
CLD	Chronic Liver Disease
C/R R	Caudate to Right lobe Ratio
DGC	Depth Gain Compensation
EOL	Edge of left lobe
FNH	Focal Nodular Hyperplasia
FNAB	Fine Needle Aspiration Biopsy
GI	Gastrointestinal
GLHW	Gray Level Co occurrence Matrix
HBV	Hepatitis B virus
HCV	Hepatitis C virus
HCC	Hepatocellular Carcinoma
U/S	Ultrasound
IDL	Interactive Data Language
OL	Outlines of liver
MCL	Midclavicular line
NTX Nodular	Texture of liver
SP	Spleenomegally
PACS	Pictures Archiving Communication System
POS	Presence of Ascites
RL	Right lobe

ROI	Region of Interest
SVM	Support Vector Machine
TAUS	Trasabdominal ultrasound scanning
TGC	Time Gain Compensation
TX	Texture of liver
USG	Ultrasonography
2-D	Tow Dimensions

Chapter one
Introduction

1.1 Introduction:

Ultrasound liver images are those images that result from the reflectance of the ultrasound signal at the incidence with the internal layers (interfaces) of the human organs; they are obtained through echography and map the structure of the human organs and the appearance of the organs tissue on the computer screen. The attenuation of the reflected signal will increase with the deepness, so the grey levels of the ultrasound image will decrease accordingly (Gherasim, 1999).

Liver diseases are taken seriously because of their vital importance to the life of the patient. Liver pathologies can be classified into two main categories according to the degree of dispersion of the disease. The first category is the *localized liver diseases* in which the pathology is concentrated in small spot(s) in one or both of the liver lobes while the rest of the liver tissue remains \normal. The second category is the *diffused liver diseases* in which at least one complete lobe of the liver is affected by the disease or, in other words, the disease is distributed over the whole liver volume. This classification does not imply that the second category is a later stage of the first or that it is more serious. Both categories encounter benign and malignant types of diseases and should be treated in totally different ways from each other (Youssef,1990, Christensen,1988 and Parker,1983).

Diffuse liver diseases are characterized through global transforms of the liver tissue, so that the entire area of the liver is affected. Hepatitis denotes the liver inflammation. Chronic hepatitis means chronic inflammation, hepato-cellular necrosis and often fibrosis, which evolves continuously during the first 6 months (Gherasim, 1999). The variations in aspect of the

ultrasound images, which are not suggestive for this disease, could be: the symmetrical growth of the liver, with more or less variations of the homogeneity of the tissue; the discrete dilation of the hepatic vessels; splenomegaly; increased echogenicity of the tissue, due to fibrosis. Cirrhosis is a diffuse liver disease characterized through the association of fibrosis, regeneration nodules and hepatocytes necrosis, with hepatic structure alteration. The tissue homogeneity decreases due to the nodules. Other changes of the liver could be: increased volume (in the case of the toxic cirrhosis) or decreased volume (viral cirrhosis); shape and contour modification (due to the nodules) ; vessels modifications. The specific variation in the appearance of the ultrasound liver images in all these cases are difficult to be observed by human eyes. Always, the biopsy is used in order to establish a diagnosis. But a non-invasive, computerized method would be preferred. Some of the diffuse liver diseases (such as steatosis, chronic hepatitis or early cirrhosis) imply transforms in the liver tissue which are difficult to be evaluated (or quantified) by human eye in ultrasound liver images. They may be characterized by an increased echogenicity, but this property is not enough in order to differentiate between them. The pathologic changes of the tissue generate alterations of physical and micro architectural properties (density, elasticity, homogeneity) of the tissue; although these alterations are difficult to be observed, they affect the propagation of the ultrasounds, during the echographic examination. For this reason, a computerized, statistical analyses of the ultrasound image texture is considered necessary. (Mojsilovic, 2000, Yeh W, 2003 and Lupsor, 2005).

1.1 Problem of the study:

All diffuse liver parenchymal diseases were confirmed by laboratory investigation especially liver fine-needle aspiration biopsy (FNAB) which causes a lot of complication like hematoma; Therefore combination of ultrasound scan results and textural analysis of ultrasound images can delimit these problems by restraining the FNAB to the highly suspected cases only.

1.2 Objectives:

1.2.1 General objective:

To characterize the ultrasound images of diffuse liver parenchymal diseases using textures analysis; in order to avoid unnecessary FNAB.

1.2.2 Specific objectives:

● To diagnose the pathological status of the diffuse liver parenchymal diseases using ultrasound and texture analysis.

● To extract textural features from liver ultrasound images.

● To develop an algorithm that can recognize different types of diffuse liver parenchymal pathology.

● To test the accuracy of the developed algorithm.

1.3 Significance of the study:

This study will helps in limiting the usage of FNAB in liver to the highly suspected cases only to avoid the complication. As well as it will reduce the cost and time of examination.

1.4 Overview of the study:

This study is concerned with characterize of diffuse liver parenchymal diseases sonographically by using textures analysis accordingly, it falls into five chapters. Chapter one is an introduction, which include introductory notes on liver anatomy, physiology, pathology and texture

analysis, as well as statement of the problem and study objectives. While Chapter two will include a comprehensive scholarly literature reviews concerning the previous studies. Chapter three deals with the methodology, where it provides an outline of material and methods used to acquire the data in this study as well as the method of analysis approach. While the results were presented in chapter four, and finally Chapter five include discussion of results, conclusion and recommendations followed by references and appendices.

Chapter two
Background and literature review

2.1 Liver Anatomy:

The liver is the largest organ in the body weighing 1400-1600 gm in the males and 1200-1400 gm in the females (Harsh, 2010) occupying a substantial portion of the upper abdominal cavity. It occupies most of the right hypochondrium and epigastrium, and frequently extends into the left hypochondrium as far as the left lateral line. As the body grows from infancy to adulthood the liver rapidly increases in size. This period of growth reaches a plateau around 18 years and is followed by a gradual decrease in the liver weight from middle age. The ratio of liver to body weight decreases with growth from infancy to adulthood. The liver weighs approximately 5% of the body weight in infancy and it decreases to approximately 2% in adulthood (Grays, 2008). The size of the liver is measures less than 15 cm (Lutz, 2011) and varies according to sex, age and body size. It has an overall wedge shape, which is in part determined by the form of the upper abdominal cavity into which it grows. (Lutz, 2011 and Gray □s, 2008)

The narrow end of the wedge lies towards the left hypochondrium, and the anterior edge points anteriorly and inferiorly. The superior and right lateral aspects are shaped by the anterolateral abdominal and chest wall as well as the diaphragm. The inferior aspect is shaped by the adjacent viscera. The capsule is no longer thought to play an important part in maintaining the integrity of the shape of the liver. The liver is usually described as having superior, anterior, right, posterior and inferior surfaces, and has a distinct inferior border (Gray □s, 2008).

Throughout life the liver is reddish brown in color, although this can vary depending upon the fat content. Obesity is the most common cause of excess fat in the liver (also known as steatosis), the liver assumes a more yellowish tinge as its fat content increases. The texture is usually soft to firm, although it depends partly on the volume of blood the liver contains and the fat content (Harsh, 2010).
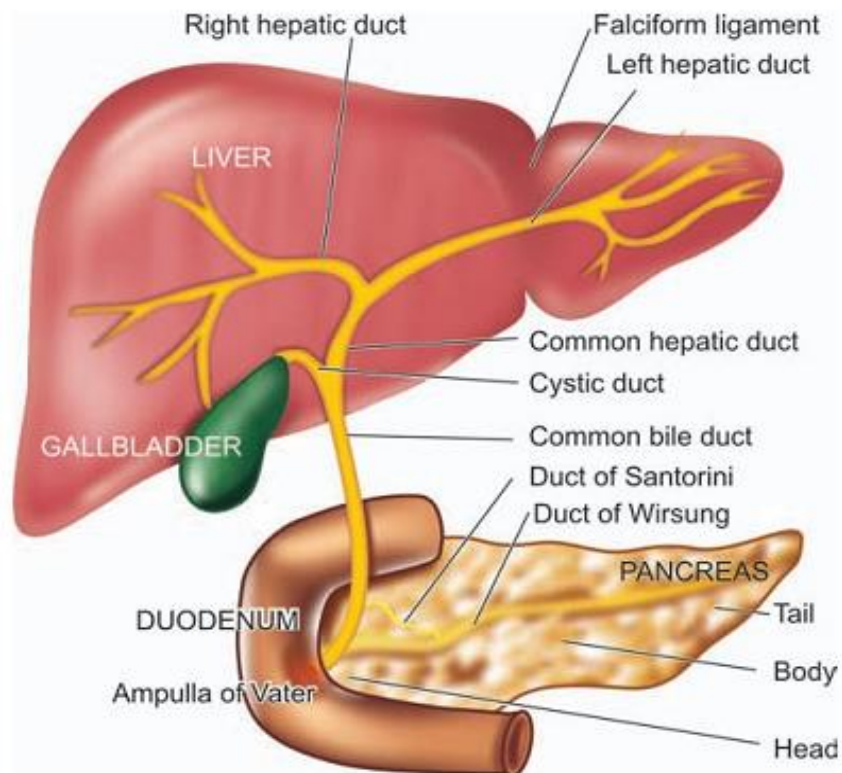
Figure (2.1). Anatomy of the liver and its relationship to

the gall bladder, pancreas and duodenum (Harsh, 2010).
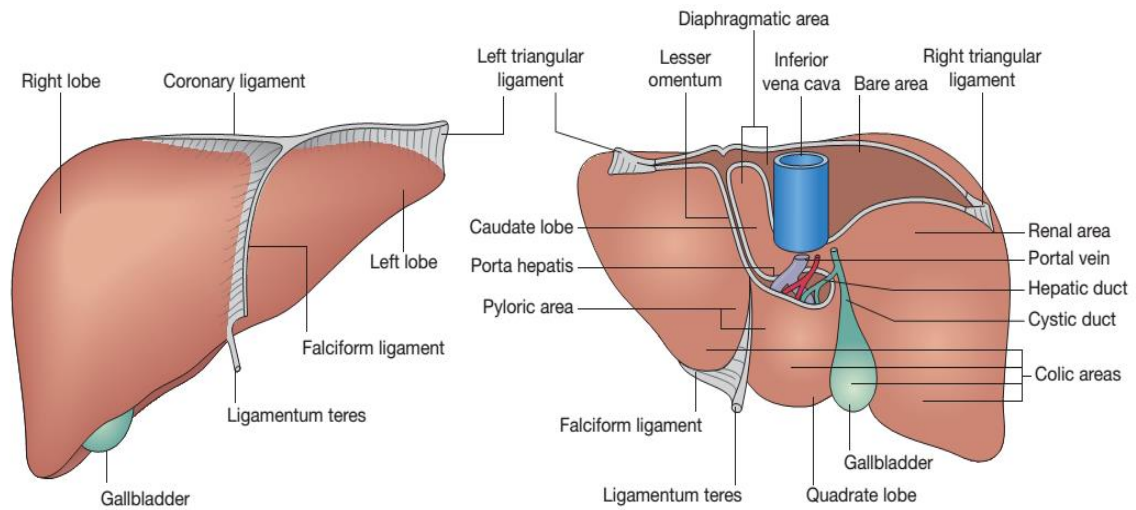
Figure 2.2 : Lobes, surfaces and ligaments of the liver viewed anterior (left)

and from aposteroinferior (right) (Thomas, 2006).

2.1.1 The Porta Hepatis:

The porta hepatis may also be referred to as the liver hilum. The three structures located within the porta hepatis are the main portal vein, common bile duct, and hepatic artery.
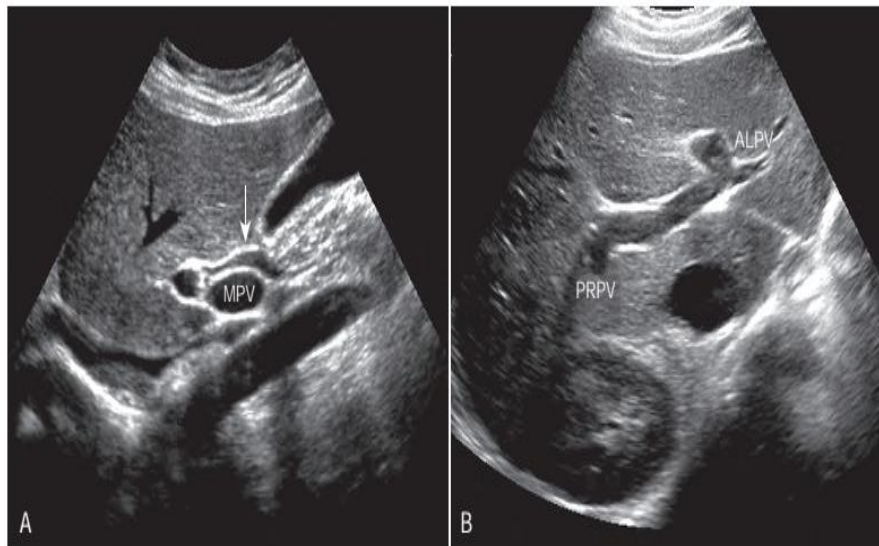
Figure (2.3) Ultrasound image of normal porta hepatis A, sagital

image and B, transverse image (Kyung, 2012).

2.1.2 Gross anatomical lobes:

Historically, the liver has been considered to be divided into right, left, caudate and quadrate lobes by the surface peritoneal and ligamentous attachments (Snell, 2012).

Right lobe:

The right lobe is the largest in volume and contributes to all surfaces of the liver. It is divided from the left lobe by the falciform ligament superiorly and the ligamentum venosum inferiorly. On the inferior face to the right of the groove formed by the ligamentum venosum there are two prominences separated by the porta hepatis: the caudate lobe lies posterior and the quadrate lobe anterior to the porta hepatis. The gallbladder lies in a shallow fossa to the right of the quadrate lobe (Snell, 2012).

Left lobe:

 The left lobe is the smaller of the two main lobes, although it is nearly as large as the right lobe in young children. It lies to the left of the falciform ligament with no subdivisions, and is substantially thinner than the right lobe, having a thin apex that points into the left upper quadrant (Snell, 2012).

Quadrate lobe:

The quadrate lobe is visible as a prominence on the inferior surface of the liver, to the right of the groove formed by the ligamentum venosum (and thus is incorrectly said to arise from the right lobe although it is functionally related to the left lobe). It lies anterior to the porta hepatis and is bounded by the gallbladder fossa to the right, a short portion of the inferior border anteriorly, the fissure for the ligamentum teres to the left, and the porta hepatis posteriorly (Snell, 2012).

Caudate lobe:

The caudate lobe is visible as a prominence on the inferior and posterior surfaces to the right of the groove formed by the ligamentum venosum: it lies posterior to the porta hepatis. To its right is the groove for the inferior vena cava. Above, it continues into the superior surface on the right of the upper end of the fissure for the ligamentum venosum. In gross anatomical descriptions this lobe is said to arise from the right lobe, but it is functionally separate (Snell, 2012).
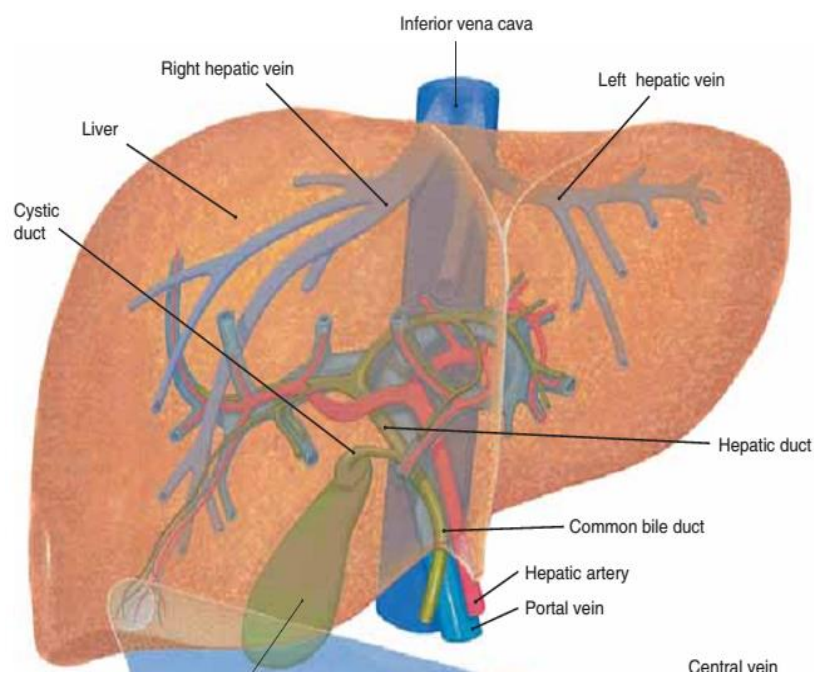
Figure(2.4) : The liver and gall bladder with blood vessels

and bile ducts (Kyung, 2012)

2.1.3 Fissures of the liver:

Knowledge of the fissures of the liver is essential for understanding liver surgery. Three major fissures, not visible on the surface, run through the liver parenchyma and harbor the three main hepatic veins (main, left and right portal fissures). Three minor fissures are visible as physical clefts of the liver surface (umbilical, venous and fissure of Gans).

2.1.4 Sectors and segments of the liver:

The sectors of the liver are made up of between one and three segments: right lateral sector = segments VI and VII; right medial sector = segments V and VIII; left medial sector = segments III and IV (and part of I); left lateral sector = segment II. Segments are numbered in an ante-clockwise spiral centered on the portal vein with the liver viewed from beneath, starting with segment I up to segment VI, and then back clockwise for the most cranial two segments VII and VIII (Rickard, 2015).
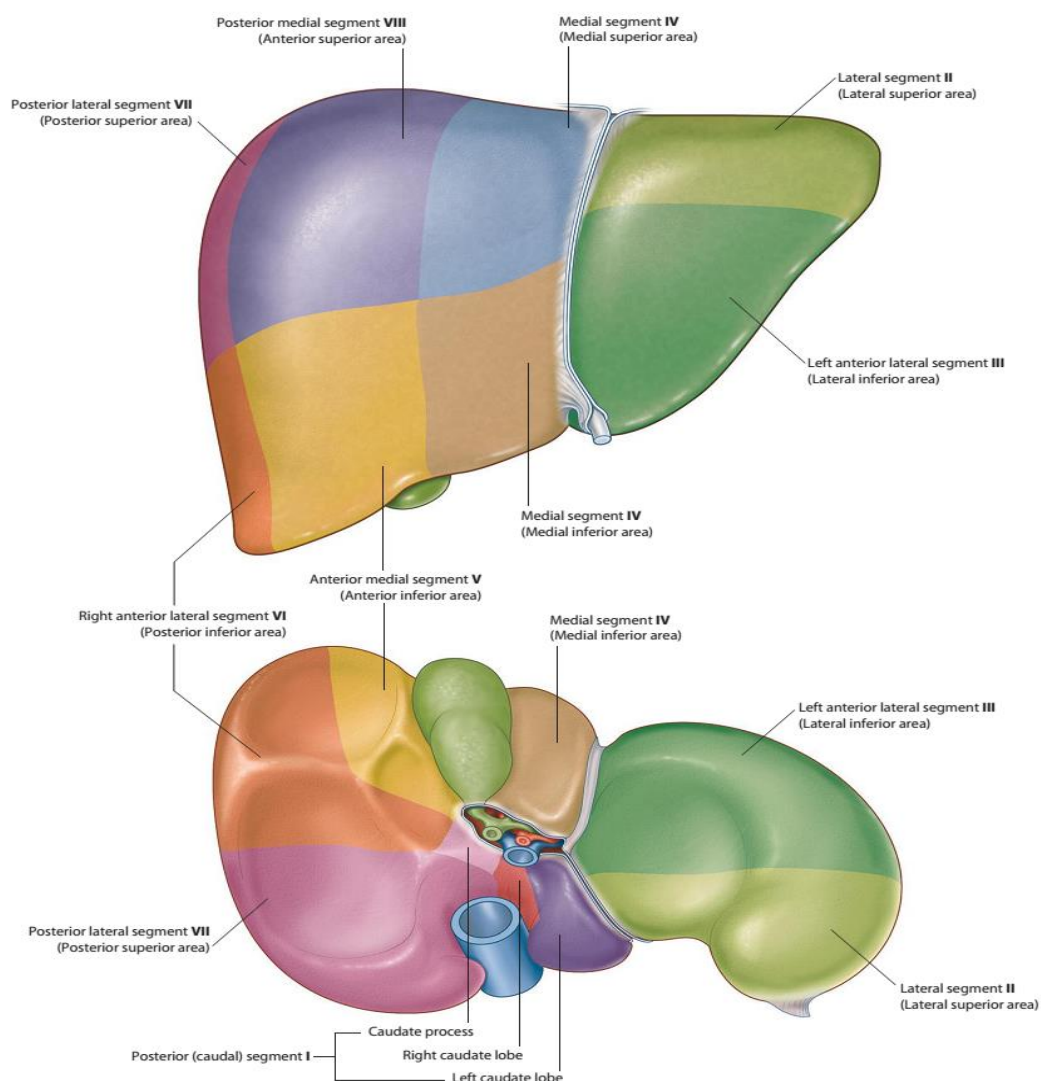
Fig. 2.5. Shows segments of the liver A. Anterior view. B. Posterior view (Rickard, 2015)

RIGHT LOBE   **LEFT LOBE**

Anterior-superior area

Posterior-superior area

Medial superior ar

Lateral superior a

Lateral inferior area

Falciform ligament

Round ligament of liver

Medial inferior area

Gallbladder

Posterior-inferior area

Anterior-inferior area

Inferior vena cava

Right hepatic vein

Left and middle hepatic veins

Right and left branches of hepatic artery

Portal vein

Bile duct

Hepatic artery

Portal triad

Gallbladder

Figure 2.6: Division of the liver based on hepatic drainage and blood supply (Rickard, 2015).

2.1.5 Supports of the liver:

The liver is stabilized and maintained in its position in the right upper quadrant of the abdomen by both static and dynamic factors. Suggested a three-tier classification of the anatomical factors: the suspensory attachments at the posterior abdominal wall to the inferior vena cava, hepatic veins, coronary and triangular ligaments (primary factors); the support provided by the right kidney, right colonic angle and

duodenopancreatic complex (secondary factors); the attachment to the anterior abdominal wall and diaphragm by the falciform ligament (tertiary factors). The inferior vena cava and the supra-hepatic veins, especially the right hepatic vein, appear to be the most important anatomical structures that support the bulk of the liver. Other factors which are responsible for the maintenance of the position of the liver within the abdominal cavity include positive intra-abdominal pressure and the movement of the diaphragm during respiration (Snell, 2012).

2.1.6 Peritoneal attachments and ligaments of the liver:

The liver is attached to the anterior abdominal wall, diaphragm and other viscera by several ligaments which are formed from condensations of the peritoneum which are Falciform ligament, Coronary ligament, Triangular ligaments, Lesser omentum, Ligamentum venosum, Porta hepatis, hepatoduodenal ligament and hilar plate and Glisson's sheat (Carol,2011).
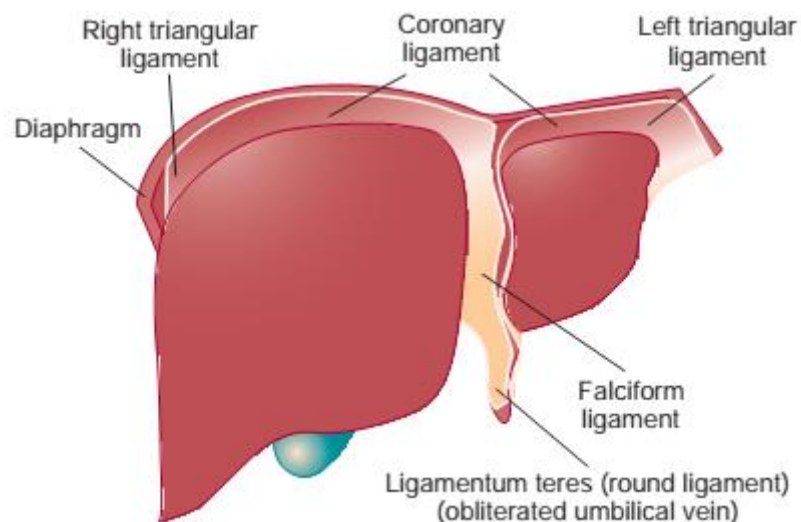
Figure 2.7. Hepatic Ligaments. Diagram of anterior surface of the liver (Carol,2011).

2.1.7 Vascular supply and lymphatic drain:

The vessels connected with the liver are the portal vein, hepatic artery and hepatic veins. The portal vein and hepatic artery ascend in the lesser omentum to the porta hepatis, where each bifurcates. The hepatic bile duct and lymphatic vessels descend from the porta hepatis in the same omentum. The hepatic veins leave the liver via its posterior surface and run directly into the inferior vena cava (Harsh, 2010).

Hepatic artery:

In adults the hepatic artery is intermediate in size between the left gastric and splenic arteries. In fetal and early postnatal life it is the largest branch of the coeliac axis. The hepatic artery gives off right gastric, gastroduodenal and cystic branches as well as direct branches to the bile duct from the right hepatic and sometimes the supraduodenal artery. After its origin from the coeliac axis, the hepatic artery passes anteriorly and laterally below the epiploic foramen to the upper aspect of the first part of the duodenum. It may be subdivided into the common hepatic artery, from the coeliac trunk to the origin of the gastroduodenal artery, and the hepatic artery 'proper', from that point to its bifurcation. It passes anterior to the portal vein and ascends anterior to the epiploic foramen between the layers of the lesser omentum. Within the free border of the lesser omentum the hepatic artery is medial to the common bile duct and anterior to the portal vein. At the porta hepatis it divides into right and left branches before these run into the parenchyma of the liver. The right hepatic artery usually crosses posterior (occasionally anterior) to the common hepatic duct. This close proximity often means that the right hepatic artery is involved in bile duct cancer earlier than the left hepatic artery. Occasionally the right hepatic artery crosses in front of the common bile duct and may be injured in surgery of the common bile duct.

It almost always divides into an anterior branch supplying segments V and VIII, and a posterior branch supplying segments VI and VII. The anterior division often supplies a branch to segment I and the gallbladder. The segmental arteries are macroscopically end-arteries although some collateral circulation occurs between segments via fine terminal branches (Gray□s, 2008).

A small number of normal variants are important to demonstrate angiographically because they may influence surgical and interventional radiological procedures. A vessel that supplies a lobe in addition to its normal vessel is defined as an accessory artery. A replaced hepatic artery is a vessel that does not originate from an orthodox position and provides the sole supply to that lobe. More commonly a replaced right hepatic artery or an accessory right hepatic artery arises from the superior mesenteric artery. In this case they run behind the portal vein and bile duct in the lesser omentum and can be identified at surgery by pulsation behind the portal vein (Gray□s, 2008).

Veins:

The liver has two venous systems. The portal system conveys venous blood from the majority of the gastrointestinal tract and its associated organs to the liver. The hepatic venous system drains blood from the liver parenchyma into the inferior vena cava (Gray □s, 2008).

Portal vein:

The portal vein begins at the level of the second lumbar vertebra and is formed from the convergence of the superior mesenteric and splenic veins. It is approximately 8 cm long and lies anterior to the inferior vena cava and posterior to the neck of the pancreas. It lies obliquely to the right and ascends behind the first part of the duodenum, the common bile duct and gastroduodenal artery. At this point it is directly anterior to the

inferior vena cava. It enters the right border of the lesser omentum, ascends anterior to the epiploic foramen to reach the right end of the porta hepatis and then divides into right and left main branches which accompany the corresponding branches of the hepatic artery into the liver. In the lesser omentum the portal vein lies posterior to both the common bile duct and hepatic artery. It is surrounded by the hepatic nerve plexus and accompanied by many lymph vessels and some lymph nodes (Gray□s, 2008).

Porto-systemic shunts:

Increased pressure within the portal venous system may result in dilatation of the portal venous tributaries: a reversal of flow may occur where these veins form anastomoses with veins which drain into the systemic venous circulation.

Hepatic veins:

Liver is drained by three major hepatic veins into the suprahepatic part of the inferior vena cava and a multitude of minor hepatic veins that drain into the intrahepatic inferior vena cava. There are three major veins are located between the four major sectors of the liver which are Right hepatic vein, Middle hepatic vein, Left hepatic vein and Minor veins (Snell, 2012).

Lymphatics:

Lymph from the liver has abundant protein content. Lymphatic drainage from the liver is wide and may pass to nodes above and below the diaphragm. Obstruction of the hepatic venous drainage increases the flow of lymph in the thoracic duct. Hepatic collecting vessels are divided into superficial and deep systems (Snell, 2012).

Innervation:

The liver has a dual innervation. The parenchyma is supplied by hepatic nerves which arise from the hepatic plexus and contain sympathetic and parasympathetic (vagal) fibers. They enter the liver at the porta hepatis and most accompany the hepatic arteries and bile ducts. A very few may run directly within the liver parenchyma. The capsule is supplied by some fine branches of the lower intercostal nerves, which also supply the parietal peritoneum, particularly in the area of the 'bare area' and superior surface (Snell, 2012).
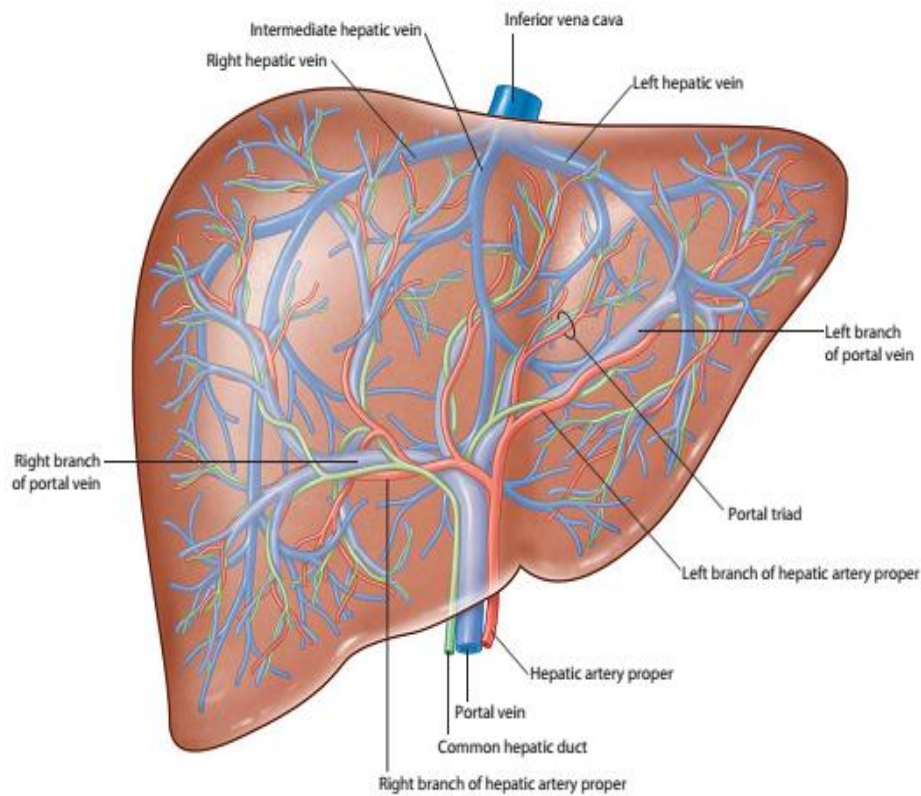
Figure 2.8. Anterior surface of liver with hepatic veins,

portal veins and associated vessels (Snell, 2012).

2.1.8 Sonographic Anatomy:

The normal liver is homogeneous, contains fine - level echoes, and is either minimally hyperechoic or isoechoic compared to the normal renal cortex. The liver is hypoechoic compared to the spleen. This relationship is evident when the lateral segment of the left lobe is elongated and wraps around the spleen (Carol, 2011), with the bright echoes of the portal triads and echo-free areas corresponding to large hepatic veins (Andrea, 2013). Its outline is smooth, the inferior margin coming to a point anteriorly. The liver is surrounded by a thin, hyperechoic capsule, which is difficult to see on ultrasound unless outlined by fluid. The smooth parenchyma is interrupted by vessels and ligaments and the liver itself provides an excellent acoustic window on to the various organs and great vessels situated in the upper abdomen. The ligaments are hyperechoic, linear structures; the falciform ligament, which separates the anatomical left and right lobes, is situated at the superior margin of the liver and is best demonstrated when surrounded by ascitic fluid. It surrounds the left main portal vein and is known as the ligamentum teres as it descends towards the infero-anterior aspect of the liver. The ligamentum venosum separates the caudate lobe from the rest of the liver. The size of the liver is difficult to quantify, as there is such a large variation in shape between normal subjects and direct measurements are notoriously inaccurate. Size is therefore usually assessed subjectively. Look particularly at the inferior margin of the right lobe which should come to a point anterior to the lower pole of the right kidney. A relatively common variant of this is the *Reidel's lobe*, an inferior elongation of segment VI on the right. This is an extension of the right lobe over the lower pole of the kidney, with a rounded margin, and is worth remembering as a possible cause of a palpable right upper quadrant 'mass'. To distinguish mild enlargement from a Reidel's lobe, look at the left lobe. If this also looks bulky, with a

rounded inferior edge, the liver is enlarged. A Reidel's lobe is usually accompanied by a smaller, less accessible left lobe (Carol, 2011).
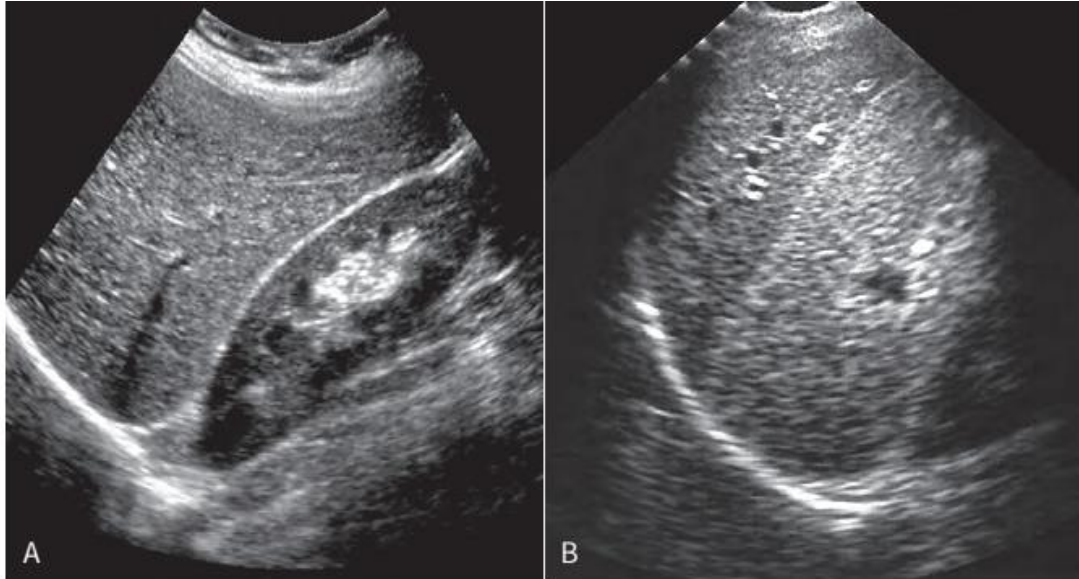
Figure 2.9. Shows normal liver echogenicity. A.the liver is more echogenic than the renal cortex. B. The liver is less echogenic than the spleen, as seen it left lobe wraps around the spleen (Carol, 2011).
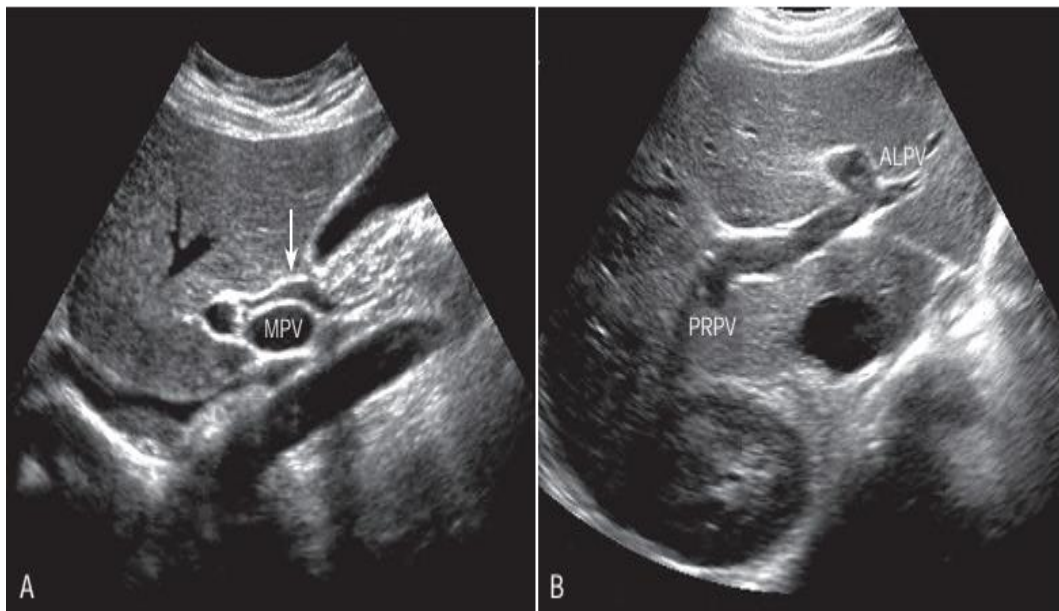
Figure 2.10. Shows normal porta hepatic. A, Sagital image and B, Transverse image (Carol, 2011).
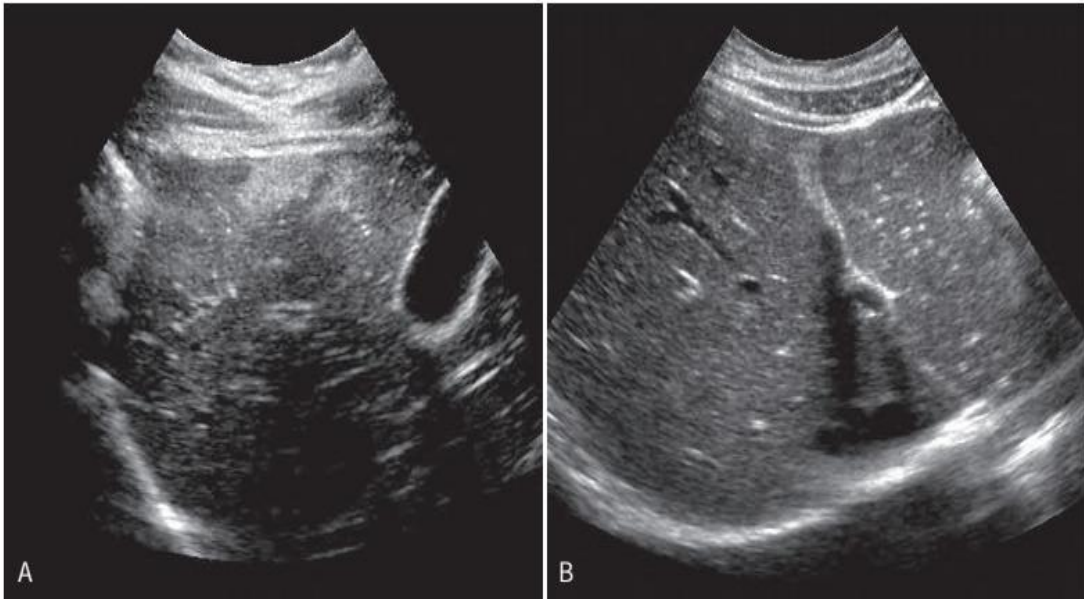
Figure 2.11. Shows falciform ligament.A, Sagital image through falciform ligament. B, Subcostal view of falciform ligament (Carol, 2011).

2.2 Microstructure:

Cells of the liver include hepatocytes, hepatic stellate cells (also known as perisinusoidal lipocytes, or Ito cells), sinusoidal endothelial cells, macrophages (Kupffer cells), the cells of the biliary tree (cuboidal to columnar epithelium) and connective tissue cells of the capsule and portal tracts (Snell, 2012).

The liver is essentially an epithelial-mesenchymal outgrowth of the caudal part of the foregut, with which it retains its connection via the biliary tree. The surface of the liver facing the peritoneal cavity is covered by a typical serosa, the visceral peritoneum. Beneath this, and enclosing the whole structure, is a thin (50–100 μm) layer of connective tissue from which extensions pass into the liver as connective tissue septa and trabeculae. Branches of the hepatic artery and hepatic portal vein, together with bile ductules and ducts, run within these connective tissue trabeculae which are termed portal tracts (portal canals). The combination of the two types of vessel and a bile duct is termed a portal triad these structures are

usually accompanied by one or more lymphatic vessels. The liver parenchyma consists of a complex network of epithelial cells, supported by connective tissue, and perfused by a rich blood supply from the hepatic portal vein and hepatic artery. The epithelial cells, hepatocytes, carry out the major metabolic activities of this organ, but additional cell types possess storage, phagocytic and mechanically supportive functions. In the mature liver, hepatocytes are arranged mainly in plates (or cords, as seen in two-dimensional sections) that are usually only one cell thick and separated by venous sinusoids which anastomose with each other via gaps in the plates. Until about seven years of age, plates are normally two cells thick. Bile secreted by the hepatocytes is collected in a network of minute tubes (canaliculi). The hepatocytes can therefore be regarded as exocrine cells, secreting bile into the alimentary tract via the hepatic ducts and bile duct. Their other metabolic functions involve complex biochemical exchanges with the blood (Harsh, 2010).

The fetal liver is a major haemopoietic organ: erythrocytes, leukocytes and platelets develop from the mesenchyme covering the sinusoidal endothelium.

2.2.1 Lobulation of the liver:

The liver is composed of small functional units called lobules. Each lobule contains numerous canals which channel blood between the cell of the lobule into a central vein (Robert, 1996). The lobule is a roughly hexagonal arrangement of plates of hepatocytes, separated by intervening sinusoids which radiate outward from a central vein, with portal triads at the vertices of each hexagon. The central vein is a tributary of the hepatic vein that drains the tissue. In some species, the classic lobular units are delimited microscopically by distinct connective tissue septa. However, the lobular organization of the human liver is not immediately evident in

histological sections: the lobules do not have distinct boundaries, and connective tissue is sparse. The plates do not pass straight to the periphery of a lobule like the spokes of a wheel but run irregularly as they anastomose and branch (Harsh, 2010).

2.3 Function of the liver:

The liver performs a wide range of metabolic activities required for homeostasis, nutrition and immune defense. For example, it is important in the removal and breakdown of toxic, or potentially toxic, materials from the blood and the regulation of blood glucose and lipids, the storage of certain vitamins, iron, and other micronutrients, and in breaking down or modifying amino acids. It is involved in a plethora of other biochemical reactions. Since the majority of these processes are exothermic, a substantial part of the thermal energy production of the body, especially at rest, is provided by the liver. The liver is populated by phagocytic macrophages, components of the mononuclear phagocyte system capable of removing particulates from the blood stream. It is an important site of haemopoiesis in the fetus. The liver functions are briefly listed as:

1. One of the many functions of the liver is synthesizes cholate and chenodeoxycholate (primary bile salts) from cholesterol (Agamemnon, 2003) and secrete bile, normally between 600 and 1000 ml/day. Bile serves two important functions: First, bile plays an important role in fat digestion and absorption. Second, bile serves as a means for excretion of several important waste products from the blood. These include especially bilirubin, an end product of hemoglobin destruction, and excesses of cholesterol (Arthur, 2006 and Stephen, 2007).

2. Manufacture of several major plasma proteins such as albumin, fibrinogen and prothrombin.

3. Metabolism of proteins, carbohydrates and lipids.

4. Storage of vitamins (A, D and B12) and iron. 5. Detoxification of toxic substances such as alcohol and drugs (Steven, 2011).

2.4 Liver pathology (Diffuse Liver Disease):

2.4.1 Fatty Liver Disease:

Is a reversible disease characterized by deposits of fat within the hepatocytes. Causes of fatty liver include obesity, alcohol abuse, chemotherapy, diabetes mellitus, pregnancy, glycogen storage disease, and the use of some drugs. Although fatty liver is typically asymptomatic, patients may present clinically with elevated liver function tests. Fatty changes within the liver can be diffuse or focal (Stephen, 2007).

2.4.2 Hepatitis:

Hepatitis is inflammation of the liver, which can ultimately lead to cirrhosis, portal hypertension, and hepatocellular carcinoma (HCC). Hepatitis can be acute or chronic.

Acute viral hepatitis is characterized by jaundice and dramatically elevated liver enzymes (aspartate aminotransaminase [AST] and alanine aminotransaminase [ALT].

Chronic viral hepatitis requires symptoms persisting for longer than 6 months**.**(George, 2009). Viral hepatitis comes in many forms, including hepatitis A, B, C, D, E, and G. The two most common forms are hepatitis A and B. Hepatitis A is spread by fecal–oral route in contaminated water or food. Hepatitis B is spread by contact with contaminated body fluids, mother-to-infant transmission, or inadvertent blood contact, as seen in the case of intravenous drug abuse or occupational exposure. An additional concern for healthcare workers is work-related exposure to hepatitis C. This form of hepatitis is also spread by means of contact with blood and body fluids. Hepatitis may also be triggered by reactions to viruses.

Patients with any form of hepatitis can experience a wide range of clinical troubles including fever, ,nausea, vomiting, fatigue, hepatosplenomegaly, dark urine, and jaundice. However, the jaundice related to hepatitis is on a cellular level and is not associated with biliary obstruction. This is referred to as non obstructive jaundice. Elevation in the liver function tests is often apparent as well. (Edward, 2010). Sonographically, a patient with hepatitis may initially have a completely normal-appearing liver. With time, hepatomegaly and splenomegaly can be observed with sonography. As the liver enlarges, it tends to become more hypoechoic. Periportal cuffing may be seen in some patients with hepatitis. This is described as an increase in the echogenicity of the walls of the portal triads. The sonographic manifestation of this phenomenon is referred to as the "starry sky" sign. The gallbladder wall may also be thickened in the presence of hepatitis (Steven, 2011).
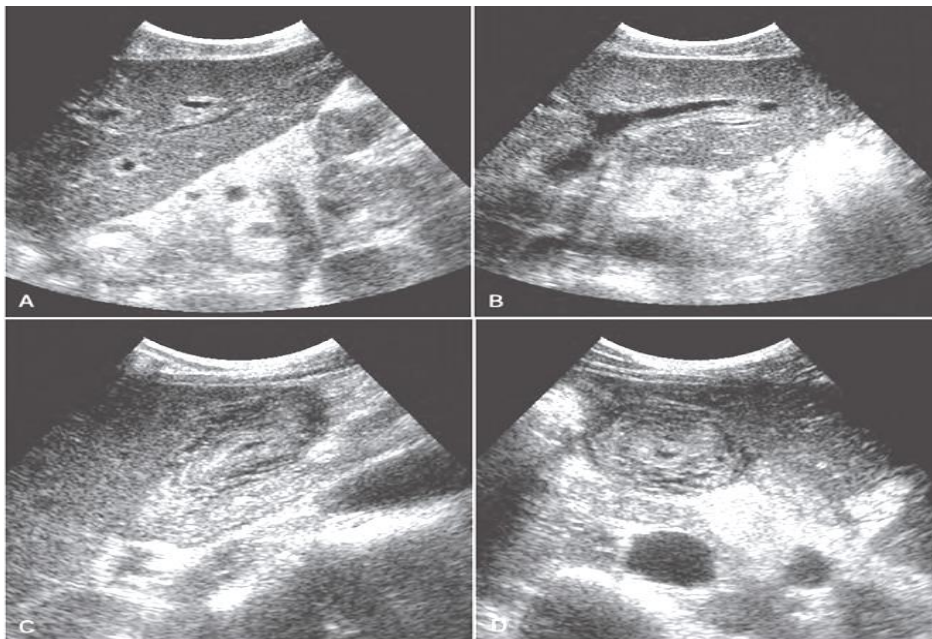
Figure 2.12. Ultrasound images A, sagittal and B, transverse, images of the left lobe of the liver show marked increased thickness and echogenisity of the soft tissue surrounding the portal vein branch. C, sagittal and D, transverse, views of the thickened gall bladder wall with extensive hypoechoic pocket of edema fluid c (Carol, 2011).

2.4.3 Cirrhosis:

Cirrhosis is a devastating liver disorder that is defined as hepatocyte death, fibrosis and necrosis of the liver, and the subsequent development of regenerating nodules. Common sequela of cirrhosis includes portal hypertension, the development of varicosities within the abdomen, portal vein thrombosis, splenomegaly, and HCC. The most common cause of cirrhosis is alcoholism. However, cirrhosis can also be caused by primary biliary cirrhosis, hepatitis, cholangitis, and hemochromatosis.

Patients may have normal laboratory findings until cirrhosis advances into end-stage liver disease. However, when laboratory abnormalities are evident, they include elevation in aspartate aminotransferase, alanine aminotransferase, lactate dehydrogenase, and bilirubin. Patients may also present with jaundice, fatigue, weight loss, diarrhea, initial hepatomegaly, and ascites (Harsh, 2010).

Sonographic findings of cirrhosis include an echogenic, small right lobe, an enlarged caudate and left lobe, nodular surface irregularity, coarse echo texture, ascites, and splenomegaly. Cirrhosis caused by alcoholism will lead to the development of nodules that typically measure less than 1 cm, while cirrhosis caused by hepatitis will cause macronodular development, or nodules that measure between 1 and 5 cm. These nodules may be readily seen when ascites surrounds the liver. If ascites is not present, a high-frequency linear transducer can be used to analyze the liver surface for lumps (Carol, 2011).
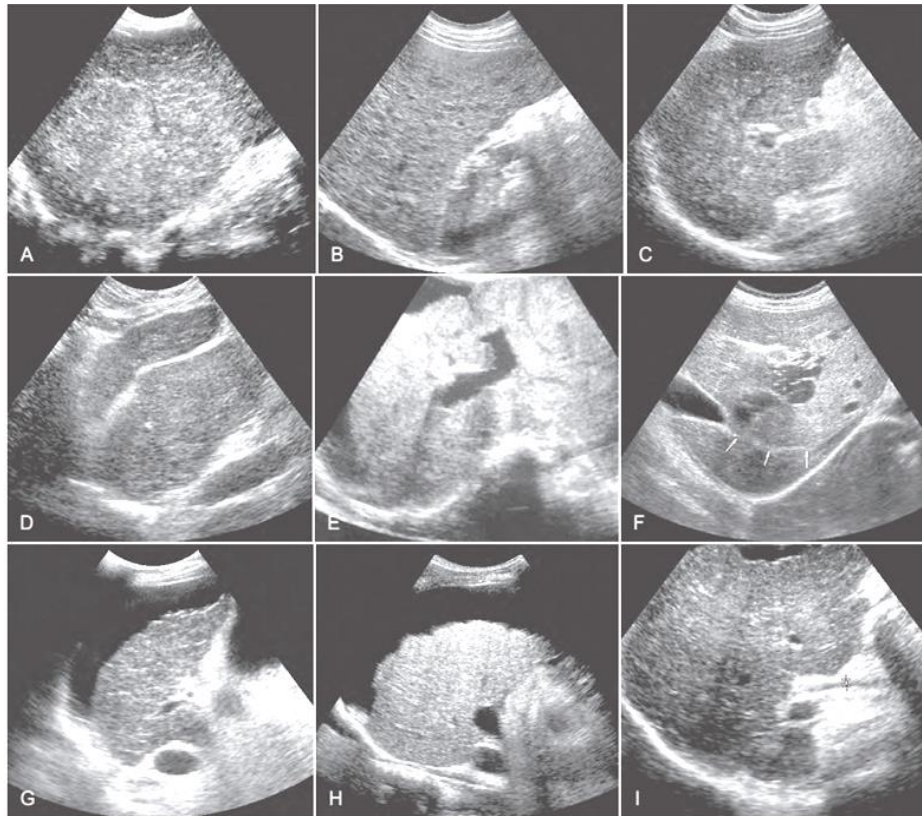
Figure 2.13. Ultrasound images of cirrhotic liver show A, Coarse parenchyma and innumerable tiny, hyperechoic nodules. B, Coarse parenchyma and innumerable tiny, hypoechoic nodules. C, Coarse parenchyma and surface nodularity. D, Sagittal image showing an enormous caudate lobe. E, Transverse sonogram shows the right lobe is small with enlarged the left lateral segment. G and H, Small, end stage liver with surface nodularity, best appreciated in patient with ascites. I, liver contour varies greatly (Carol, 2011).

2.4.4 Budd–Chiari Syndrome:

Budd–Chiari syndrome is described as the occlusion of the hepatic veins, with possible co-existing occlusion of the inferior vena cava. Budd–Chiari can be seen secondary to a congenital webbing disorder, coagulation abnormalities, tumor invasion from HCC, thrombosis, oral contraceptive use, pregnancy, and trauma. Clinical symptoms of this abnormality, when found in female patients on oral contraception, include ascites, right upper quadrant pain, hepatomegaly, and possibly splenomegaly. Other patients

may suffer from extensive upper abdominal pain and elevated liver function (Carol, 2011).

2.4.5 Focal Liver Diseases:

Hepatic Cysts:

True hepatic cysts are usually not encountered until middle age. They are often associated with autosomal dominant polycystic kidney disease. Clinically, hepatic cysts are asymptomatic and they do not alter liver function tests. They are often multiple, and they may not always conform to the sonographic appearance of a simple cyst, as their shape can be somewhat irregular. Clusters of cysts may be noted, which may suggest a complex appearance. However, all other simple cysts criteria should be present, including smooth wall, acoustic enhancement, and they should be entirely anechoic (Carol, 2011).

Hydatid Liver Cyst:

A hydatid liver cyst may also be referred to as an echinococcal cyst. These cysts develop most commonly from a parasite referred to as *Echinococcus granulosus*. This parasite is a tapeworm that lives in dog feces. Food contaminated by the infected feces is consumed indirectly by sheep, cattle, goat, and possibly humans. Therefore, there is a higher prevalence of hydatid disease in sheep- and cattle-raising countries such as the Middle East, Australia, and the Mediterranean. The parasite moves from the bowel through the portal vein to enter the liver (Steven, 2011).

Pyogenic Hepatic Abscess:

Most commonly arises as a complication of an intra-abdominal infection with direct portal venous spread to the liver. Clinical presentation may be variable but fever, pain, pleurisy, nausea and vomiting are all common. USG- Frankly purulent abscesses appear cystic, with the fluid ranging from echo-free to highly echogenic. Occasionally gas producing

organisms give rise to echogenic foci with a posterior reverberation artifact. The abscess wall can vary from well-defined to irregular and thick (Sumeet, 2013).

Amebic Hepatic Abscess:

An amebic hepatic abscess comes from a parasite that grows in the colon and invades the liver via the portal vein. It is typically transmitted through contaminated water found in places like Mexico, Central America, South America, India, and Africa. Therefore, patients who present with amebic abscesses may have traveled out of the country in recent times. Clinical features may be hepatomegaly, right upper quadrant pain, general malaise, or signs of dysentery, which include bloody diarrhea, abdominal pain, and fever. Sonographically usually appears as a round or oval-shaped lesion, absence of a prominent abscess wall, hypoechogenicity, distal acoustic enhancement, fine low level echoes and contiguity with the diaphragm (Sumeet, 2013).

Hepatic Candidiasis:

Patients who are immunocompromised can develop hepatic candidiasis. For example, cancer patients, recent organ transplant patients, or those with human immunodeficiency virus are prone to develop this fungal abscess within their liver. Candidiasis results from the spread of fungus, namely *Candidaalbicans*, in the blood. Besides being immunocompromised, patients may have right upper quadrant pain, fever, and hepatomegaly.

Sonographic findings include multiple hyperechoic masses with hypoechoic borders. These masses may be described as "halo" or "bull's-eye" lesions (Steven, 2011).

Hepatocellular Adenoma:

The hepatocellular adenoma, which may also be referred to as a hepatic adenoma or liver cell adenoma, is a rare benign liver tumor. It is often associated with the use of oral contraceptives. Patients are typically asymptomatic with an adenoma. Hepatic adenomas do have thepropensity to become malignant and are often surgically removed for that reason. The sonographic appearance of a hepatic adenoma is variable, including hypoechoic, hyperechoic, isoechoic, or mixed echogenicities (Steven, 2011).

Cavernous Hemangioma:

The most common benign liver tumor is the cavernous hemangioma. They are more common in women. Hepatic hemangiomas are usually incidentally detected and asymptomatic. The most common location of the cavernous hemangioma is within the right lobe of the liver and they characteristically appear as a small, hyperechoic mass measuring less than 3 cm. Unfortunately, hemangiomas may also appear hypoechoic or complex, and therefore they can be sonographically indistinguishable from metastatic liver disease (Steven, 2011and Murray, 2014).

Hepatic Hematoma:

A hepatic hematoma can be a consequence of trauma or surgery. Patients will have a decreased hematocrit. Hematomas can be located within the liver parenchyma, termed intrahepatic, or around the liver, which is termed subcapsular. Hematomas can appear solid or complex depending on their age. Initial hemorrhage appears echogenic, and over time as it resolves, it will appear more cystic or complex. Therefore, in the acute stage, an intrahepatic hematoma may be difficult to visualize with sonography (Steven, 2011).

Focal Nodular Hyperplasia:

Focal nodular hyperplasia (FNH) has been cited as the second most common benign liver tumor and more commonly incidentally discovered in women. The mass is composed of a combination of hepatocytes and fibrous tissue. It typically contains a central scar that is not always detected with sonography. Patients who have FNH are most often asymptomatic. Sonographically, FNH may have varying sonographic appearances including isoechoic, echogenic, and hypoechoic. FNH has been referred to as a "stealth lesion" because it may be difficult to identify secondary to its slight sonographic disparity from normal liver parenchyma. The central scar, when seen, will appear as a hypoechoic or hyperechoic, linear structure within the mass. Hypervascularity within the scar can be identified by using color Doppler (Harsh, 2010).

Hepatic Lipoma:

The hepatic lipoma is rarely encountered in the liver. Patients are asymptomatic and its sonographic appearance is that of a hyperechoic mass.

Hepatocellular Carcinoma:

HCC is the most common primary form of liver cancer, although it is not encountered as often as metastatic liver disease. HCC is most often seen in men, and frequently accompanied by cirrhosis or chronic hepatitis. (Steven, 2011)The major etiologies of HCC are now well defined and include chronic viral hepatitis B, C and D, toxins and drugs (e.g. alcohol, aflatoxins, anabolic steroids), metabolic liver diseases (e.g. hereditary hemochromatosis, a1-antitrypsin deficiency) and to an as yet less clearly defined extent, non-alcoholic fatty liver disease. On a global scale, chronic hepatitis B virus (HBV) and HCV infection account for well over 80% of HCCs (Zakim, 2006).

The malignant mass associated with HCC is referred to as a hepatoma. Hepatomas can invade the portal veins or hepatic veins. Narrowing of the hepatic veins, with possible tumor invasion into the inferior vena cava, is termed Budd–Chiari syndrome. The sonographic findings of HCC are unpredictable. There may be an individual mass or multiple masses present at the time of diagnosis. HCC may appear as a solitary, small, hypoechoic mass, or as heterogeneous masses scattered throughout the liver.A hypoechoic halo may be noted around the hepatoma as well (Steven, 2011).

Hepatic Metastasis:

The liver is a common location for metastatic disease to manifest. Metastatic liver disease is much more common than primary liver cancer. The malignant cells from other sites enter the liver through the portal veins or lymphatic channels. Primary cancers that metastasize to the liver include the gallbladder, colon, stomach, pancreas, breast, and lung, with the latter being the most common primary source. Patients with hepatic metastasis often present with weight loss, jaundice, right upper quadrant pain, hepatomegaly, and ascites. Liver function tests will be abnormal as well. The sonographic findings of metastatic liver disease are variable, often depending on the location of the primary cancer. Metastatic cancer from the gastrointestinal tract and pancreas tends to be calcified tumors. Hypoechoic masses may be from the breast, lung, or lymphoma. Hyperechoic masses may be from the kidney or pancreas (Steven, 2007).

Hepatoblastoma:

The hepatoblastoma is a malignant pediatric liver tumor. It has been cited as the most common malignant tumor of childhood.10 These aggressive tumors are most often discovered before age 5, with half of the cases identified in children less than 1 year old. There is a high incidence of

hepatoblastoma in children who have Beckwith–- Wiedemann syndrome. Like liver carcinoma in the adult, hepatoblastomas will cause an elevation in serum -fetoprotein. These tumors can invade surrounding vasculature and may obstruct the biliary tree as well (Stephen, 2007).

Liver transplant and postsurgical complications:

A liver transplant should appear similar to a normal native liver. All vasculature should appear patent and have normal waveforms. Signs of rejection can be documented sonographically. Complications of a liver transplant include biliary strictures, cholangitis, biliary sludge and stones, hepatic artery thrombosis, hepatic artery stenosis, hepatic artery pseudoaneurysms, celiac artery stenosis, portal vein stenosis and thrombosis, and fluid collections (Steven, 2011).

2.5 Ultrasound Physics:

All diagnostic ultrasound applications are based on the detection and display of acoustic energy reflected from interfaces within the body. These interactions provide the information needed to generate high-resolution, gray-scale images of the body, as well as display information related to blood flow.

2.5.1 Wavelength and Frequency:

Sound is the result of mechanical energy traveling through matter as a wave producing alternating compression and rarefaction. Pressure waves are propagated by limited physical displacement of the material through which the sound is being transmitted. A plot of these changes in pressure is a sinusoidal waveform, in which the Y axis indicates the pressure at a given point and the X axis indicates time. Changes in pressure with time defied the basic units of measurement for sound. The distance between corresponding points on the time pressure curve is defined as the

wavelength (λ), and the time (T) to complete a single cycle is called the period. The number of complete cycles in a unit of time is the frequency *(f)* of the sound. Frequency and period are inversely related. If the period (T) is expressed in seconds, $f = 1/T$, or $f = T \times sec-1$. The unit of acoustic frequency is the hertz (Hz); 1 Hz = 1 cycle per second. High frequencies are expressed in kilohertz (kHz; 1 kHz = 1000 Hz) or megahertz (MHz; 1 MHz = 1,000,000 Hz). In nature, acoustic frequencies span a range from less than 1 Hz to more than 100,000 Hz (100 kHz). Human hearing is limited to the lower part of this range, extending from 20 to 20,000 Hz. Ultrasound differs from audible sound only in its frequency, and it is 500 to 1000 times higher than the sound we normally hear. Sound frequencies used for diagnostic applications typically range from 2 to 15 MHz, although frequencies as high as 50 to 60 MHz are under investigation for certain specialized imaging applications (Carol, 2011).
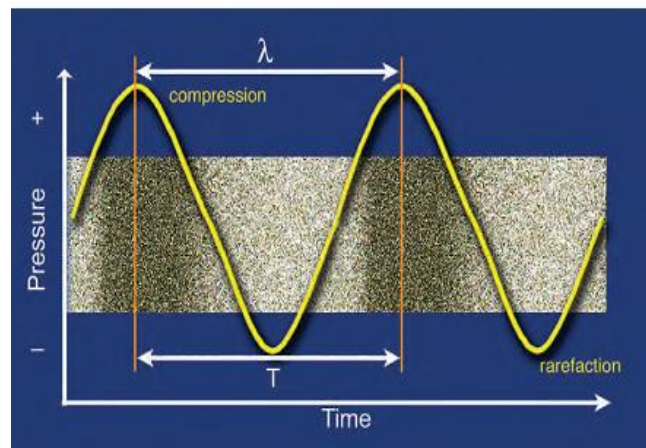
Figure 2.14. Shows sound wave (Carol, 2011).

2.5.2 Propagation of Sound:

In most clinical applications of ultrasound, brief bursts or pulses of energy are transmitted into the body and propagated through tissue. Acoustic pressure waves can travel in a direction perpendicular to the direction of the particles being displaced (transverse waves), but in tissue

32

and fluids, sound propagation is along the direction of particle movement (longitudinal waves). The speed at which the pressure wave moves through tissue varies greatly and is affected by the physical properties of the tissue. Propagation velocity is largely determined by the resistance of the medium to compression, which in turn is influenced by the density of the medium and its stiffness or elasticity. It is increased by increasing stiffness and reduced by decreasing density. In the body, propagation velocity may be regarded as constant for a given tissue and is not affected by the frequency or wavelength of the sound (Carol, 2011).

2.5.3 Distance Measurement:

Propagation velocity is a particularly important value in clinical ultrasound and is critical in determining the distance of a reflecting interface from the transducer. Much of the information used to generate an ultrasound scan is based on the precise measurement of time and employs the principles of echo-ranging. If an ultrasound pulse is transmitted into the body and the time until an echo returns is measured, it is simple to calculate the depth of the interface that generated the echo, provided the propagation velocity of sound for the tissue is known (Carol, 2011).

2.5.4 Acoustic impedance (Z):

Is determined by product of the density (ρ) of the medium propagating the sound and the propagation velocity (c) of sound in that medium (Z = ρc). Interfaces with large acoustic impedance differences, such as interfaces of tissue with air or bone, reflect almost all the incident energy. Interfaces composed of substances with smaller differences in acoustic impedance, such as a muscle and fat interface, reflect only part of the incident energy (Carol, 2011).

2.5.5 Reflection:

The way ultrasound is reflected when it strikes an acoustic interface is determined by the size and surface features of the interface. If large and relatively smooth, the interface reflects sound much as a mirror reflects light. Such interfaces are called specular reflectors because they behave as "mirrors for sound." The amount of energy reflected by an acoustic interface can be expressed as a fraction of the incident energy; this is termed the reflection coefficient (R). If a specular reflector is perpendicular to the incident sound beam, the amount of energy reflected is determined by the following relationship: $R = (Z2-Z1)2 / (Z2 + Z1)2$ where Z1 and Z2 are the acoustic impedances of the media forming the interface (Carol, 2011).

Because ultrasound scanners only detect reflections that return to the transducer, display of specular interfaces is highly dependent on the angle of insonation (exposure to ultrasound waves). Specular reflectors will return echoes to the transducer only if the sound beam is perpendicular to the interface. If the interface is not at a 90-degree angle to the sound beam, it will be reflected away from the transducer, and the echo will not be detected. Most echoes in the body do not arise from specular reflectors but rather from much smaller interfaces within solid organs. In this case the acoustic interfaces involve structures with individual dimensions much smaller than the wavelength of the incident sound. The echoes from these interfaces are scattered in all directions. Such reflectors are called diffuse reflectors and account for the echoes that form the characteristic echo patterns seen in solid organs and tissues. The constructive and destructive interference of sound scattered by diffuse reflectors results in the production of ultrasound speckle, a feature of tissue texture of sonograms of solid organs. For some diagnostic applications, the nature of

the reflecting structures creates important conflicts. For example, most vessel walls behave as specular reflectors that require insonation at a 90-degree angle for best imaging, whereas Doppler imaging requires an angle of less than 90 degrees between the sound beam and the vessel (Carol, 2011).
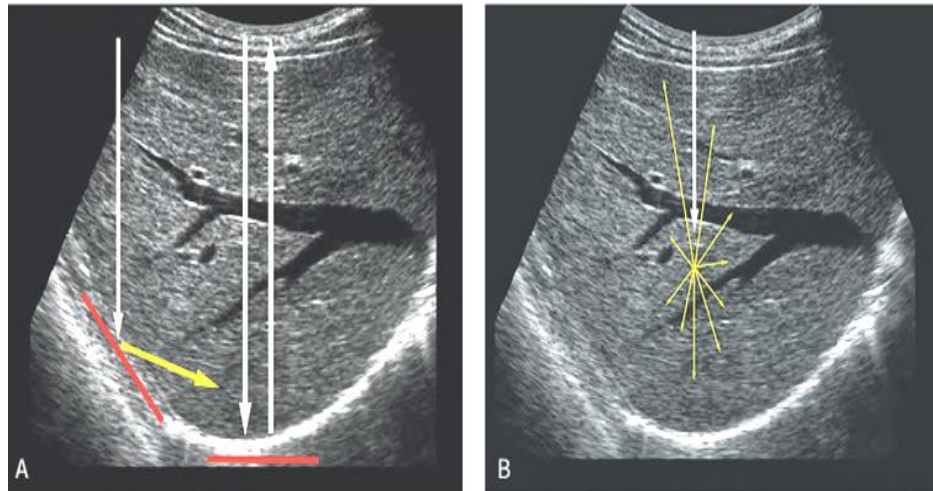
Figure 2.15. Ultrasound images represent A, Specular reflector.

B, Diffuse reflector (Carol, 2011).

2.5.6 Refraction:

Another event that can occur when sound passes from a tissue with one acoustic propagation velocity to a tissue with a higher or lower sound velocity is a change in the direction of the sound wave. This change in direction of propagation is called refraction and is governed by Snell's law: **Sin 1/ Sin 2 = C1/C2**

Where **Sin 1** is the angle of incidence of the sound approaching the interface, **Sin 2** is the angle of refraction, and c1 and c2 are the propagation velocities of sound in the media forming the interface (Carol, 2011).
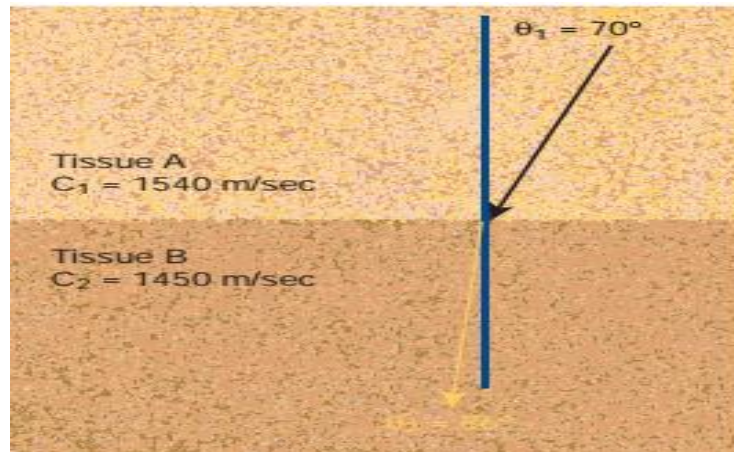
Figure 2.16. Shows Refraction(Carol, 2011).

2.5.7 Attenuation:

An ultrasound wave can be attenuated by several mechanisms as it travels through tissue. The most important mechanism is absorption, in which ultrasound energy is converted into heat. As well as absorption, the intensity in the beam may be reduced due to scattering of ultrasound out of the beam and to divergence or spreading of the beam with distance. Attenuation depends on the insonating frequency as well as the nature of the attenuating medium. High frequencies are attenuated more rapidly than lower frequencies, and transducer frequency is a major determinant of the useful depth from which information can be obtained with ultrasound. Attenuation determines the efficiency with which ultrasound penetrates a specific tissue and varies considerably in normal tissues (Carol, 2011).

Intensity (I) is used to describe the spatial distribution of power and is calculated by dividing the power by the area over which the power is distributed, as follows: **I (W/ cm2) = Power (W) / Area (cm2)**
The attenuation of sound energy as it passes through tissue is of great clinical importance because it influences the depth in tissue, from which useful information can be obtained. This in turn affects transducer

selection and a number of operator-controlled instrument settings, including time (or depth) gain compensation, power output attenuation, and system gain levels. Attenuation is measured in relative rather than absolute units. The **decibel** (dB) notation is generally used to compare different levels of ultrasound power or intensity. This value is 10 times the log10 of the ratio of the power or intensity values being compared (Carol, 2011).
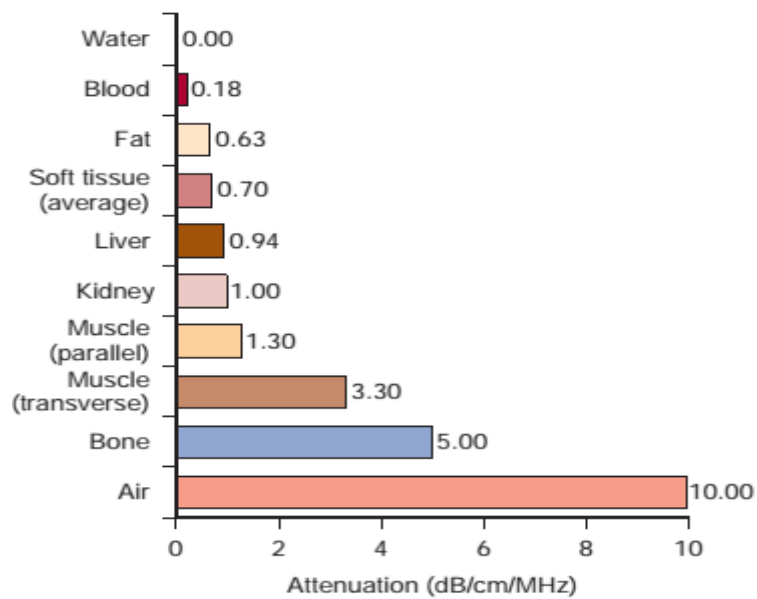
Figure 2.17. Demonstrate attenuation when a sound passes through tissue(Carol, 2011).

2.5.8 Instrumentation:

Ultrasound scanners are complex and sophisticated imaging devices, but all consist of the following basic components to perform key functions:

• Transmitter or pulser to energize the transducer • Ultrasound transducer itself • Receiver and processor to detect and amplify the backscattered energy and manipulate the reflected signals for display • Display that presents the ultrasound image or data in a form suitable for analysis and interpretation • Method to record or store the ultrasound image (Peter, 2010).

Transmitter:

Most clinical applications use pulsed ultrasound, in which brief bursts of acoustic energy are transmitted into the body. The source of these pulses, the ultrasound transducer, is energized by application of precisely timed, high-amplitude voltage. The maximum voltage that may be applied to the transducer is limited by federal regulations that restrict the acoustic output of diagnostic scanners. Most scanners provide a control that permits attenuation of the output voltage. Because the use of maximum output results in higher exposure of the patient to ultrasound energy, prudent use dictates use of the output attenuation controls to reduce power levels to the lowest levels consistent with the diagnostic problem (Carol, 2011).

The transmitter also controls the rate of pulses emitted by the transducer, or the pulse repetition frequency (PRF). The PRF determines the time interval between ultrasound pulses and is important in determining the depth from which unambiguous data can be obtained both in imaging and Doppler modes. The ultrasound pulses must be spaced with enough time between the pulses to permit the sound to travel to the depth of interest and return before the next pulse is sent (Carol, 2011).

Transducer:

A transducer is any device that converts one form of energy to another. In ultrasound the transducer converts electric energy to mechanical energy, and vice versa. In diagnostic ultrasound systems the transducer serves two functions: converting the electric energy provided by the transmitter to the acoustic pulses directed into the patient and serving as the receiver of reflected echoes, converting weak pressure changes into electric signals for processing (Carol, 2011).

Ultrasound transducers use piezoelectricity, a principle discovered by Pierre and Jacques Curie in 1880. Piezoelectric materials have the unique

ability to respond to the action of an electric field by changing shape. They also have the property of generating electric potentials when compressed. Changing the polarity of a voltage applied to the transducer changes the thickness of the transducer, which expands and contracts as the polarity changes. This results in the generation of mechanical pressure waves that can be transmitted into the body. The piezoelectric effect also results in the generation of small potentials across the transducer when the transducer is struck by returning echoes. Positive pressures cause a small polarity to develop across the transducer; negative pressure during the rarefaction portion of the acoustic wave produces the opposite polarity across the transducer. These tiny polarity changes and the associated voltages are the source of all the information processed to generate an ultrasound image or Doppler display. When stimulated by the application of a voltage difference across its thickness, the transducer vibrates. The frequency of vibration is determined by the transducer material. When the transducer is electrically stimulated. A range or band of frequencies results. The preferential frequency produced by a transducer is determined by the propagation speed of the transducer material and its thickness. In the pulsed wave operating modes used for most clinical ultrasound applications, the ultrasound pulses contain additional frequencies that are both higher and lower than the preferential frequency. The range of frequencies produced by a given transducer is termed its bandwidth. Generally, the shorter the pulse of ultrasound produced by the transducer, the greater is the bandwidth (Carol, 2011).

Interference of pressure waves results in an area near the transducer where the pressure amplitude varies greatly. This region is termed the near field, or Fresnel zone. Farther from the transducer, at a distance determined by the radius of the transducer and the frequency, the sound field begins to

diverge, and the pressure amplitude decreases at a steady rate with increasing distance from the transducer. This region is called the far field, or Fraunhofer zone. In modern multi element transducer arrays, precise timing of the filing of elements allows correction of this divergence of the ultrasound beam and focusing at selected depths. Only reflections of pulses that return to the transducer are capable of stimulating the transducer with small pressure changes, which are converted into the voltage changes that are detected, amplified, and processed to build an image based on the echo information (Carol, 2011).

Receiver:

When returning echoes strike the transducer face, minute voltages are produced across the piezoelectric elements. The receiver detects and amplifies these weak signals. The receiver also provides a means for compensating for the differences in echo strength, which result from attenuation by different tissue thickness by control of time gain compensation (TGC) or depth gain compensation (DGC). Sound is attenuated as it passes into the body, and additional energy is removed as echoes return through tissue to the transducer. Because echoes returning from deeper tissues are weaker than those returning from more superficial structures, they must be amplified more by the receiver to produce a uniform tissue echo appearance. Another important function of the receiver is the compression of the wide range of amplitudes returning to the transducer into a range that can be displayed to the user. The ratio of the highest to the lowest amplitudes that can be displayed may be expressed in decibels and is referred to as the dynamic range. In a typical clinical application, the range of reflected signals may vary by a factor of as much as 1 : 1012, resulting in a dynamic range of up to 120 dB. Although the amplifiers used in ultrasound machines are capable of

handling this range of voltages, gray-scale displays are limited to display a signal intensity range of only 35 to 40 dB (Carol M, 2011).
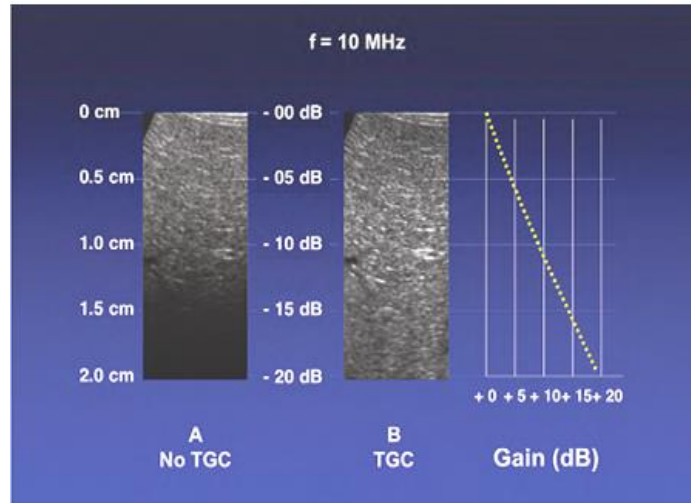
Figure 2.18. Demonstrate the effect of time gain compensation (Carol, 2011).

Compression and remapping of the data are required to adapt the dynamic range of the backscattered signal intensity to the dynamic range of the display Compression is performed in the receiver by selective amplification of weaker signals. Additional manual post processing controls permit the user to map selectively the returning signal to the display. These controls affect thebrightness of different echo levels in the image and therefore determine the image contrast (Carol, 2011).
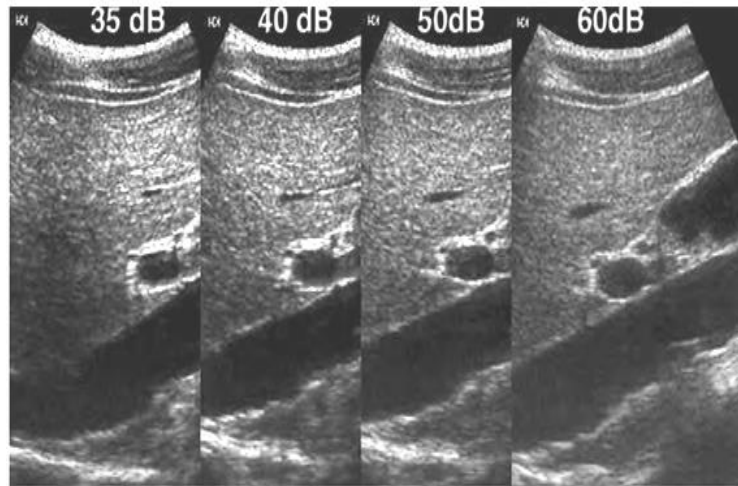
Figure 2.19. Diagram demonstrate

the dynamic range (Carol, 2011).

Image Display:

Ultrasound signals may be displayed in several ways. Imaging has evolved from simple A-mode and bistable display to high-resolution, real-time, grayscale imaging. The earliest A-mode devices displayed the voltage produced across the transducer by the backscattered echo as a vertical deflection on the face of an oscilloscope. The horizontal sweep of the oscilloscope was calibrated to indicate the distance from the transducer to the reflecting surface. In this form of display, the strength or amplitude of the reflected sound is indicated by the height of the vertical deflection displayed on the oscilloscope. With A-mode ultrasound, only the position and strength of a reflecting structure are recorded. Another simple form of imaging, M-mode ultrasound, displays echo amplitude and shows the position of moving reflectors. M-mode imaging uses the brightness of the display to indicate the intensity of the reflected signal. The time base of the display can be adjusted to allow for varying degrees of temporal resolution, as dictated by clinical application (Carol, 2011).
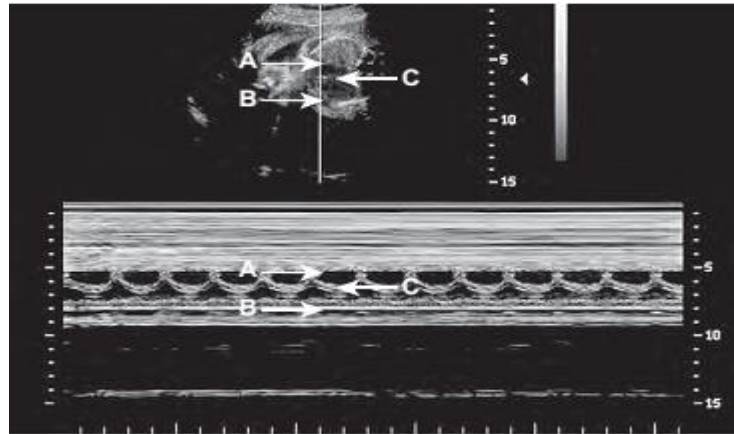
Figure 2.20. Shows M- mode display (Carol, 2011).

The mainstay of imaging with ultrasound is provided by real-time, gray-scale, B-mode display, in which variations in display intensity or brightness are used to indicate reflected signals of differing amplitude. To generate a two-dimensional (2-D) image, multiple ultrasound pulses are sent down a series of successive scan lines, building a 2-D representation of echoes arising from the object being scanned. When an ultrasound image is displayed on a black background, signals of greatest intensity appear as white; absence of signal is shown as black; and signals of intermediate intensity appear as shades of gray. If the ultrasound beam is moved with respect to the object being examined and the position of the reflected signal is stored, the brightest portions of the resulting 2-D image indicate structures reflecting more of the transmitted sound energy back to the transducer. In most modern instruments a digital memory of 512×512 or 512×640 pixels is used to store values that correspond to the echo intensities originating from corresponding positions in the patient. At least 28, or 256, shades of gray are possible for each pixel, in accord with the amplitude of the echo being represented. The image stored in memory in this manner can then be sent to a video monitor for display. Because B-mode display relates the strength of a backscattered signal to a brightness

level on the display device (usually a video display monitor), it is important that the operator understand how the amplitude information in the ultrasound signal is translated into a brightness scale in the image display. Each ultrasound manufacturer offers several options for the way the dynamic range of the target is compressed for display, as well as the transfer function that assigns a given signal amplitude to a shade of gray. Although these technical details vary among machines, the way the operator uses them may greatly affect the clinical value of the fial image. In general, it is desirable to display as *wide* a dynamic range as possible, to identify subtle differences in tissue echogenicity. Real-time ultrasound produces the impression of motion by generating a series of individual 2-D images at rates of 15 to 60 frames per second. Real-time, 2-D, B-mode ultrasound is now the major method for ultrasound imaging throughout the body and is the most common form of B-mode display. Real-time ultrasound permits assessment of both anatomy and motion. When images are acquired and displayed at rates of several times per second, the effect is dynamic, and because the image reflects the state and motion of the organ at the time it is examined, the information is regarded as being shown in real time. In cardiac applications the terms "2-D echocardiography" and "2-D echo" are used to describe real-time, B-mode imaging; in most other applications the term "real-time ultrasound" is used. Transducers used for real-time imaging may be classified by the method used to steer the beam in rapidly generating each individual image, keeping in mind that as many as 30 to 60 complete images must be generated per second for real-time applications (Carol, 2011).
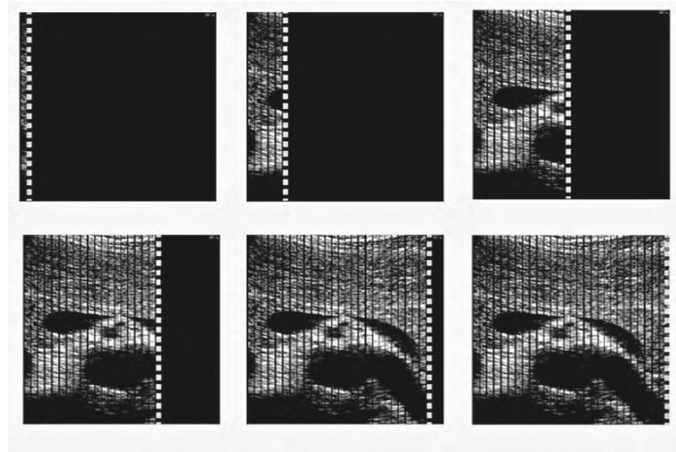
Figure 2.21. Shows B- mode display (Carol, 2011).

● *Steering* may be done through mechanical rotation or oscillation of the transducer or by electronic means.
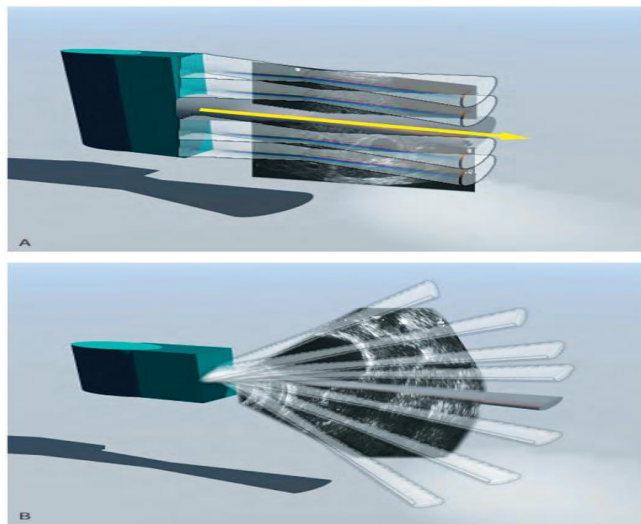
Figure 2.22. Shows beam steering (Carol, 2011).

Electronic beam steering is used in linear array and phased array transducers and permits a variety of image display formats. Most electronically steered transducers currently in use also provide electronic focusing that is adjustable for depth.

Mechanical beam steering may use single-element transducers with a field focus or may use annular arrays of elements with electronically controlled focusing. For real-time imaging, transducers using mechanical

or electronic beam steering generate displays in a rectangular or pie-shaped format. For obstetric, small parts, and peripheral vascular examinations, linear array transducers with a rectangular image format are often used. The rectangular image display has the advantage of a larger field of view near the surface but requires a large surface area for transducer contact. Sector scanners with either mechanical or electronic steering require only a small surface area for contact and are better suited for examinations in which access is limited (Carol, 2011).

2.5.9 Mechanical Sector Scanners:

Early ultrasound scanners used transducers consisting of a single piezoelectric element. To generate real-time images with these transducers, mechanical devices were required to move the transducer in a linear or circular motion. Mechanical sector scanners using one or more single-element transducers do not allow variable focusing. This problem is overcome by using annular array transducers. Although important in the early days of real-time imaging, mechanical sector scanners with field-focus, single-element transducers are not presently in common use (Carol, 2011).

Array

Current technology uses a transducer composed of multiple elements, usually produced by precise slicing of apiece of piezoelectric material into numerous small units, each with its own electrodes. Such transducer arrays may be formed in a variety of configurations. Typically, these are linear, curved, phased, or annular arrays. High-density 2-D arrays have also been developed. By precise timing of the filing of combinations of elements in these arrays, interference of the wave fronts generated by the individual elements can be exploited to change the direction of the ultrasound beam, and this can be used to provide a steerable beam for the

generation of real-time images in a linear or sector format. (Andrew, 2013).

Linear Arrays:

Linear array transducers are used for small parts, vascular, and obstetric applications because the rectangular image format produced by these transducers is well suited for these applications. In these transducers, individual elements are arranged in a linear fashion. By filing the transducer elements in sequence, either individually or in groups, a series of parallel pulses is generated, each forming a line of sight perpendicular to the transducer (Andrew, 2013).

Curved Arrays:

Linear arrays that have been shaped into convex curves produce an image that combines a relatively large surface field of view with a sector display format. Curved array transducers are used for a variety of applications, the larger versions serving for general abdominal, obstetric, and transabdominal pelvic scanning. Small, high-frequency, curved array scanners are often used in transvaginal and transrectal probes and for pediatric imaging (Andrew, 2013).

Phased Arrays:

In contrast to mechanical sector scanners, phased array scanners have no moving parts. A sector field of view is produced by multiple transducer elements field in precise sequence under electronic control. By controlling the time and sequence at which the individual transducer elements are field, the resulting ultrasound wave can be steered in different directions as well as focused at different depths. By rapidly steering the beam to generate a series of lines of sight at varying angles from one side of the transducer to the other, a sector image format is produced. This allows the

fabrication of transducers of relatively small size but with large fields of view at depth. These transducers are particularly useful for intercostal scanning, to evaluate the heart, liver, or spleen, and for examinations in other areas where access is limited applications. For evaluation of deeper structures in the abdomen or pelvis more than 12 to 15 cm from the surface, frequencies as low as 2.25 to 3.5 MHz may be required. When maximal resolution is needed, a high frequency transducer with excellent lateral and elevation resolution at the depth of interest is required (Andrew, 2013).

Figure 2.23.   Shows Ultrasound transducers for regional blocks. The photograph includes (left to right) broad linear, small footprint linear,curved, sector and hockey-stick transducers (Andrew, 2013).

2.5.10 Image display and storage:

With real-time ultrasound, user feedback is immediate and is provided by video display. The brightness and contrast of the image on this display are determined by the ambient lighting in the examination room, the brightness and contrast settings of the video monitor, the system gain setting, and the TGC adjustment. The factor most affecting image quality in many ultrasound departments is probably improper adjustment of the video display, with a lack of appreciation of the relationship between the video display settings and the appearance of hard copy or images viewed on a workstation. Because of the importance of the real-time video display in providing feedback to the user, it is essential that the display and the lighting conditions under which it is viewed are standardized and matched to the display used for interpretation. Interpretation of images and archival storage of images may be in the form of transparencies printed on film by optical or laser cameras and printers, videotape, or digital picture archiving and communications system (PACS). Increasingly, digital storage is being used for archiving of ultrasound images (Jane, 2004).

Image quality:
The key determinants of the quality of an ultrasound image are its spatial, contrast, and temporal resolution, as well as freedom from certain artifacts.

Spatial Resolution: The ability to differentiate two closely situated objects as distinct structures is determined by the spatial resolution of the ultrasound device, it is must be considered in three planes, with different determinants of resolution for each. Axial resolution, the maximum resolution along the beam axis, is determined by the pulse length. Because ultrasound frequency and wavelength are inversely related, the pulse length decreases as the imaging frequency increases. Because the pulse

length determines the maximum resolution along the axis of the ultrasound beam, higher transducer frequencies provide higher image resolution. In addition to axial resolution, resolution in the planes perpendicular to the beam axis must also be considered (Jane, 2004).
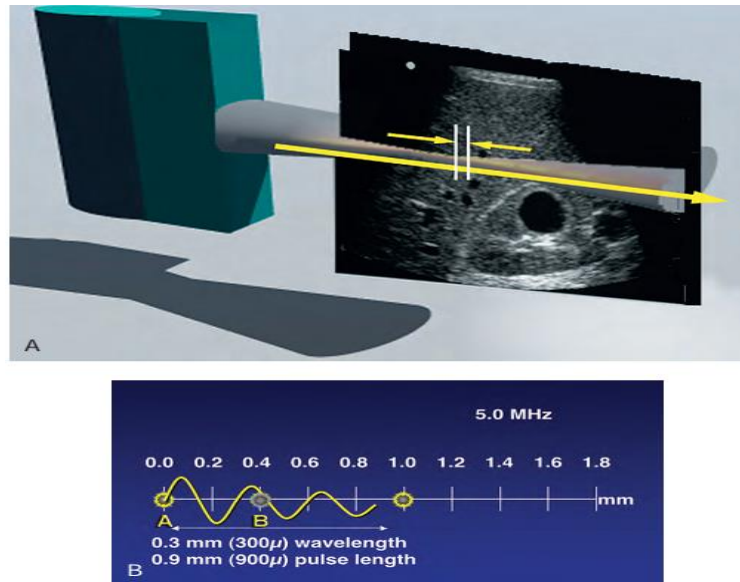
Figure 2.24. Shows Axial resolution (Carol, 2011).

Lateral resolution refers to resolution in the plane perpendicular to the beam and parallel to the transducer and is determined by the width of the ultrasound beam. Azimuth resolution, or elevation resolution, refers to the slice thickness in the plane perpendicular to the beam and to the transducer. Ultrasound is a tomographic method of imaging that produces thin slices of information from the body, and the width and thickness of the ultrasound beam are important determinants of image quality. Excessive beam width and thickness limit the ability to delineate small features and may obscure shadowing and enhancement from small structures, such as breast micro calcifications and small thyroid cysts. The width and thickness of the ultrasound beam determine lateral resolution and elevation resolution, respectively. Lateral and elevation resolutions

are significantly poorer than the axial resolution of the beam. Lateral resolution is controlled by focusing the beam, usually by electronic phasing, to alter the beam width at a selected depth of interest. Elevation resolution is determined by the construction of the transducer and generally cannot be controlled by the user (Jane, 2004).
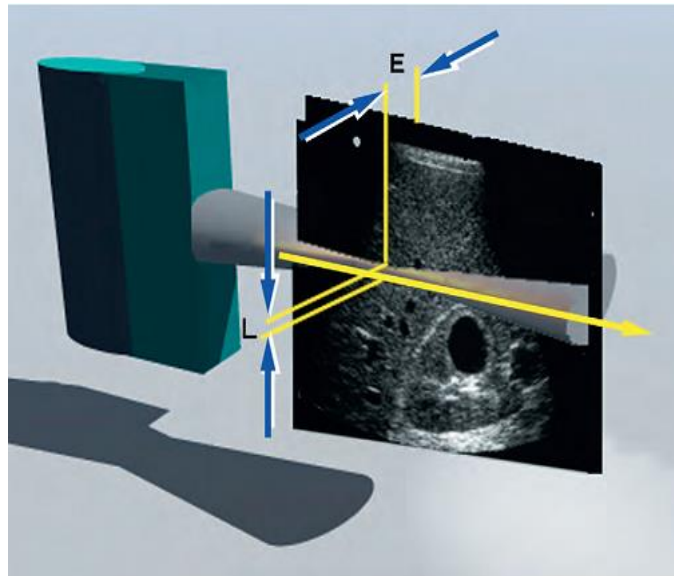
Figure 2.25. Shows lateral resolution (Carol, 2011).

2.6 Ultrasound Examination technique:

2.6.1 Patient Preparation:

It is recommended that a patient undergo a period of fasting prior to upper abdominal imaging to maximize the distension of the gall bladder and to reduce food residue and gas in the upper GI tract which may reduce image quality or precluded liver imaging. This is essential for full imaging of the liver and related biliary tree but may not be required in an acute situation such as trauma where imaging of the gall bladder is not immediately essential. A patient may take small amounts of still water by mouth prior to scan, particularly for taking any medications. There is some evidence that smoking can reduce image quality when scanning upper abdominal structures and it is good practice to encourage a patient not to smoke for

6-8 hours prior to US scan. Smoking increases gas intake into upper GI tract and may reduce image quality. Also, some chemicals in tobacco are known to cause contraction of the smooth muscle of the GI tract and this can cause contraction of the gall bladder, even when fasting has occurred, and the gall bladder cannot be scanned (Christoph, 2004).

2.6.2 Sonographic technique:

TAUS usually begins with the patient in the supine position. The examiner is on the patient's right side and the ultrasound machine is on the same side toward the head of the bed. A 3.5 MHz curvilinear transducer is the most common one used in adults. The curvilinear transducer requires a larger, flatter surface for optimal contact. When a smaller "footprint" (size of the contact surface) is necessary, such as viewing through an intercostal space, a phased array transducer can be used. Ideally, prior to TAUS, the patient should fast for 6 h. This decreases bowel gas and allows gallbladder distension. Standard scanning planes for TAUS are: longitudinal (sagittal, coronal) and transverse. Most TAUS scanning is done with light contact with coupling accomplished with gel. When holding the transducer, it is helpful to stabilize your hand by placing the base of the hypothenar eminence against the body. This allows for fine probe movement during the examination. The initial transducer placement depends on the type of study or organ of interest. The same is true for the initial transducer orientation. Transducer movement during TAUS includes all the techniques previously described (Ellen, 2014).

The patient should be examined from the sub- to the intercostal in the decubitus position as well in the modified, slightly oblique, positions with the right arm above the head and the right leg stretched during all respiration cycles to identify the best approach and to avoid artefacts

caused by the thorax. Examination in the standing position is also helpful owing to the liver moving caudally with gravity. Scanning from the sub- or intercostal probe positions (depending on the individual anatomy) avoids interposed lung, which can occur in the right posterolateral (superficial) parts of the liver when using the intercostal approach. There are other examination techniques that can also be used, but these will not be mentioned here in detail (Jan 2013). One measurement of liver size is done in the mid-clavicular line from highest peak of the diaphragm down to the caudal liver end. This has a maximum dimension 18 cm. Another possibility to measure the liver size is in the mid-clavicular line to measure ventrodorsal dimension (depth) and cranio-caudal dimension (length). The maximum length is 15 cm and depth 13 cm, maximum for both dimensions together is 28 cm. In many diseases, the caudate lobe is larger than the rest. In the liver cross section, measurement of this lobe relative to the rest, the quotient should be normally less than 0.55 (Jan Tuma, 2013).
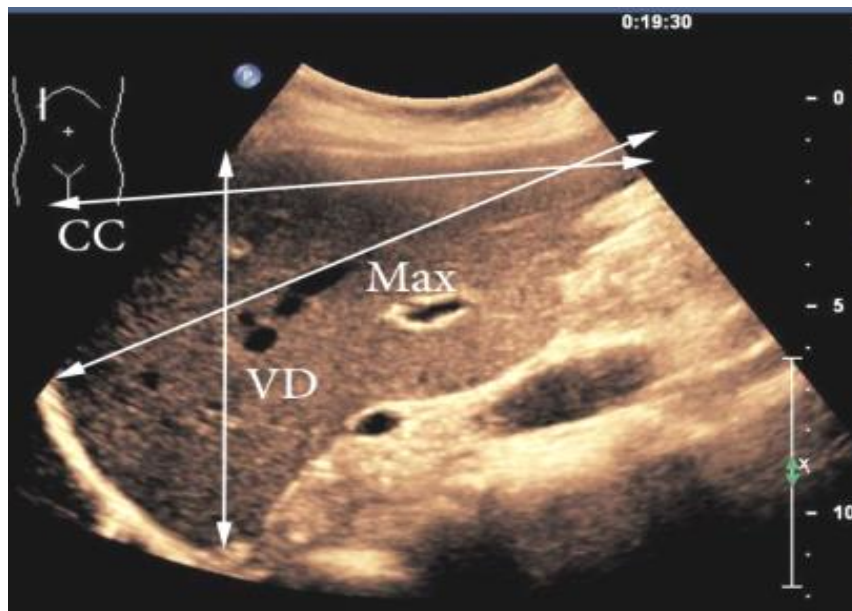
Figure 2.26. Measurement of liver size: Length CC, cranio-caudal; depth VD,ventrodorsal and the maximum distance of diaphragmatic dome to the lower edge of the liver in the MCL Max (Jan, Tuma 2013).
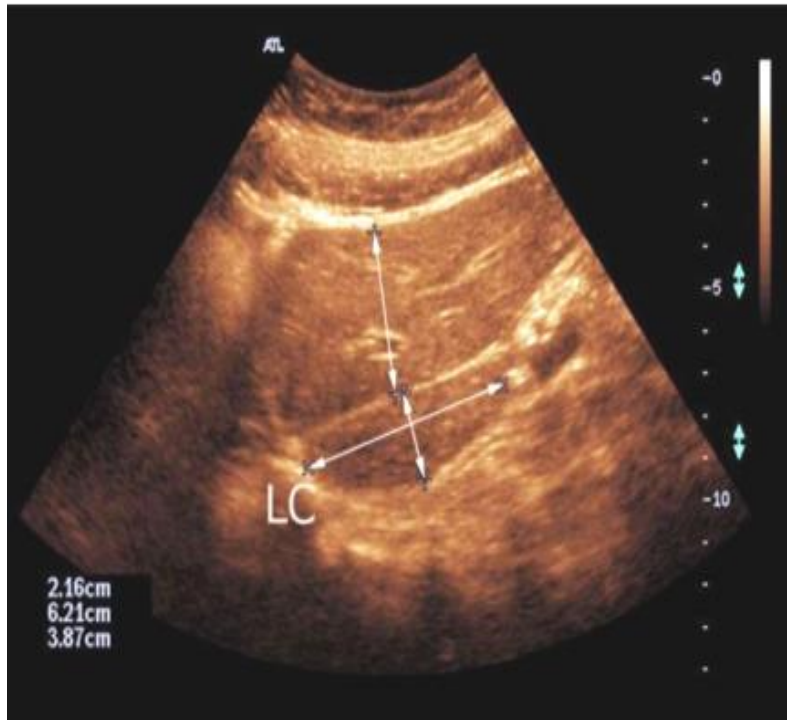
Figure 2.27. Measurement of the size of the caudate lobe and the overlying segments (Jan, Tuma 2013).
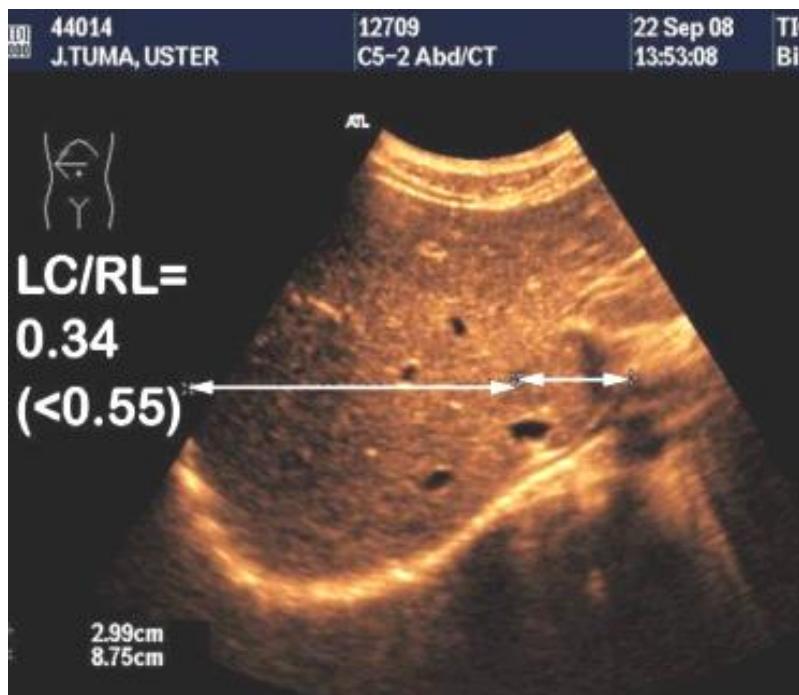
Figure 2.28. Measurement of the size of the caudate lobe and the right lobes. The ratio of caudate lobe CL / right lobes, RL should be <0.55 (here 0.34, normal) (Jan, Tuma 2013).
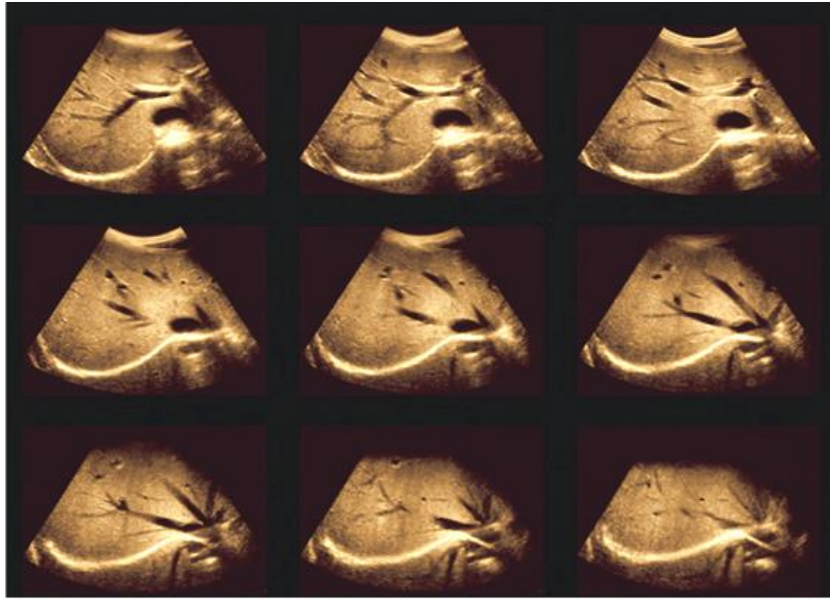
Figure 2.29. Ultrasound images show normal liver(Jan, Tuma 2013).

2.7 Texture-Based Methods Previously Used for Ultrasound Liver Disease Characterization:

The first and simplest methods used in order to do texture-based analysis of the ultrasound images were those based on first order statistics. The grey level histograms and the grey level histogram width, GLHW – a measure denoting the difference between the highest and lowest grey level and also the number of the histogram bars were used in (Kazuo et al., 1998) in order to quantify the sonographic echogenicity. A histogram-based method for diffuse liver disease identification was used in (Ossawa et al, 1996). The first order statistics were found not enough for a complete characterization of the properties of the liver tissue in order to differentiate between diffuse liver diseases. Second order statistics, based on the Gray Level Cooccurence Matrix, were used in (Valckx and,Thijssen, 1997,Cavouras, 1997 and Yeh, 2003). Some second order statistics like the GLCM mean, GLCM variance, homogeneity, entropy, angular second moment, contrast, correlation

formedthe feature vector and a classification method likek nearest neighbour (k-nn), Support Vector Machine (SVM) or Artificial Neural Networks (ANN) was used. In (Cavouras et al., 1997) a decision tree was implemented in order to differentiate between normal and bad liver (first stage), steatosis and cirrhosis (second stage), respectively different degrees of steatosis and cirrhosis (last stage). The differentiation between normal and bad liver was made using features like GLCM mean and GLCM angular second moment, at the second stage the relevant features were autocorrelation, GLCM mean and GLCM variance, and at the last stage second order statistics like GLCM based variance, entropy, sum entropy and difference entropy were used. In order to perform classification at each stage, the Multilayer Perceptron (MLP) was used. In order to analyse the signal modifications induced by the diffuse liver diseases, transform-based methods were also used. The wavelet transform was applied in (Mojsilovic and Yeh, 2003), used a nonseparable quincunx wavelet transform with a 2-D diamond shaped filter in orderto zoom in the differences which exist between the different ultrasound images of the various diffuse liver diseases. The quincunx wavelet also had the role of eliminating the diagonal noise from the ultrasound liver images. The Hartley transform was also applied in (Paik and Fox, 1988), in order to differentiate between the diffuse liver diseases, but it is considered that the authors have not yet proved well enough its efficiency. The feature vector formed by features based on the spatial grey level dependence matrices, the Fourier spectrum, the grey level difference statistics and the Laws texture energy measures is considered not good enough in order to provide the expected speed and accuracy of the results. Other features, based on multiple resolution imagery and on the fractional

Brownian motion model are used instead. The fractal-based features proved 90% accuracy. Other texture-based methods used in order to characterizethe diffuse liver diseases in ultrasound images are the attenuation and backscattering coefficient, run-length matrices and RF signal parameters (Kadah,1996).

2.8 Previous studies:

Ulrich et al. (1985) aimed to investigate the diagnostic accuracy of computerized B- Scan texture analysis and conventional ultrasonography in diffuse parenchymal and malignant liver disease; In his study there were one hundred seventy - four consecutive patients with a broad spectrum of liver pathology and 20 healthy controls without any clinical, biochemical, and virological evidence or history of liver disease were examined. In 71 of these patients liver histology was evaluated in operative or biopsy specimen. Together with the 20 normals, these patients formed our data base which was used to develop a diagnostic classification for normal liver and diffuse parenchymal and malignant liver tissue changes. The patients with diffuse parenchymal disease were further subclassified into ultrasonic patterns prevalent in chronic active and persistent hepatitis, cirrhosis/fibrosis, fatty infiltration of the liver and combination of cirrhosis/fibrosis with fatty infiltration. For prospective computerized analysis, the " hold one out" method was employed. His study resulted that; Computerized B- scan image analysis had an overall prospective accuracy of 96%. Diffuse disease was classified with an accuracy of 98 % and malignant liver disease with 89 %, respectively. The sub classification accuracy for patients with diffuse parenchymal disease was 79 %, for the individual subgroup it ranged between 70% and 82%. He concluded that: The diagnostic classes, normal, diffuse parenchymal and malignant disease are clearly differentiated by

computerized images analysis which is superior to subjective evaluation of liver echograms. Computerized images also renders a reliable and clinically useful diagnostic sub classification of diffuse parenchymal disease into echopattern changes prevalent in chronic hepatitis, cirrhosis/fibrosis, fatty infiltration and a mixed state of cirrhosis/fibrosis with fatty infilteration which cannot be achieved by conventional liver ultrasound.

Alan, et.al (2010) were aimed to assess studies reporting the diagnostic performance of ultrasound imaging for identifying chronic liver disease (CLD) in a high risk population. In their study there were two authors independently used the quality assessment of diagnostic accuracy studies (QUADAS) checklist to assess the methodological quality of the selected studies. Inter-observer reliability of the QUADAS tool was assessed by measuring the degree of agreement (percent agreement, κ statistic) between the reviewers for each assessment prior to a consensus meeting. The characteristics of each study population, sensitivity and specificity results for the index tests, and results of any testing for observer agreement were extracted from the reports. Receiver Operator Characteristic plots were generated using Microsoft Excel 2003 software and used to graphically display the diagnostic performance data and to explore the relationships between the reported ultrasound techniques and study characteristics, and methodology quality. Their *Study resulted that:* Twenty-one studies published between 1991 and 2009 were retained for data extraction, analysis and assessment for methodological quality. Assessment of methodology quality was performed on the 21 selected studies by two independent reviewers (RA & KT) using the QUADAS assessment tool. Across all studies the mean number of responses within the QUADAS assessment tool was 10 (range 7-13) for "Yes", 1 (range 0-

3) for "No" and 3 (range 0-6) for "unclear". Inter-rater agreement for assessment of methodology quality was significantly greater than chance when assessing for representative spectrum, clear selection criteria, appropriate delay between reference and index tests, adequate descriptions of the index and reference tests, reference and index test blinding, and if relevant clinical information was provided. Seven studies reported moderate to high observer agreement for ultrasound techniques. Studies which clearly reported blinding performed better than the other studies for diagnostic accuracy, and lower diagnostic accuracy was evident for populations with lower prevalence of disease. Assessment of the liver surface using ultrasound consistently had moderate diagnostic accuracy across studies which demonstrated good research methodology. Other techniques demonstrated variable or poor to fair diagnostic accuracy. *Authors were concluded that:* Ultrasound of the liver surface is a useful diagnostic tool in patients at risk of CLD when assessing whether they should undergo a liver biopsy.

Marcia, et al (2011) aimed to evaluate the role of ultrasonography in the assessment of histopathological changes in patients with chronic hepatitis C, with emphasis on hepatic steatosis. In this study liver ultrasonography results were compared with histopathological findings of liver biopsy of 192 patients with chronic hepatitis C virus infection. All the US examinations followed a single protocol, analyzing the following aspects: echogenicity, echotexture and attenuation. The patients sample was divided into two groups as follows: patients with sonographic changes and patients with no sonographic changes. Sonographic findings of both groups were compared with histopathological findings after liver biopsy. This study showed that: Statistically significant intergroup differences were observed just regarding architectural changes grades 0 and 3 and

hepatic steatosis. Attenuation was the sonographic criterion that was best correlated with hepatic steatosis., with an intermediate rate of agreement with the diagnosis of hepatic steatosis. Considering the specificity of 77.9% and the negative predictive value of 95.5%, the authors highlight the capacity of the method to demonstrate the probability of absence of hepatic steatosis.

Needleman (1986) who investigated the sonography of diffuse benign liver disease: accuracy of pattern recognition and grading in which sonograms of 110 patients were compared to recently performed liver biopsies for evaluation of the accuracy of sonography in predicting the type (pattern) of pathology and its grade of severity (mild, moderate, or severe) in a wide variety of diffuse liver processes. There were two distinct, abnormal sonographic patterns: the fatty-fibrotic pattern seen primarily with cirrhosis, chronic hepatitis, and/or fatty infiltration, and the centrilobular pattern seen primarily with acute hepatitis. Study showed that, sonography was 88% accurate in assigning the correct pattern to the corresponding pathology (sensitivity 89%, specificity 86%, p less than 0.001). The degree of accuracy was dependent on the grade of pathologic severity, with mild disease offering the greatest difficulty; moderate and severe diseases were accurately detected and placed in the correct pattern in all cases. Sonographic grading of the severity of disease was far less precise (63% overall). This study concluded that sonography can distinguish between two abnormal sonographic patterns of diffuse benign liver disease as well as between normal and abnormal patterns.

A retrospective study on ultrasound findings in hepatitis. In which the ultrasound images of the liver in patients with hepatitis was undertaken. Two distinct ultrasound patterns were detected. In acute hepatitis, the predominant findings were accentuated brightness and more extensive

demonstration of the portal vein radicle walls and overall decreased echogenicity of the liver. Chronic hepatitis primarily revealed decreased brightness and number of portal vein radicle walls and overall increased liver echogenicity. In addition, the pathological severity closely paralleled these ultrasound patterns. This study confirmed the same acute hepatitis ultrasound findings with close correlation to the clinical severity. These distinct ultrasound patterns will help to evaluate patients with suspected acute and chronic hepatitis and more accurately define intrahepatic causes of jaundice. As stated by Kurtz AB, et.al (1980).

Delia in 2005 aimed to do accurate analysis and recognition of ultrasound liver images, in order to identify diffuse liver diseases like steatosis, cirrhosis and hepatitis. In order to do a proper tissue analysis from ultrasound images. Firstly they used that: The first and simplest methods to do texture-based analysis of the ultrasound images were those based on first order statistics. The grey level histograms and the grey level histogram width, GLHW – a measure denoting the difference between the highest and lowest grey level and also the number of the histogram bars were used.. In order to quantify the sonographic echogenicity. A histogram-based method for diffuse liver disease identification was used. The first order statistics were found not enough for a complete characterization of the properties of the liver tissue in order to differentiate between diffuse liver diseases. Second order statistics, based on the Gray Level Co occurence Matrix, were used Some second order statistics like the GLCM mean, GLCM variance, homogeneity, entropy, angular second moment, contrast, correlation formed the feature vector and a classification method like k nearest neighbour (k-nn), Support Vector Machine (SVM) or Artificial Neural Networks (ANN) was used. Their study using recognition method based on features like the mean

grey level values as a function of distance, the second order statistics of GLCM as a function of distance and on the k nearest neighbor method for classification, found the following recognition rates for the optimal value of k=9: 86% for normal liver. 90% for steatosis. 50% for cirrhosis. 85% for hepatitis. In conclusion*: elaborated a classification method based on the Grey Level Co-occurrence Matrix (GLCM) second order statistics and mean grey level in order to distinguish diffuse liver diseases in ultrasound liver images. The texture-based method has been proved to be suited for liver tissue characterization, in cases in which the corresponding changes cannot be noticed by the human eyes on echography. The computerized method replaces the previously used invasive methods, dangerous for the subjects.

Ricardo (2000) aimed to evaluate the Usefulness of Ultrasound in the Classification of Chronic Liver Disease. In his study there were 115 US liver images from 115 patients, including 26 normal livers (ωN), 26 chronic hepatitis without cirrhosis (ωCHC), 27 compensated cirrhosis (ωCC) and 36 decompensated cirrhosis (ωDC), were involved in the experiments. The patients were selected from the Gastroenterology Department of the Santa Maria Hospital, in Lisbon, with known diagnosis based on liver biopsy results. A ROI of 128×128 pixels along the medial axis was extracted from each image. No acquisition protocol was used due to the use of the pre-processing algorithm. A semi-automatic procedure to stage this disease is proposed based on ultrasound liver images, clinical and laboratorial data. In the core of the algorithm two classifiers are used: a k nearest neighbor and a Support Vector Machine, with different kernels. The classifiers were trained with the proposed multi-modal feature set and the results obtained were compared with the laboratorial and clinical feature set. His results showed that using ultrasound based

features, in association with laboratorial and clinical features, improve the classification accuracy. The support vector machine, polynomial kernel, outperformed the others classifiers in every class studied. For the Normal class they achieved 100% accuracy, for the chronic hepatitis with cirrhosis 73.08%, for compensated cirrhosis 59.26% and for decompensated cirrhosis 91.67%. He concluded that: The proposed multifeature and multiclassifier system, based on a pre-processing US image decomposition proved to be a useful approach to the CLD classification problem. The results presented in this study show that it is possible to identify the different stages of CLD based on US liver images, particularly textural and contour parameters, laboratorial and clinical features. The group with the most severe stage, ωDC, is well identifiable, while patients in lower stages, ωCHC and ωCC, need further analysis.

Vishakha 2015 aimed to classify Liver Disease Based on US Images. In which, an automatic hierarchical procedure to classify and stage liver disease using ultrasound images is described. The database for this work is the ultra sonographic images of liver disease along with the healthy conditions. Initially the contrast enhancement is applied to the input image that helps to identify the object, after that discrete wavelet transform is applied which helps to remove the speckle noise, then the approximate component is subjected to K-mean clustering which segments the image with respect to the minimum Euclidian distance. The classification strategy is performed using the classifier such as Neural Network. This study concluded that Neural Network was a useful diagnosis tool which may reduce, but does not replace, liver biopsy and it is useful for the doctors for the second opinion.

Chapter Three
Materials and Methods

3.1 Materials:

- An ultrasound machines of facilities as shown in the following table:

U/S machine name	Honda	Alpinion	General Electric
Model	HS 2000	E- CUPE 7	LOGIQ **5**
Movement	Portable	Mobile	Mobile
Type of probe	Curvilinear	- Curvilinear	- Curvilinear
Energy of probe	3.5 MHz	- 3.5 MHz	- 3.5 MHz

- *All these machines have Printer with thermal paper.*
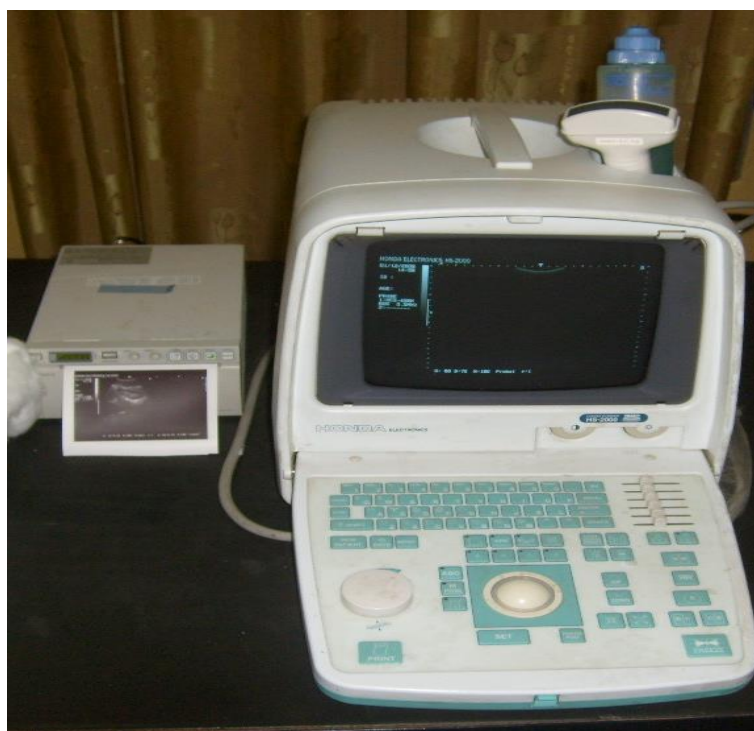
Figure (3.1). Shows Honda 2000 Machine which used in this study

Figure (3.2). Shows General electric LOGIQ 5 which used in this study

Figure (3.3). Shows E-CUPE 7 which used in this study.

- **Sony printer with thermal paper.**
- **Computer for data analysis.**

3.2 Design of the study:

This study is analytic study used liver ultrasound images for normal patient as control and patients with liver cirrhosis, Hepatitis type B and C for classification texturally and characterization ultrasonographically.

3.3 Population of the study:

The population of this study was patient with normal free from any liver lesion for control groups as well as patient with liver cirrhosis, Hepatitis

type B and C all acquired with the same machine and similar overall gain. Patients associated with other liver complications were excluded.

3.4 Sample size and type:

This study consisted of 200 patients 60 patients have normal liver, 60 have hepatitis B, 60 have cirrhosis and 20 patients have hepatitis C. All patients under study having ultrasonography images showing the disease or normal area in the center of the image at focal zone, the sample selected conveniently.

3.5 Place and duration of the study:

This study was carried out in the period from September 2013 to May 2016 in Khartoum state at College of Radiologic Sciences (Sudan university for science and Technology), Ribat Teaching hospital and Ibn Sina teaching hospital.

3.6 Methods of data collection:

Using a special data collection sheet (questionnaire), sample of 200 patient with normal free from any lesion for control groups as well as patient with liver cirrhosis, Hepatitis type B and C were studied by trans abdominal ultrasound scanning and data was collected using a data collecting sheet which designed to evaluate liver anatomy, size, texture, shape, surface characteristics (outlines and left upper border), right and caudate lobe sizes, portal hypertenstion, presence of ascites and spleenomegally**.**

3.7 Technique*: (Imaging protocols)*
3.7.1 Trans abdominal U/S scanning:
Patient Preparations:

The bladder must be full enough, gives patient 4 to 5 glasses of fluid and examined after one hour. Do not allow the patient to micturate,

Alternatively fill the bladder through a urethral catheter with sterile normal saline, Stop when patient feels uncomfortable.

Position of the patient:

The patient should lie supine but may need to be rotated obliquely. The patient should be relaxed, lying comfortably and breathing quietly, lubricates the lower abdomen with coupling agent. Hair any where on the abdomen will trap air bubbles so apply coupling agent generously. [49]

Choice of transducer:

Uses a curve linear probe of 3.5 MHZ frequency.

Scanning technique:

Start with a longitudinal scans from the Xiphoid process and we must be angle the probe sharply to the right for setting the gain, move the probe to the right until the right lateral border of the liver appears clearly in the center of the screen. Then move the probe to the left until the left lateral border of the liver appears clearly in the center of the screen, return to the right until the right lateral border of the liver appears clearly in the center of the screen. Adjusted the gain of the image and freeze it, I measured the liver span by putting the probe saggital , subcostal and in midclavicular line. Any area appears abnormal must be viewed in several projections then rock slide and saving the image. After that I do a transverse scanning tomeasured the right and caudate lobes transversely. During scan researcher evaluate the liver shape, if it is normal or abnormal; also evaluate the liver texture, portal vein size, left edge of the liver, presence of ascites and finally measured spleen size. Then saving the image.

Finally complete the abdomen pelvic examination by the scanning remainder abdominal organs mainly gall bladder to detect any associated pathologies.

Ultrasonographic sonograms took place and information of the patient was collected using special data collecting sheet and stored within USB.

3.7.2 Methods of analysis:

Discriminant analysis:

Discriminant analysis provides a basis for classifying not only the sample used to compute the discriminant function, but also any other observations that can have value for all the variables by generating a ***classification function***. In this way, discriminant analysis can be used to classify other variables into defined classes. The number of classification functions is equal to the number of classes. Each function allows the computation of a classification score for each variable by applying an equation, which takes the following form:

$$S_i = a_i + \sum_{j=1}^{n} W_{ij} \times V_j$$

where S_i is the resultant classification score for the ith class,

$i = 1, 2, 3...K$ with K being the numbers of classes,

a_i is a constant for the ith class,

$W_{i,j}$ is a weight function for the jth variable for the ith class,

$j = 1, 2, 3..n$ with n being the number of variables.

V_j denotes the value of the jth variable.

Thus, a classification is achieved by multiplying each variable for an individual case by its corresponding weight in the different classes and adding these products together in each class. This process results in a single classification score for each class. Once the classification score is computed, the case is thus classified as belonging to the class in which it has achieved the highest score, and the process is continued in the same fashion for the rest of the variables.

Interactive Data Language:

After that ultrasound images were stored in computer disk were uploaded into the computer based software Interactive Data Language (IDL) the user clicks on an areas represents the background, normal liver parenchyma (for normal), then for disease patients on liver cirrhosis region, Hepatitis type B and C; in these areas These textural features include mean, variance, Skewness, Kurtosis, energy and entropy. A window of 3×3 pixel was generated and first order textural feature for the classes were generated. After extraction of the textural features from all images; data concerning the liver tissues (normal liver, liver cirrhosis, Hepatitis type B and C) entered into SPSS with its classes to generate a classification score using stepwise linear discriminate analysis; to select the most discriminate features that can be used in the classification of liver tissues in ultrasound images. Where scatter plot using discriminate function were generated as well as classification accuracy and linear discriminate function equations to classify the liver tissues into the previous classes without segmentation process for unseen images in routine work.

3.8 Ethical approval:

The ethical approval was granted from the hospital and the radiology department; which include commitment of no disclose of any information concerning the patient identification.

Chapter Four

Results

The crosstabulation table is the basic technique for examining the relationship between two categorical (nominal or ordinal) variables, possibly controlling for additional layering variables.

The crosstabulation shows the frequency of each response at each store location. Therefore the crosstabulation tables were formulated to show the relationship between the following variables according to their condition: liver anatomy, size, texture, shape, surface characteristics (outlines and left upper border), right and caudate lobe sizes, portal hypertenstion, presence of ascites and spleenomegally.

Table4.1 Shows marital status distribution.

MS	Frequency	Percent
Single	51	25.5%
Married	149	74.5%
Total	200	100.0%

There were 149 patients (74.5%) out of 200 cases under study were married and 51 (25.5 %) were singles.
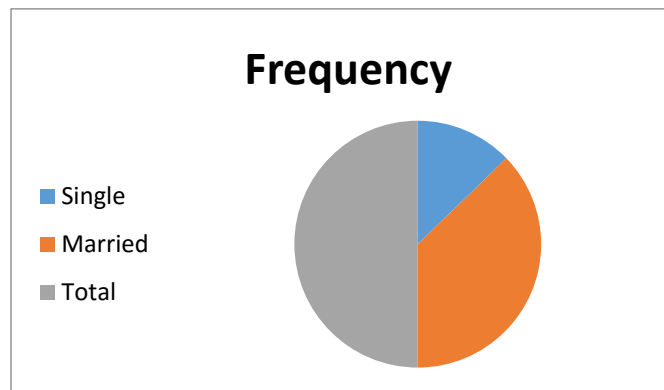
Figure 4.1 Shows marital status distribution.

Table 4.2 Types of diseases distribution.

Disease	Frequency	Percent
Normal	60	30.0%
Liver cirrhosis	60	30.0%
Hepatitis B	60	30.0%
Hepatitis C	20	10.0%
Total	200	100.0%

There were 60 (30%) cases out of 200 cases under study have normal liver, 60 (30%) patients have liver cirrhosis, 60 (30%) patients have hepatitis B and 20(10%) patients have hepatitis C.

Figure 4.2 .Shows diseases distribution
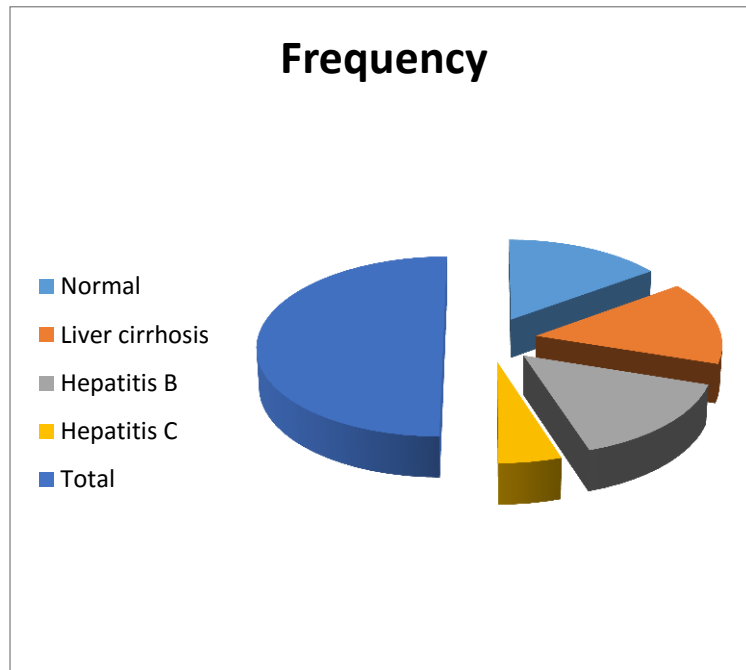
Table 4.3 Crosstabulation of liver disease with vomiting.

Disease	Vomiting		Total
	not found	found	
Normal	60	0	60
Liver cirrhosis	22	38	60
Hepatitis B	28	32	60
Hepatitis C	19	1	20
Total	129	71	200

All normal cases and 19 patients out of 20 patients with hepatitis C have not vomiting, while other one patient has vomiting, 38 cases out of 60 patients with liver cirrhosis have vomiting and 32 patients out of 60 cases with hepatitis have vomiting.
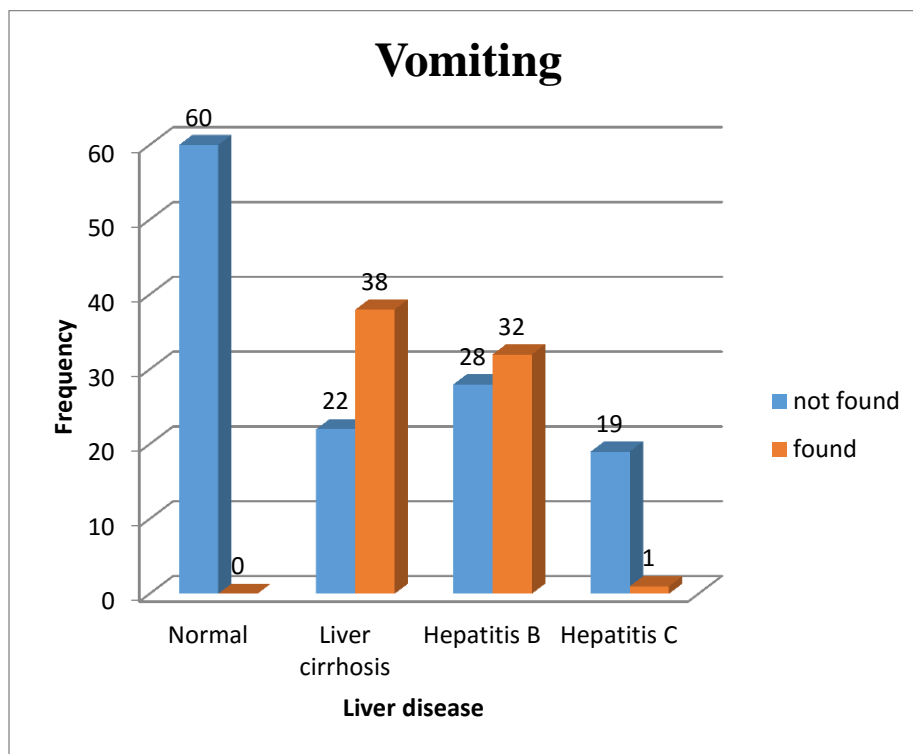
Figure 4.3. bar graph shows the cases distribution of liver in case of normal, cirrhosis and hepatitis with vomiting.

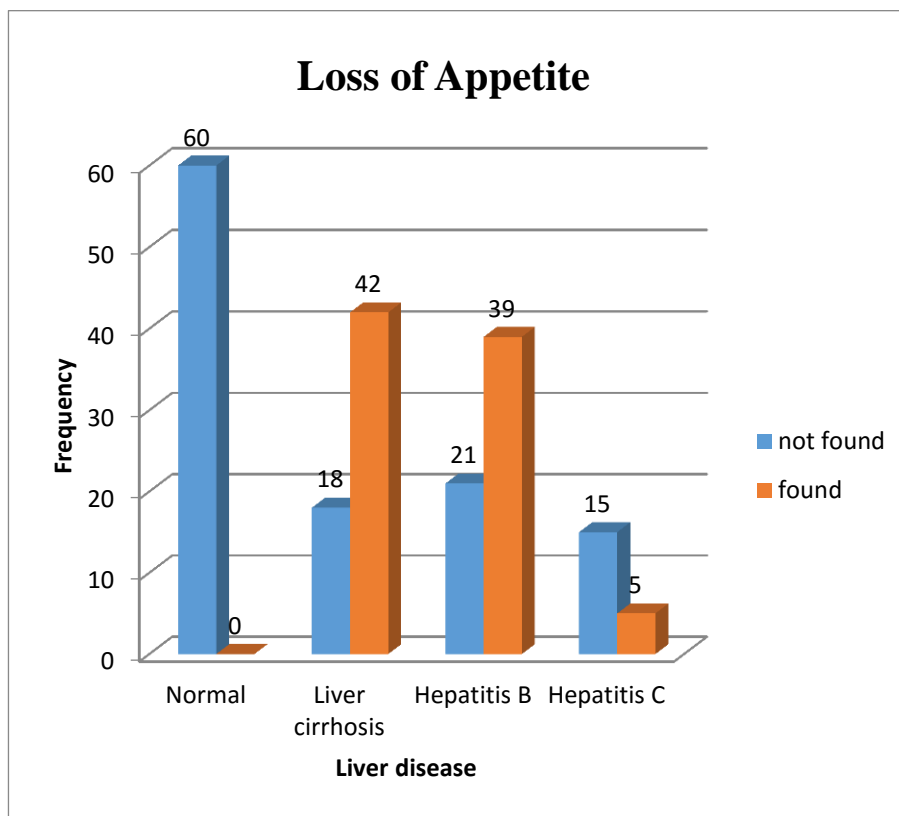**Table 4.4 Crosstabulation of liver disease with loss of appetite.**

Disease	Loss of Appetite		Total
	not found	found	
Normal	60	0	60
Liver cirrhosis	18	42	60
Hepatitis B	21	39	60
Hepatitis C	15	5	20
Total	114	86	200

All normal cases and 15 patients out of 20 cases with hepatitis C have not loss of appetite, while other 5 patients have loss of appetite, 42 cases out of 60 patients with liver cirrhosis have loss of appetite and 39 patients out of 60 cases with hepatitis have loss of appetite.
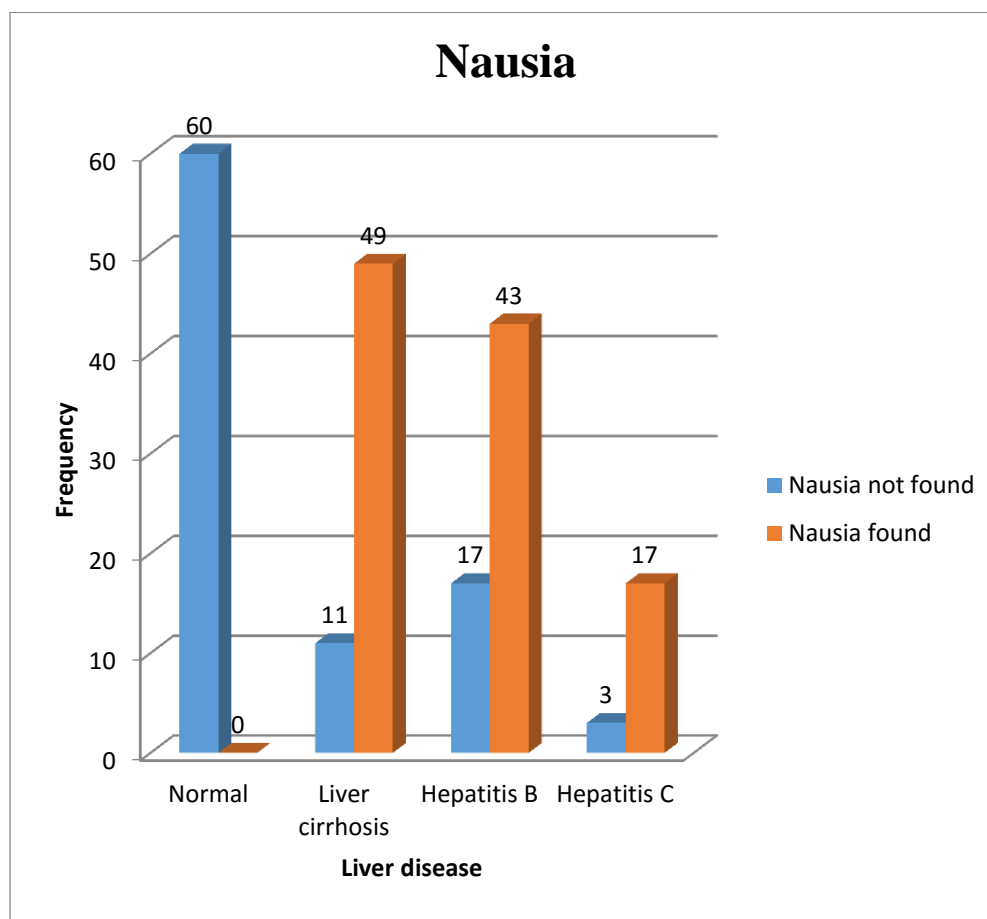

Figure 4.4. bar graph shows the cases distribution of liver in case of normal, cirrhosis and hepatitis with loss of Appetite.

Table 4.5 Crosstabulation of liver disease with nausea.

Disease	Nausea		Total
	Not found	Found	
Normal	60	0	60
Liver cirrhosis	11	49	60
Hepatitis B	17	43	60
Hepatitis C	3	57	20
Total	91	109	200

All normal cases and 3 patients out of 20 patients with hepatitis C have not nausea, while other 17 patients have nausea, 49cases out of 60 patients with liver cirrhosis have nausea and 43 patients out of 60 cases with hepatitis have nausea.

Figure 4.5. bar graph shows the cases distribution of liver in case of normal, cirrhosis and hepatitis with nausea.

Table 4.6 Crosstabulation of liver disease with loss weight.

Disease	Loss_of_Weight		Total
	not found	found	
Normal	60	0	60
Liver cirrhosis	8	52	60
Hepatitis B	18	42	60
Hepatitis C	20	0	20
Total	106	94	200

All normal cases and patients with hepatitis C have not loss of weight, 52 cases out of 60 patients with liver cirrhosis have loss of weight and 42 patients out of 60 cases with hepatitis have loss of weight.
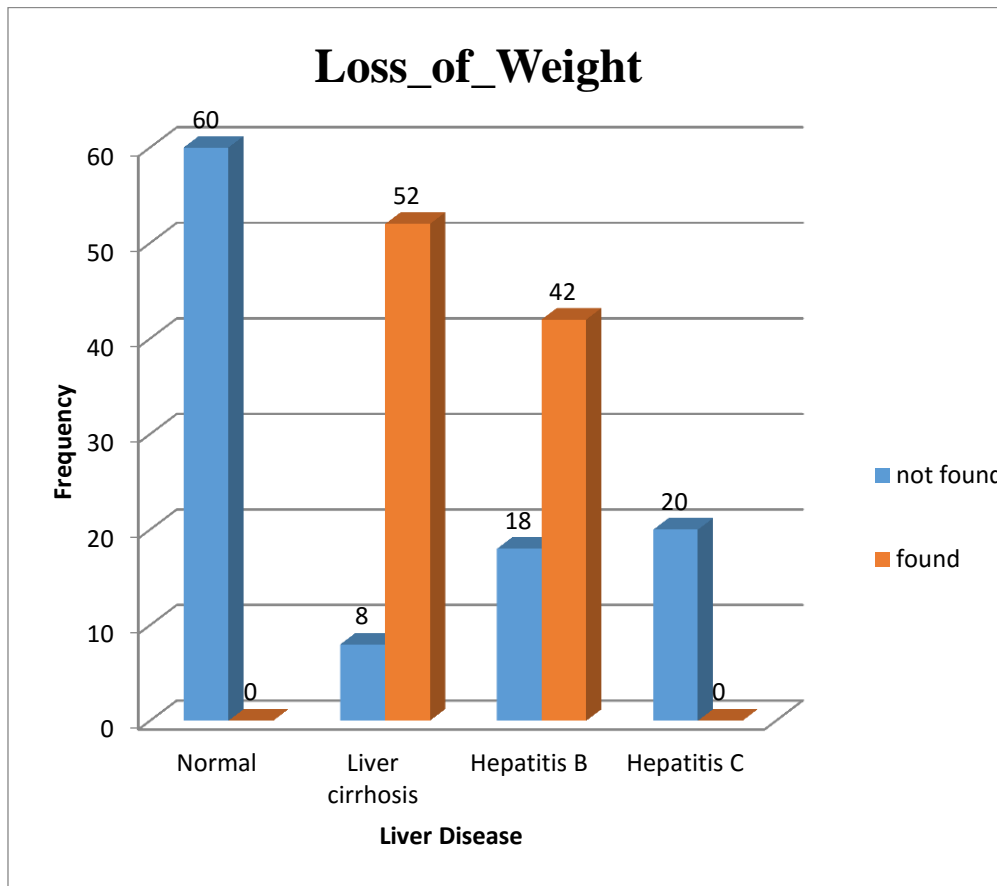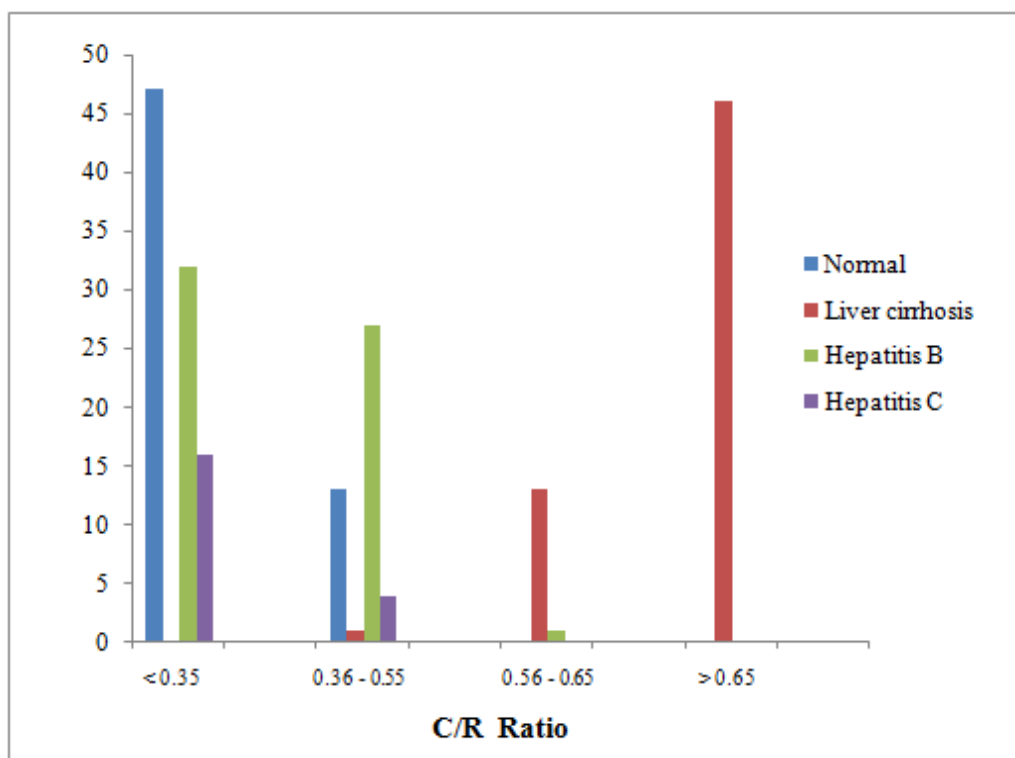

Figure 4.6. bar graph shows the cases distribution of liver in case of normal, cirrhosis and hepatitis with loss of weight.

Table 4.7 . Crosstabulation of liver disease with C/R lobe ratio.

Disease	C/R lobe Ratio				Total
	>0.35	0.36 - 0.55	0.55-0.64	<0 .65	
Normal	47	13	0	0	60
Liver cirrhosis	0	1	13	46	60
Hepatitis B	32	27	1	0	60
Hepatitis C	16	4	0	0	20
Total	95	45	14	46	200

There were 47 cases out of 60 normal patients have C/R R >0.35, 32 cases out of 60 patients with hepatitis B have C/R R >0.35, 16 cases out of 20 patients with hepatitis C have C/R R >0.35, but no any cirrhotic case had C/R R >0.35. Also there were 46 cases out of 60 cirrhotic patients have C/R R <0 .65, while there was no any case from other liver classes had C/R R <0 .65.
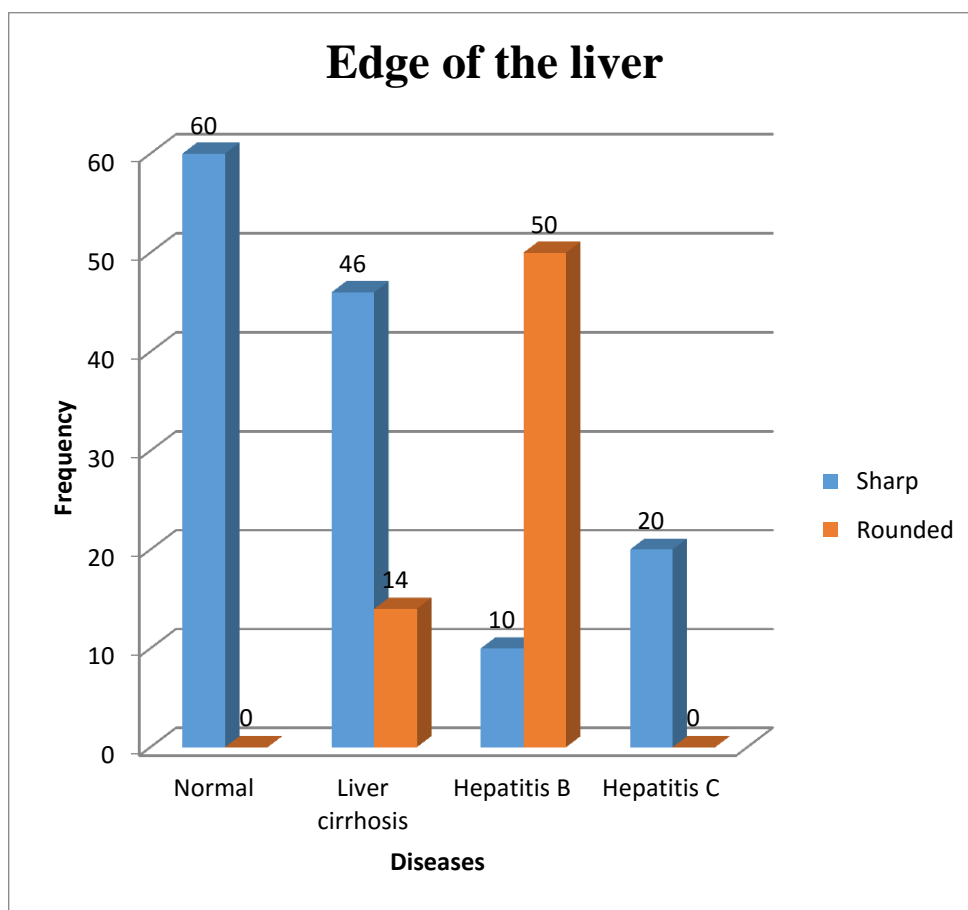

Figure 4. 7. bar graph shows the distribution of C/R lobe ratio in case of normal, cirrhosis and hepatitis.

Table 4.8. Crosstabulation of liver disease with left edge of liver.

Disease	Edge_of_Left lobe		Total
	Sharp	Rounded	
Normal	60	0	60
Liver cirrhosis	56	4	60
Hepatitis B	10	50	60
Hepatitis C	20	0	20
Total	146	54	200

All normal cases and patients with hepatitis C have sharp upper left liver edge, while there were 4 patients out of 60 patients have cirrhosis have pounded upper left edge and 50 patients out of 60 cases with hepatitis B have pounded upper left liver edge and other cases have sharp upper left liver edge.
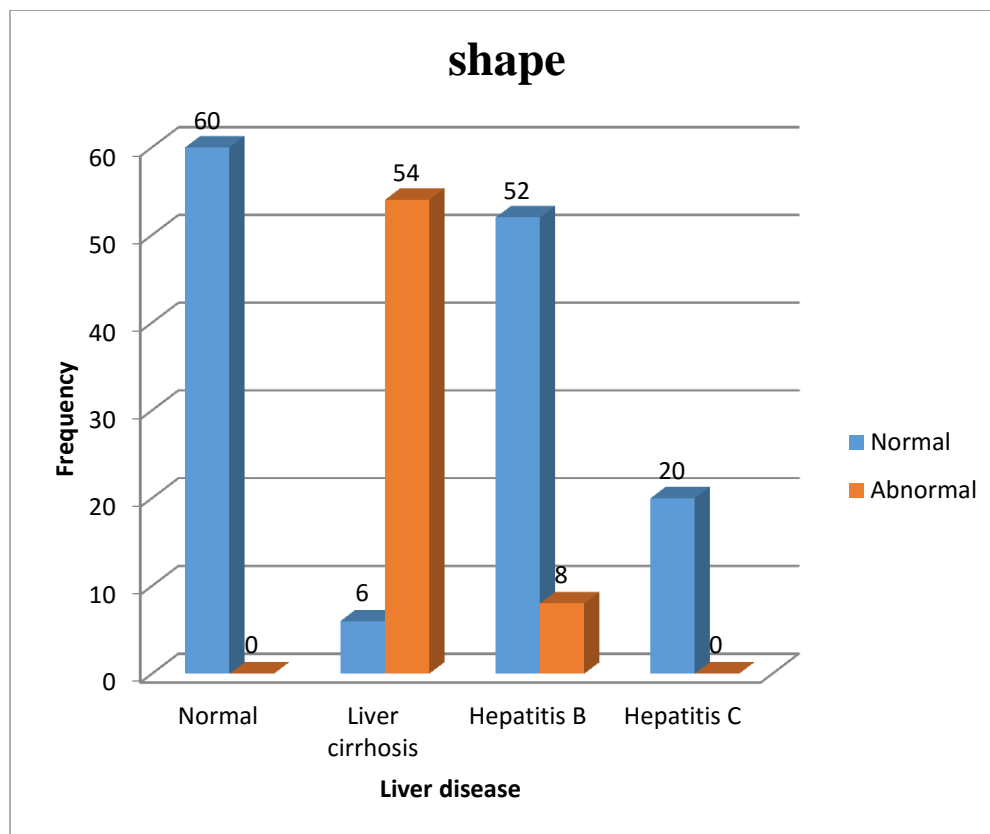

Figure 4. 8. bar graph shows the distribution of liver edge status in case of normal, cirrhosis and hepatitis.

Table 4.9 Crosstabulation of liver disease with liver shape.

Disease		shape		Total
		Normal	Abnormal	
	Normal	60	0	60
	Liver cirrhosis	6	54	60
	Hepatitis B	52	8	60
	Hepatitis C	20	0	20
	Total	142	58	200

All normal cases and cases with hepatitis C under study have normal liver shape but there were 54 patients out of 60 cases with liver cirrhosis have abnormal liver shape, while other 6 patients have normal liver shape and there were 8 patients out of 60 cases with hepatitis B have abnormal liver shape while other 52 patients have normal liver shape.
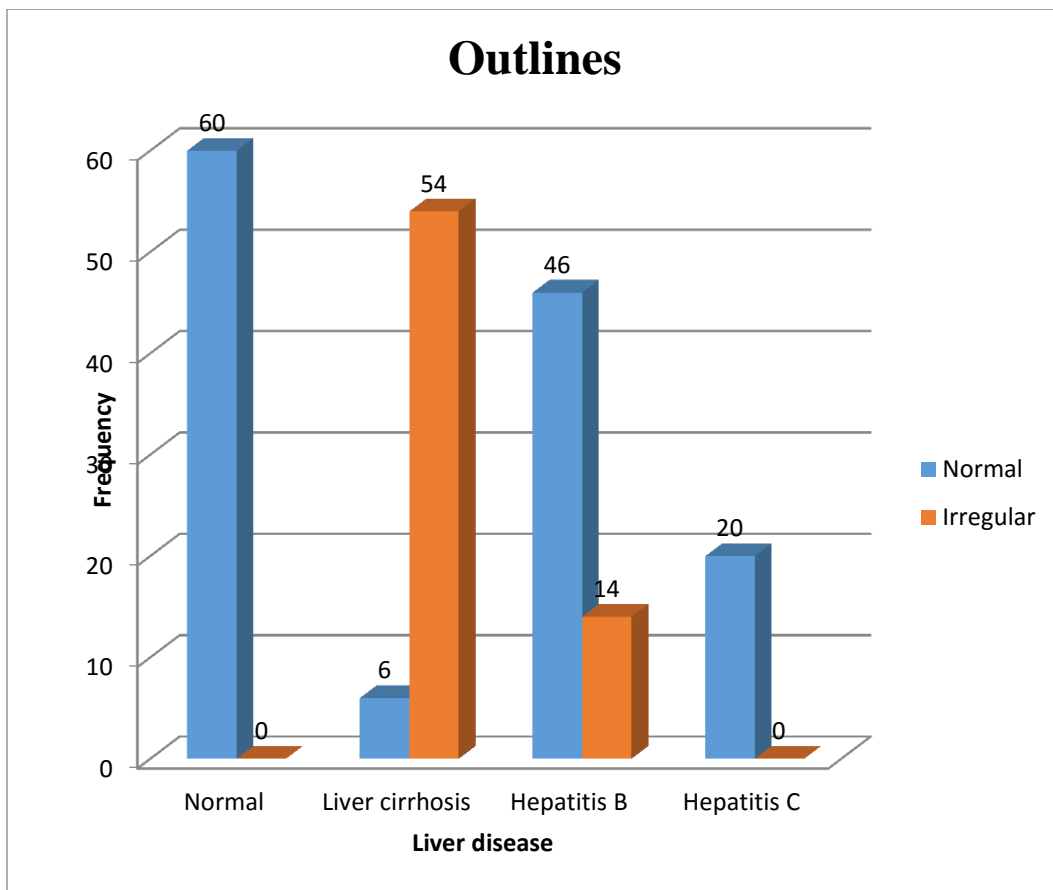

Figure 4.9. Bar graph shows the percentage distribution of liver shape in case of normal, cirrhosis and hepatitis.

Table 4.10 Crosstabulation of liver disease with liver outlines.

Disease	outlines		Total
	Normal	Irregular	
Normal	60	0	60
Liver cirrhosis	6	54	60
Hepatitis B	46	14	60
Hepatitis C	20	0	20
Total	132	68	200

All normal cases and cases with hepatitis C under study have normal liver out lines, but there were 54 patients out of 60 cases with liver cirrhosis have irregular liver outlines, while other 6 patients have regular liver outlines and there were 14 patients out of 60 cases with hepatitis B have irregular liver outlines while other 46 patients have normal liver outlines.
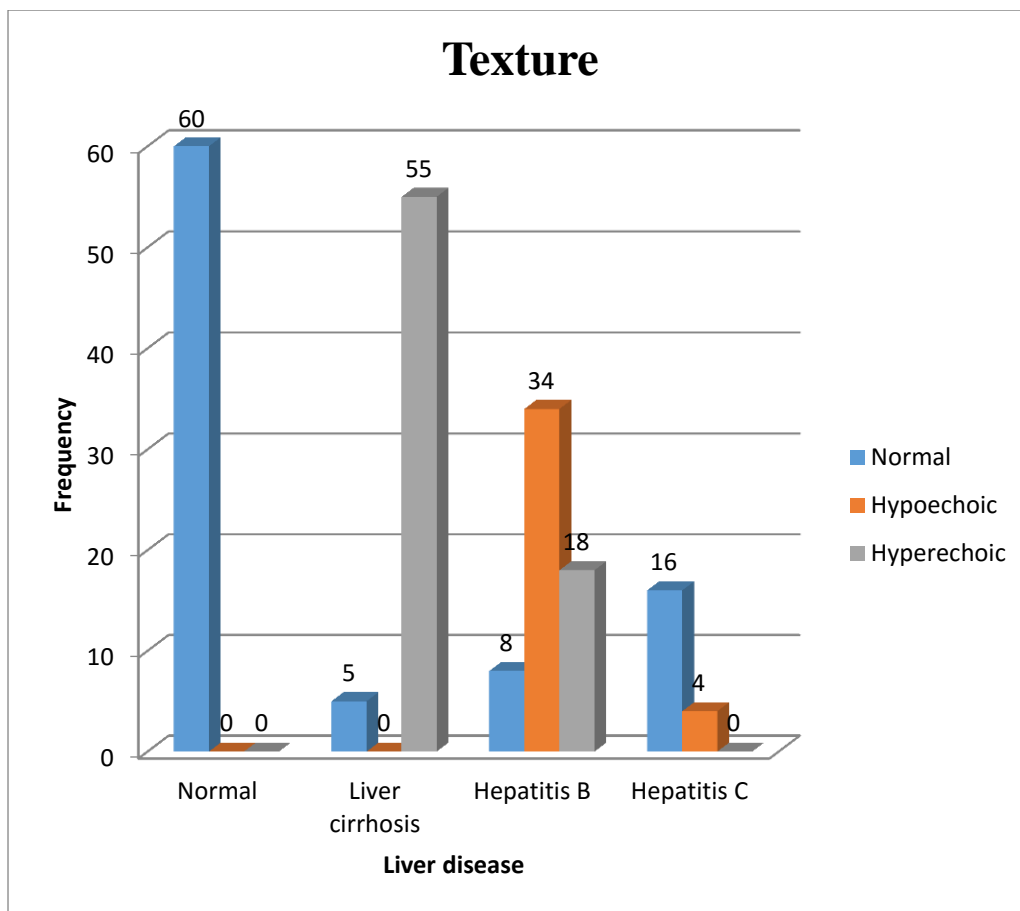

Figure 4.10. Bar graph shows the percentage distribution of liver outline status in case of normal, cirrhosis and hepatitis.

Table 4.11. Crosstabulation of liver disease with liver texture.

Disease	Texture			Total
	Normal	Hypoechoic	Hyperechoic	
Normal	60	0	0	60
Liver cirrhosis	5	0	55	60
Hepatitis B	8	34	18	60
Hepatitis C	16	4	0	20
Total	89	38	73	200

All normal cases and 16 patients with hepatitis C under study have normal liver texture and other four patients of them have hypo echoic texture. There were 5 patients out of 60 cases with liver cirrhosis have normal liver texture, while other 55 patients have hyper echoic liver texture, there were 16 patients out of 60 cases with hepatitis B have normal liver texture, 18 patients have hypo echoic liver texture, while other 18 patients have hyper echoic liver texture.

Figure 4.11. bar graph shows the percentage distribution of liver echo texture in case of normal, cirrhosis and hepatitis.

Table 4.12. Crosstabulation of liver disease with nodular liver Texture.

Disease	Nodular_texture		Total
	No	Yes	
Normal	60	0	60
Liver cirrhosis	5	55	60
Hepatitis B	60	0	60
Hepatitis C	20	0	20
Total	145	55	200

There were 55 patients out of 60 cases with liver cirrhosis have nodular liver texture, while other all 145 cases under study have not nodular liver texture.
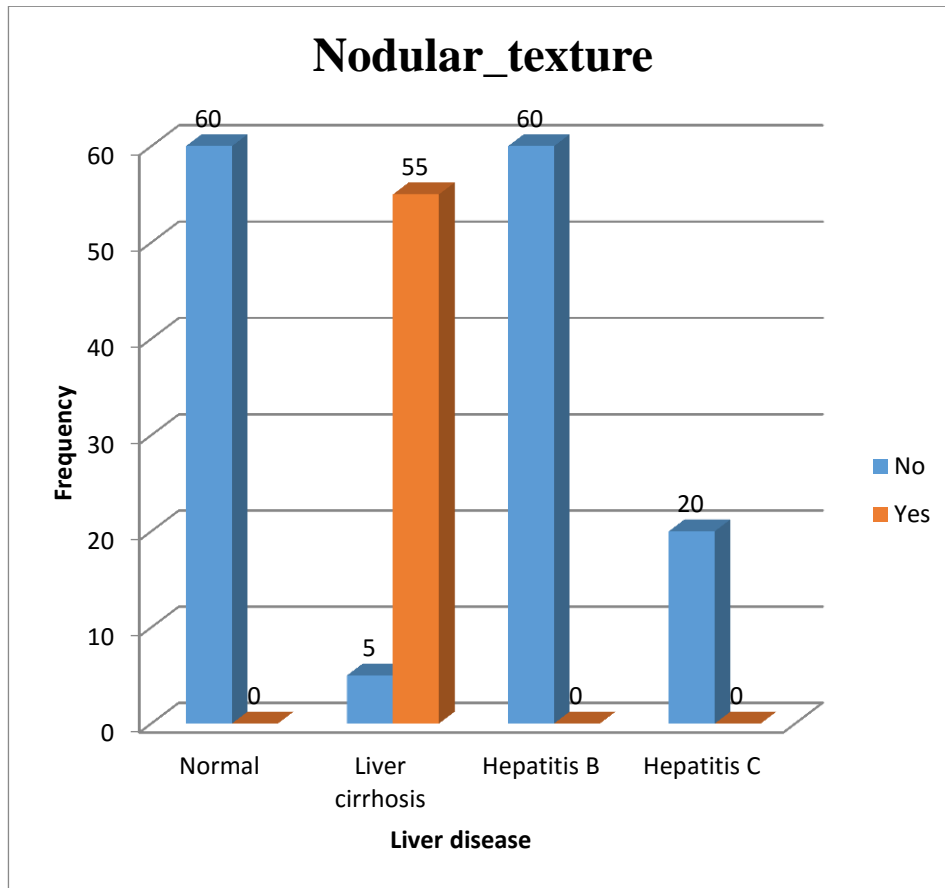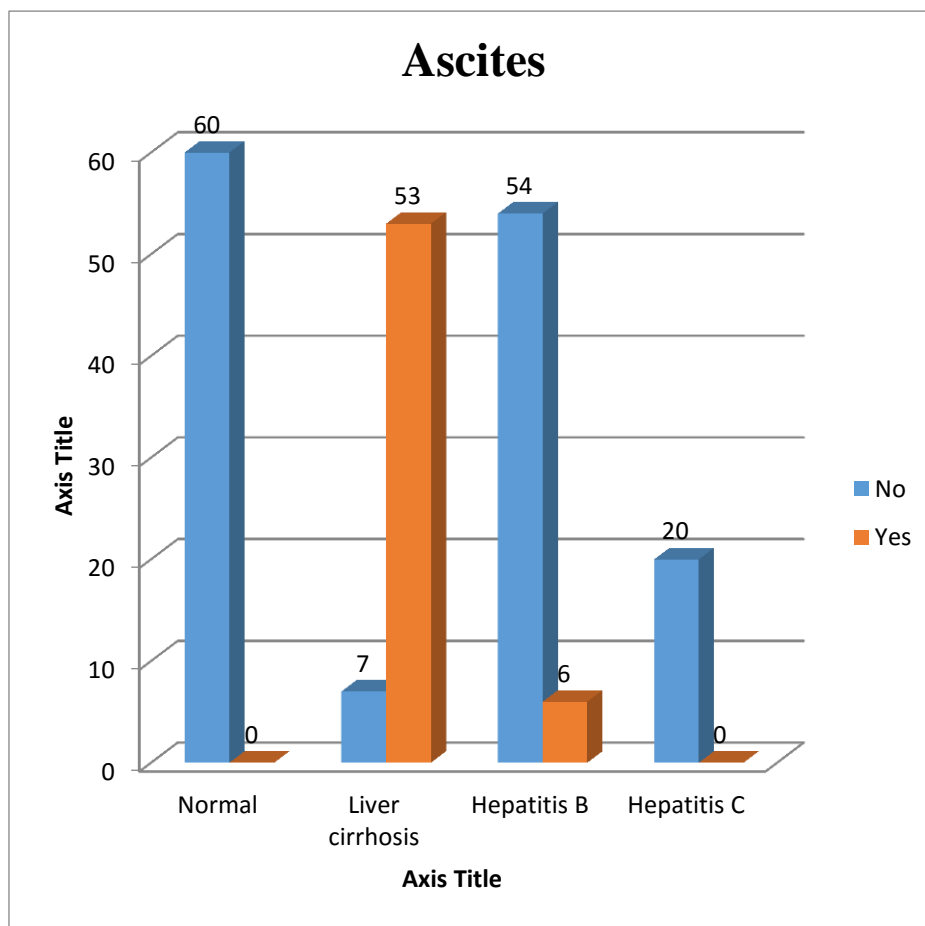

Figure 4.12. bar graph shows the percentage distribution of liver nodular echo texture in case of normal, cirrhosis and hepatitis.

Table 4.13. Crosstabulation of liver disease with presence of ascites

Disease		Precense_of_ascites		Total
		No	Yes	
	Normal	60	0	60
	Liver cirrhosis	7	53	60
	Hepatitis B	54	6	60
	Hepatitis C	20	0	20
Total		141	59	200

All normal cases and cases with hepatitis C under study have not ascites, but there were 53 patients out of 60 cases with liver cirrhosis have ascites, while other 7 patients have not ascites and there were 6 patients out of 60 cases with hepatitis B have ascites while other 54 patients have not ascites.
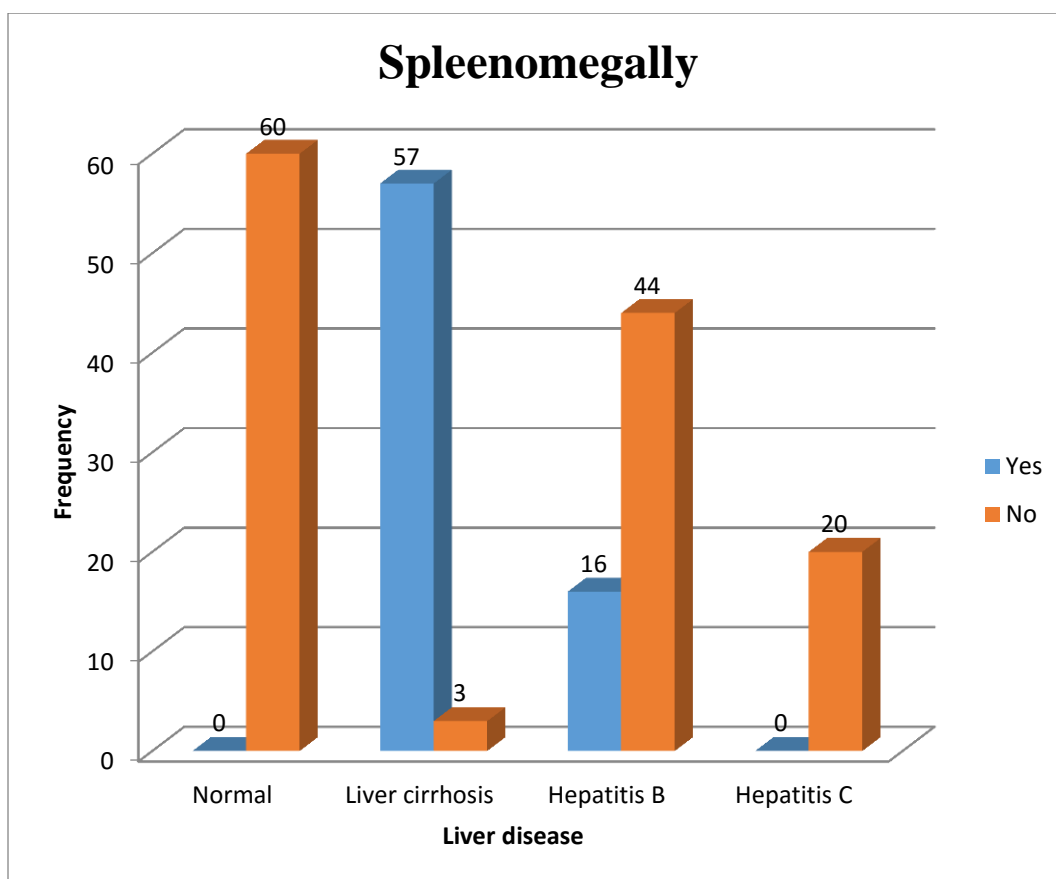

Figure 4.13. bar graph shows the percentage distribution of liver ascites status in case of normal, cirrhosis and hepatitis.

Table 4.14. Crosstabulation of liver disease with spleenomegally

Disease	Spleenomegally		Total
	Yes	No	
Normal	0	60	60
Liver cirrhosis	57	3	60
Hepatitis B	16	44	60
Hepatitis C	0	20	20
Total	73	127	200

All normal cases and cases with hepatitis C under study have normal spleenomegally, but there were 57 patients out of 60 cases with liver cirrhosis have spleenomegally, while other 3patients have normal spleen and there were 16 patients out of 60 cases with hepatitis B have spleenomegally while other 44 patients have normal spleen.

Figure 4.14. bar graph shows the percentage distribution of splenomegaly status in case of normal, cirrhosis and hepatitis.

Table 4.15 ANOVA

		Sum of Squares	F	Sig.
Age	Between Groups	18358.372	43.773	.000
	Within Groups	27400.983		
	Total	45759.355		
RT_lobe_Size	Between Groups	115.138	44.586	.000
	Within Groups	168.717		
	Total	283.855		
Caudate Size	Between Groups	105.013	102.913	.000
	Within Groups	66.667		
	Total	171.680		
Ratio	Between Groups	3.420	345.047	.000
	Within Groups	.648		
	Total	4.068		
Liver span	Between Groups	414.220	94.597	.000
	Within Groups	286.079		
	Total	700.299		
PVD	Between Groups	615.905	81.021	.000
	Within Groups	496.650		
	Total	1112.555		
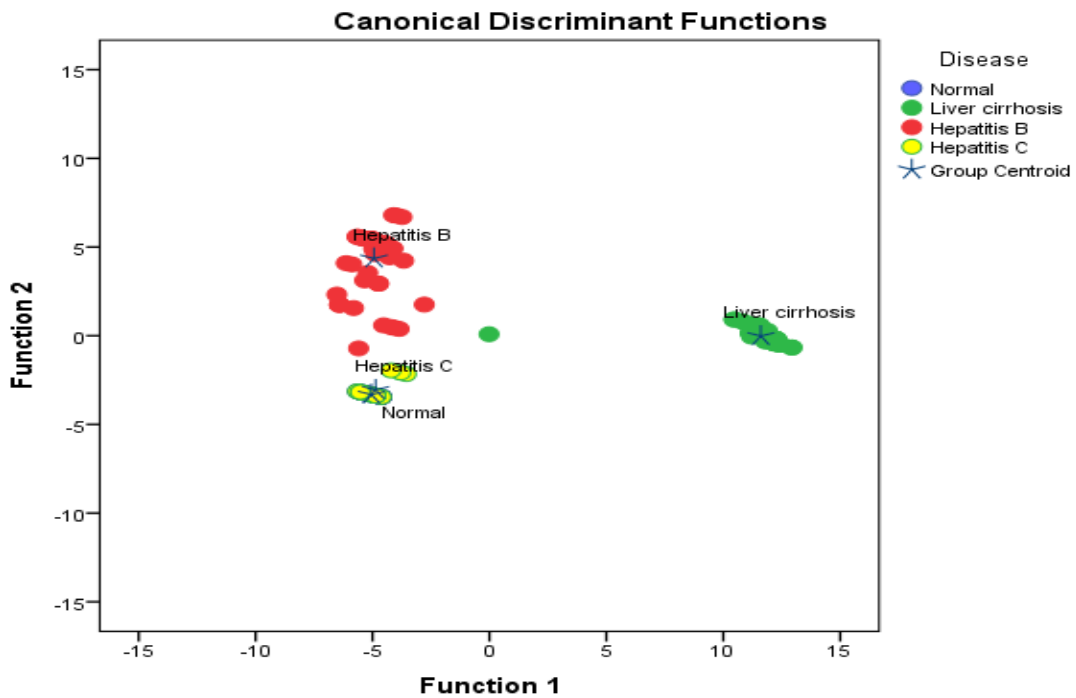
Figure 4.15 Scatter plot show the classification liver classes ((normal, hepatais B, hepatitis C and cirrhotic liver) using linear discriminant analysis

Table 4.16 a confusion matrix shows the classification score using linear discriminant analysis and ultrasound features as input variable
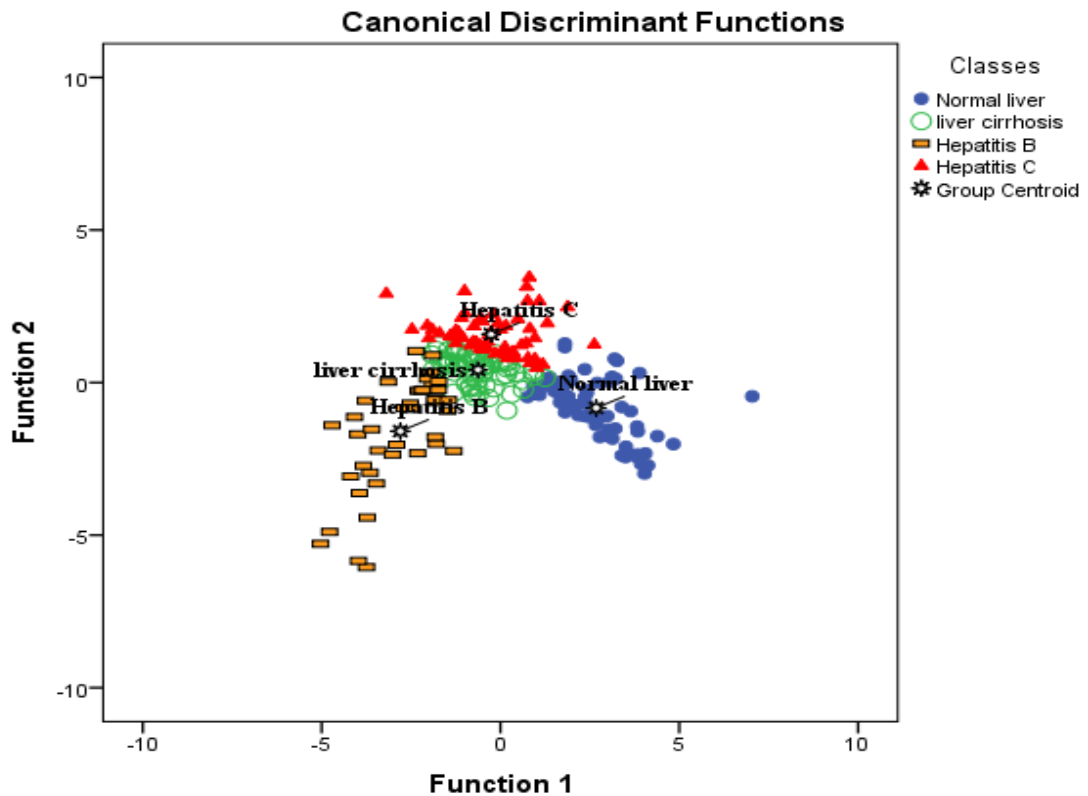
Original	Predicted Group Membership				Total
	Normal	Liver cirrhosis	Hepatitis B	Hepatitis C	
Normal	83.3	0	0	16.7	100%
Liver cirrhosis	0	98.3	0	1.7	100%
Hepatitis B	0	0	91.7	8.3	100%
Hepatitis C	55	0	0	45	100%
86.5% of original grouped cases correctly classified.					

Table 4.17. Calcification function used to classify the liver as classes ((normal, hepatitis B, hepatitis C and cirrhotic liver) using linear discriminant.

| **Classification Function Coefficients**				
	Disease			
	Normal	Liver cirrhos	Hepatitis B	Hepatitis C
Edge_of_L	-9.377	-18.892	-3.780	-10.038
Outlines	397.987	596.161	396.891	398.096
Texture	14.822	33.298	26.625	16.467
N_texture	475.862	720.100	496.143	479.175
Ratio	134.139	223.186	121.193	131.265
P_of_asc	46.246	47.656	83.459	46.633
Spleenomegally	24.295	.262	14.136	23.532
(Constant)	-513.245	-1091.112	-590.994	-515.622
Fisher's linear discriminant functions				

Figure 4.16. Scatter plot show the classification liver classes ((normal, hepatais B, hepatitis C and cirrhotic liver) using linear discriminant analysis

Table 4.18

| Classes		Predicted Group Membership				Total
		Normal liver	liver cirrhosis	Hepatitis B	Hepatitis C	
Original groups	Normal liver	**92.5**	4.5	0.0	3.0	100.0
	liver cirrhosis	0.0	**97.1**	0.0	2.9	100.0
	Hepatitis B	0.0	30.2	**69.8**	0.0	100.0
	Hepatitis C	1.7	25.0	0.0	**73.3**	100.0

84.9% of original grouped cases correctly classified
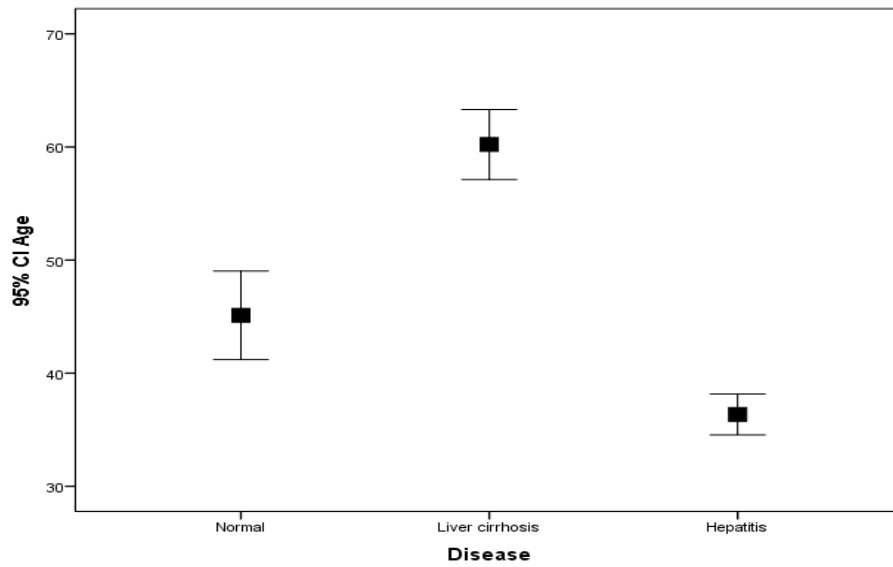
Figure 4.17 (A) An error bar graphs of the patient's age for the different classes of liver (normal, hepatitis B, hepatitis C and cirrhotic liver).
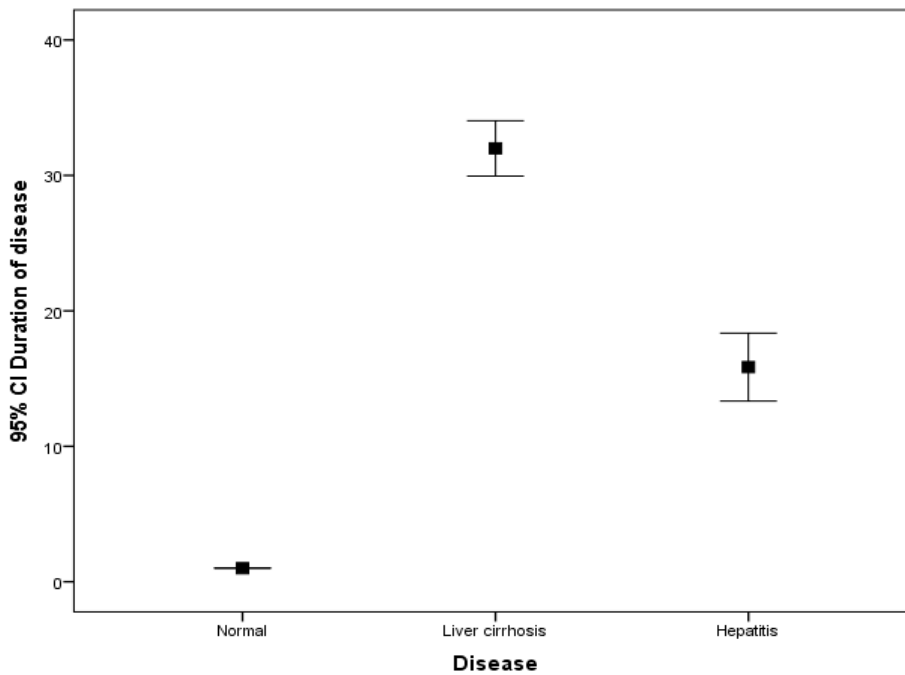
Figure 4.17(B). An error bar graphs of the duration of disease for the different classes of liver (normal, hepatitis B, hepatitis C and cirrhotic liver).
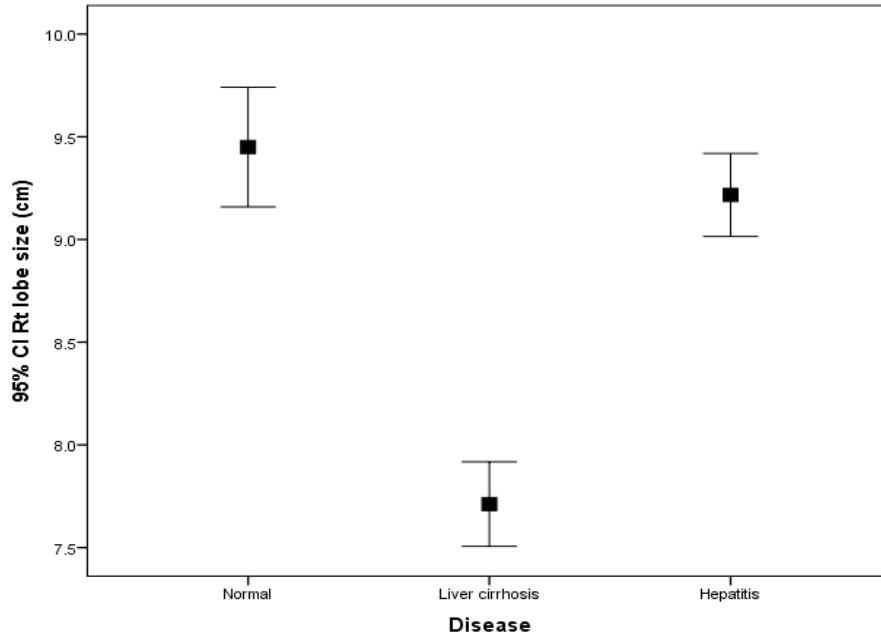
Figure 4.17(C) An error bar graphs of the right lobe size for the different classes of liver (normal, hepatitis B, hepatitis C and cirrhotic liver).

Figure 4.17(D) An error bar graphs of the caudate right lobe ratio for the different classes of liver (normal, hepatais B, hepatitis C and cirrhotic liver).

Figure 4.17(E) An error bar graphs of the liver span for the different classes of liver (normal, hepatitis B, hepatitis C and cirrhotic liver).
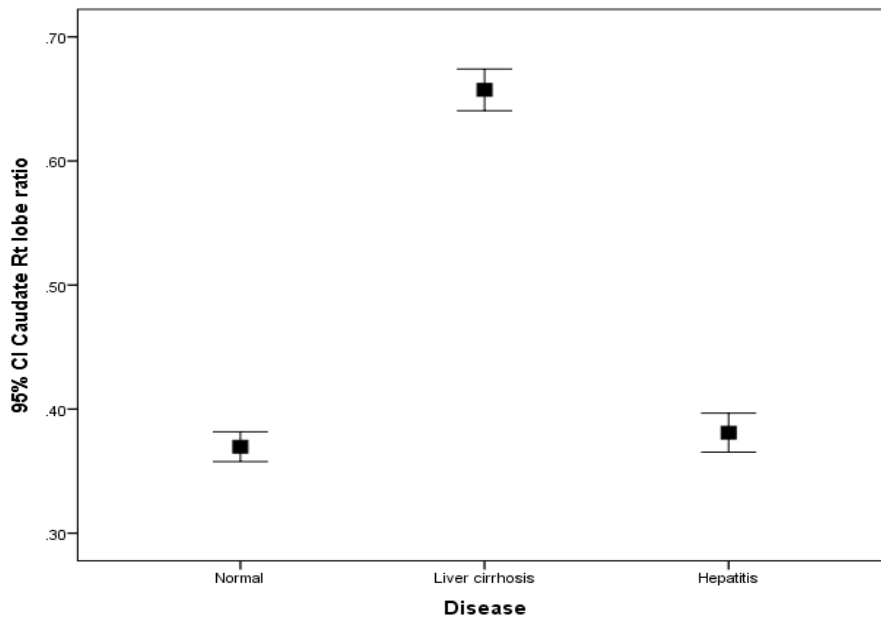

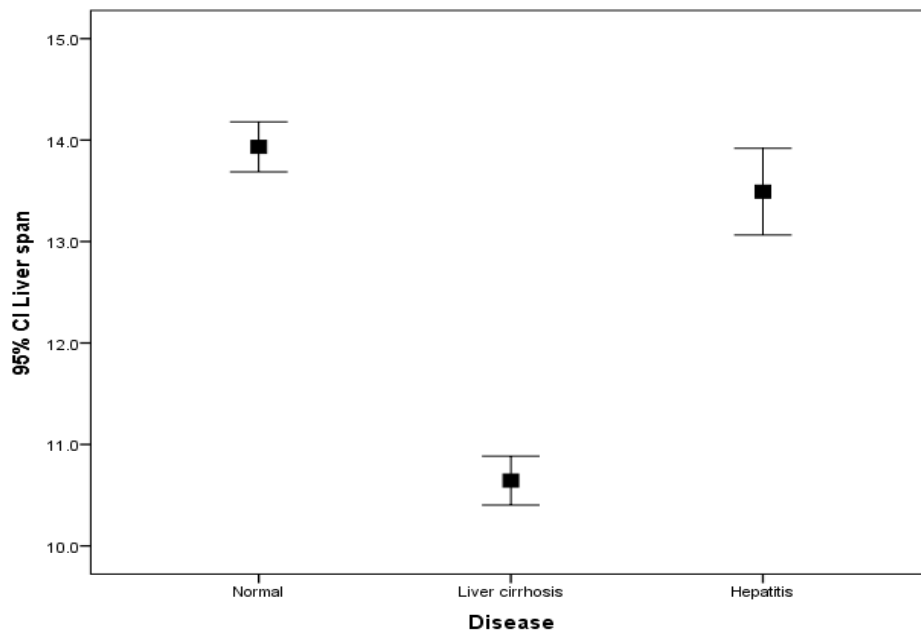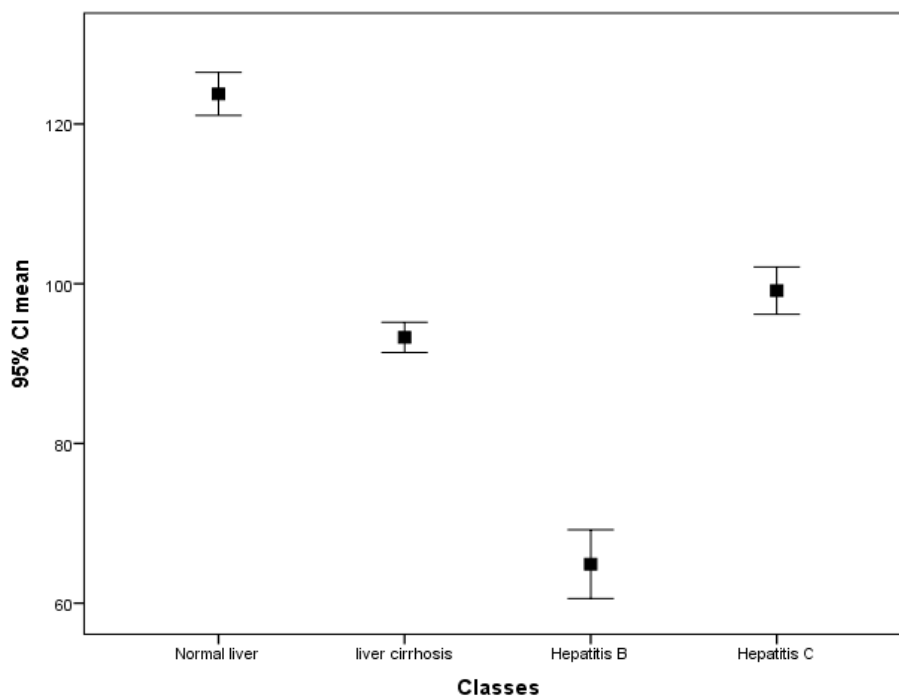**Figure 4.18. An error bar graphs of the mean textural features `for the different classes of liver (normal, hepatitis B, hepatitis C and cirrhotic liver).**

Figure 4.19. An error bar graphs of the variance textural features for the different classes of liver (normal, hepatitis B, hepatitis C and cirrhotic liver).

Figure 4.20. An error bar graphs of the energy textural features for the different classes of liver (normal, hepatitis B, hepatitis C and cirrhotic liver).
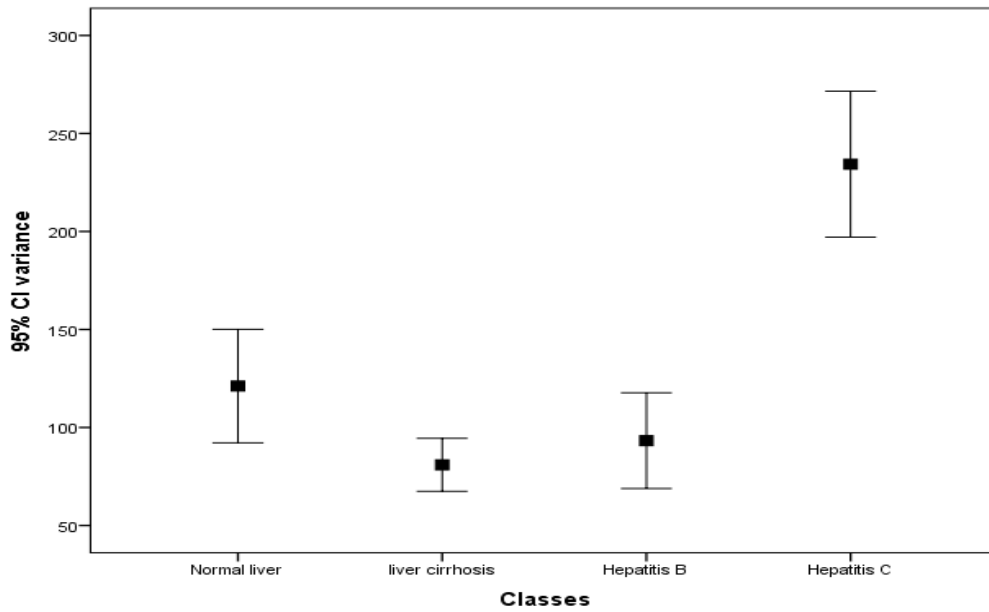
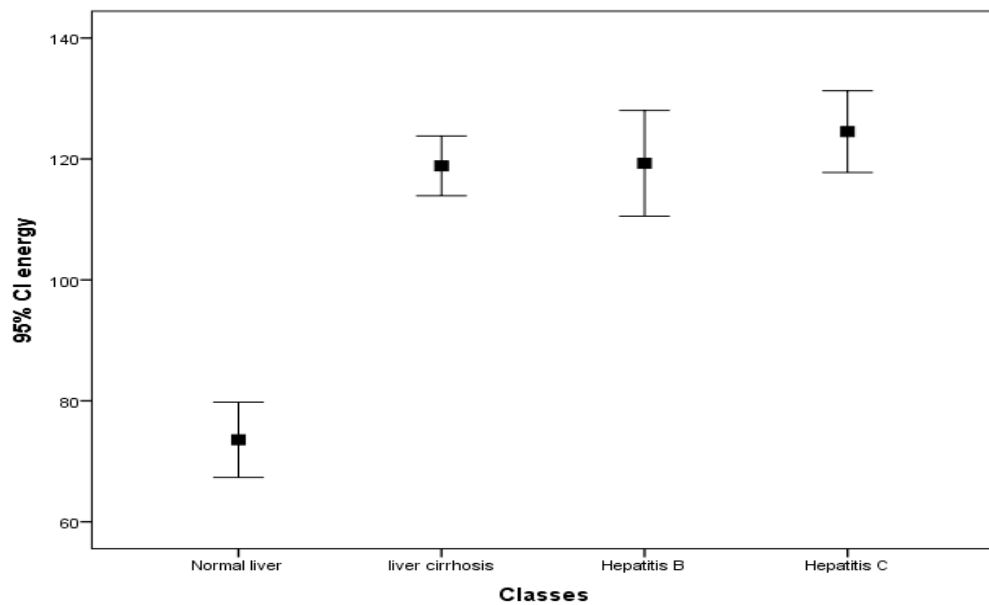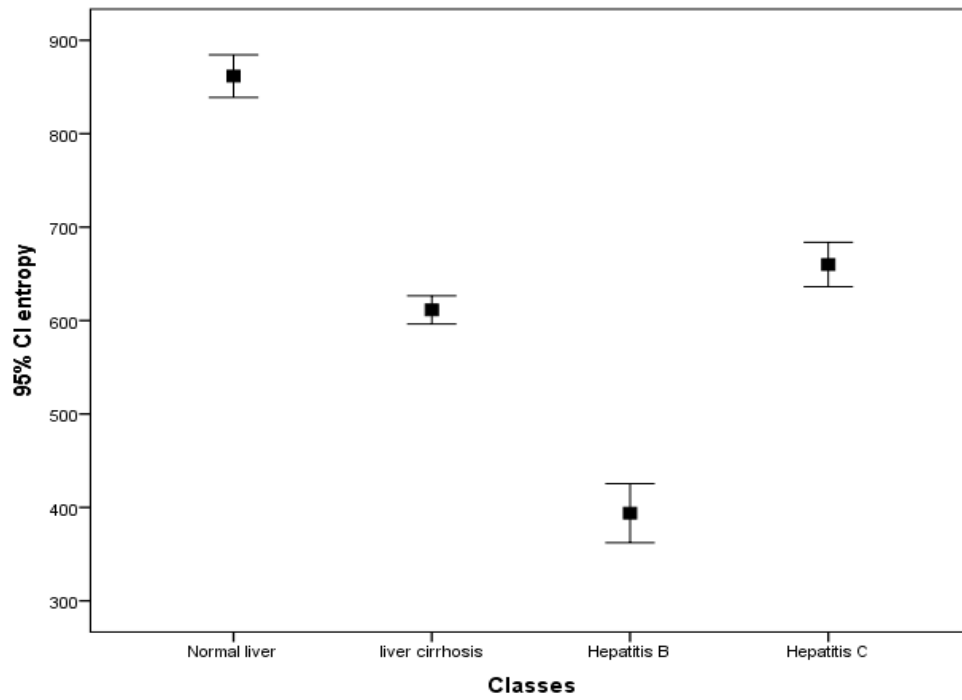**Figure 4.21. An error bar graphs of the entropy textural features for the different classes of liver (normal, hepatitis B, hepatitis C and cirrhotic liver).**

Chapter five
Discussion, conclusion and recommendation

The main aim of this study was to classify the liver ultrasound images into normal liver tissues and abnormal (liver cirrhosis region, Hepatitis type B and C) using linear discriminant analysis.

5.1 Discussion

In (tables 4.3, 4.4, 4.5 and 4.6) which show clinical findings in patients with normal liver, hepatitis B, hepatitis C and cirrhotic liver it has been found that the major clinical findings associated with hepatitis B and cirrhosis, this usually due to aggressiveness of hepatitis B and long duration of diseases that taken until liver becomes cirrhotic.

In this study the Rt lobe of the liver was measured including the caudate lobe and hence the caudate Rt lobe ratio as well as the portal vein size, duration of disease and age of the patient whom diagnosed as having liver cirrhosis or hepatitis type B and C including patient with normal liver measures. All these data were classified using linear discriminant analysis using stepwise method to select the well correlated variable with the specified disease (classes); therefore portal vein diameter and caudate lobe size were excluded by the stepwise method from the analysis due to their insignificant correlation with dependent variable (classes).

The classification result as shown in the scatter plot demonstrates well separation of the liver characteristics according to their class (disease) i.e. remarkable concentration around the class center; with an overall accuracy of 86.5% (Table 4.16).

In the same essence the results reveals that the normal liver can be identified by an accuracy of (83.3%) while the sensitivity of diagnosing

liver cirrhosis was 98.3%, for hepatitis type B the sensitivity was 91.7% where 10% of the cases showed measures similar to the normal liver; this occurs specially in early stage. And for hepatitis type C the sensitivity was 45% where 55% of the cases showed some likelihood to the normal liver; This means in patients with hepatitis C, ultrasonography has limitations in the characterization of histopathological changes and therefore it is not reliable in diagnosis of hepatitis C, similar result has been achieved by Marcia et al. therefore results of classification concerning hepatitis C doesn't worth much attention concerning the scope of this study.

The variable used to discriminate between the different classes showed different resolving power; where the age of the patient differentiate between the livers cirrhosis measures and the normal and hepatitis (Figure 4.17(A)) which associated with older patient. While duration of disease in average can differentiate between the three classes; where livers cirrhosis got the higher duration in respect to hepatitis type B (Figure 4.17 (B)), the Rt liver lobe showed a shrunken size in average for patient with livers cirrhosis relative to the other classes (Figure 4.17 (D)) this situation lead to high ratio (caudate lobe Rt lobe). Arbitrary liver span depicted similar essence as the Rt lobe of the liver (Figure 4.17(E)).

These variable (which included in the classification process) showed a significant difference between the normal and abnormal groups (cirrhosis and hepatitis) using ANOVA analysis at $p = 0.05$ (Table 4.15).

Also the study using B-mode qualitative data showed that the edge of the liver has a Pounded edge in more than 53% of case in liver cirrhosis and hepatitis B versus sharp edge in case of normal liver and hepatitis C (Table 4.8).

The shape of the liver showed normal shape in hepatitis patients relatively similar to normal (87%) while in cirrhosis 90% of the cases gives an

abnormal outline due to the nodularity and fibrotic tissues that replaces the normal tissues (Table 4.9), but in case of outline only liver cirrhosis also showed 90% of abnormal outline attributed to the same cause of abnormal shape (Figure 4.10).

Concerning the liver echo texture; liver cirrhosis showed hyperechoic texture appearance in 92% of the patients while 57% of the patient with hepatitis showed hypoecoic (Figure 4.11), while ascites mainly associated with Cirrhosis in 90% of the cases (Figure 4.13) , splenomegaly mainly associated with liver cirrhosis (Figure 4.14). All these findings mean that the ultrasound finding in hepatitis B, usually enlarged liver size (more than 15 cm), hypo echoic texture with pounded upper left edge in acute stage, while in chronic stage ultrasound usually shows that normal liver size or hypotrophied, hyper echoic texture with pounded upper left edge. But in liver cirrhosis ultrasound mainly shows shrunken liver, hyper echoic with nodular texture, abnormal shape, irregular outlines, ascites and spleenomegally dye to portal hypertension. Therefore this study found that Ultrasound of the liver surface is a useful diagnostic features in patients at risk of chronic liver diseases when assessing whether they should undergo a liver biopsy Richard Alan, Kerry Thoirs and Maureen Philips achieved same result and sonography can distinguish between two abnormal sonographic patterns of diffuse benign liver disease as well as between normal and abnormal patterns. Same result a achieved by L Needleman, et al, Kurtz AB, et, al and Ricardo Ribeiro, et, al.

The researcher in this study also applied pattern recognition analysis by extracting textural features from all images that represents the classes of the study using first order textural feature which include six features extracted from normal and abnormal images of ultrasound (liver) using 3×3 window. From these features, four of them showed significant

correlation with the predefined classes (normal liver, liver cirrhosis region, Hepatitis type B and C) they include mean, <u>variance</u>, <u>energy</u>, and <u>entropy</u>; to classify the liver into cirrhosis, Hepatitis type B and C and normal liver tissues the features of the classified regions of the whole images (as raw data) were classified furthers using linear discriminate analysis.

The result of the classification showed that the normal classes were classified well from the rest of the tissues although it has characteristics mostly similar to surrounding tissue (Figure 4.15) with a classification accuracy of 92.5%, while liver cirrhosis showed a sensitivity of 97.1%, Hepatitis type B and C showed a classification accuracy of 70%, and 73.3% respectively Table (4.18).

From the discriminant power point of view in respect to the applied features the mean can differentiate between all the classes successfully (Figure 4-18), similarly the entropy (Figure 4-21) showed the same discriminant power. Mean and entropy can successfully differentiate between the normal liver texture and Hepatitis type B from the rest of the tissues, but they reveals spars differentiation between the other tissues (liver cirrhosis, and Hepatitis type B); because they both had almost similar average grey level and heterogeneity. The variance discriminates between Hepatitis type C and the rest of the tissue (Figure 4-19) but with high variation (confidence interval) and final energy gives more emphases on normal liver than the other tissue types. This situation lead to efficient classification of normal liver and liver cirrhosis compared to the other two classes relatively.

In summary normal liver and other abnormal liver tissues in ultrasound images for simplicity can be diagnosed as normal or abnormal (according to its type by using the following simple equation after extracting the

associated features using a window of 3×3 pixel from the region of interest; the biggest classification score assume the tissue type:

Normal liver = *(mean × 48.6) + (variance × 0.16) + (energy × 0.29) + (entropy × -5.10) – 453.52.*

Liver cirrhosis = *(mean × 51.31) + (variance × 0.17) + (energy × 0.36) + (entropy × -6.35) – 418.29.*

Hepatitis B = *(mean × 48.1) + (variance × 0.15) + (energy × 0.34) + (entropy × -5.98) – 412.72.*

Hepatitis C = *(mean × 52.03) + (variance × 0.18) + (energy × 0.38) + (entropy × -6.43) – 502.72.*

This means that Computerized images also renders a reliable and clinically useful diagnostic sub classification of diffuse parenchymal disease into echo pattern changes and the computerized method replaces the previously used invasive methods, dangerous for the subjects. Same results achieved by Delia, et al. and Ulrich et al.

5-2 Conclusion:

This study was proved that ultrasound is a reliable and accurate in diagnosis of liver disorders, it differentiates between normal, hepatitis B and liver cirrhosis, but it is not accurate in diagnosis of hepatitis C.

The U/S features of acute hepatitis were: Enlarged liver span (More than 15 cm), hypoechoic echopattern and pounded upper edge of the left lobe, while in chronic hepatitis, hyperechoic echopattern, slightly small liver size and pounded upper edge of left lobe, similarly in liver cirrhosis the features of U/S usually are: Shrunken liver size (less than 15 cm), irregular outlines, abnormal shape, abnormal texture (Hyper echoic and heterogeneous) with presence of nodule, splenomegaly, presence of ascites and increased the C/R lobe ratio more than = 0.65 %.

Texture analysis can be adopted as a method of classification to describe microscopic changes occurs in the liver, which does not reveal itself ultrasonographically. So Normal liver and other abnormal liver tissues in ultrasound images for simplicity can be diagnosed as normal or abnormal(according to its type by using the following simple linear equations after extracting the associated features using a window of 3×3 pixel from the region of interest; the biggest classification score assume the tissue type:

Normal liver = *(mean × 48.6) + (variance × 0.16) + (energy × 0.29) + (entropy × -5.10) – 453.52.*

Liver cirrhosis = *(mean × 51.31) + (variance × 0.17) + (energy × 0.36) + (entropy × -6.35) – 418.29.*

Hepatitis B = *(mean × 48.1) + (variance × 0.15) + (energy × 0.34) + (entropy × -5.98) – 412.72.*

Hepatitis C = *(mean × 52.03) + (variance × 0.18) + (energy × 0.38) + (entropy × -6.43) – 502.72.*

By using discriminant analysis also characteristics extracted from ultrasound scan can be used for quantitative analysis, therefore the following equations can be applied to new cases for prediction of the type of normal liver, hepatitis B, hepatitis C and liver cirrhosis, these are:-

Normal liver = (EOL *-9.377) + (OL*397.987) + (TX *14.822) + (NTX *475.862) + (C/RR *134.139) + (POS *46.246) + (SP*24.295) -184.244

Liver cirrhosis = (EOL *-18.892) + (OL*596.161) + (TX *33.298) + (NTX *720.100) + (C/RR *223.186) + (POS *47.656) + (SP*0.262) - 1091.112.

Hepatitis B = (EOL *-3.780) + (OL*396.891) + (TX *26.625) + (NTX *496.143) + (C/RR *121.193) + (POS *83.459) + (SP*14.136) -590.994

Hepatitis C = (EOL *-10.038) + (OL*398.096) + (TX *16.467) + (NTX *479.175) + (C/RR *131.265) + (POS *46.633) + (SP*23.532) – 515.62

5-3 Recommendation:

● Younger people i.e. (50 years or smaller) and those who have high sexual activity are advised to do U/S scanning routinely to exclude the presence of liver disorders, because U/S is a cheap, safe and reliable.

● The author recommends that the Government should introduce the modern ultrasound machines and increase the training institutes of ultrasound and computer programs for increasing the sonologists skills and experiences.

● If there is any indication of liver disorder appears in U/S scanning, the patient images must be analyzes by the linear discriminate equations provided by this study.

● Texture analysis tools are not usually available, and it is expensive. According to its high values in diagnosis of liver disorders and differentiated between types, study advised the ministry of health to indorsing it, until it is become available for any doctor and patient.

● According to the high cost of scientific research which the researcher was faced, the government should appeal universities in Sudan and companies to support the researchers in order to improve plans of treating and management of such diseases.

● Further studies should be carried out in this field on many aspects such as increasing the number of patients, to show the relation between normal liver and diffuse liver diseases, comparing between the role of U/S scanning and other diagnostic tools, using color Doppler ultrasonography and texture analysis.

References:

Agamemnon D. Stefan S. 2003 Color Atlas of Physiology 5th edition. Printed in Germany by: Appl Druck GmbH & Co. KG, Wemding, Germany. Hieme Stuttgart. New York.

Youssef A.M.and A.A. Sharawi. 1990 ''KSODATA Clustering Analysis for Diffuse Liver Diseases,'' Proceedings of the IEEE Symposium on Ultrasound, Philadelphia.

Andrea G. Rockall. 2013 Diagnostic imaging 7th edition published by A. Rockall, A. Hatrick, P. Armstrong, M. Wastie.. Library of Congress Cataloging-in-Publication Data.

Andrew T. G, 2013. Atlas Of Ultrasound – Guided Regional Anesthesia . 2nd edition. Saunders, an imprint of Elsevier Inc. ISBN: 978-

Armstrong, M. Wastie. 2013. Diagnostic Imaging. 7th editions Rockall, A. Hatrick, P. First published in print format G. Kudesia and T. Wreghitt. Mosby, Inc., an affiliate of Elsevier Inc.

Arthur C. Guyton. Jackson, M. 2006 Textbook of Medical Physiology. International Edition. Elsevier Inc. Library of Congress Cataloging-in-Publication Data,

Asim K. Frank A Chervenak. 2006. Donald School Textbook of Ultrasound in Obstetrics and Gynecology. This edition published in the Taylor & Francis e-Library.

Betty B. T, 2007. Pocket protocol for ultrasound scanning. 2nd edition Saunders, an imprint of Elsevier Inc.

Carol M. Rumack. 2011. Diagnostic Ultrasound, 4th edition. Mosby, Inc, an affiiate of Elsevier Inc.

Christensen D.A., 1988. Ultrasound Bioinstrumentation, John Wiley and Sons, New York.

Delia M, Sergiu N, Bogdan F and Monica L. 2005 (Texture-Bassed Methods in Biomedical Image Recognition of Diffuse Liver Diseases). http://ace.ucv.ro/sintes12/SINTES12_2005/SOFTWARE%20ENGINEER ING/35.

Edward F. Goljan, 2010. Rapid Review Series Pathology. 3rd edition. Pliladelphia, PA: 19103-2899   by Mosby. Inc an affiliate of Elsevier Inc.

Ellen J. Hagopian • Junji Machi. 2014, Abdominal Ultrasound for Surgeons. Springer Science + Business Media New York.

Farideh J, and Janice Mc Currie. 2008 Clinical Physiology and Pharmacology The Essentials.   John Wiley & Son , Ltd.   Printed and bound in Singapore by Markono Pte. Ltd.

George R. Wettach, Thomas W. Palmrose, Terry K. Morgan, 2009. Usmle Road Map Pathology. The Mc Graw-Hill Companies

Gordon C. Cook and Alimuddin Zumla. Manson □s 2008 Tropical Diseases 22th edition.. Saunders Elsevier.

Haim A. 2010 Basics of Biomedical Ultrasound For Engineers. John Wiley & Sons, Inc., Hoboken, New Jersey, United States of America Published simultaneously in Canada.

Harald Lutz, Elisabetta Buscarini .2011. Manual of Diagnostic Ultrasound. Vol. 1- 2nd edition World Health Organization. Printed in Malta by Gutenberg Press Ltd.

Harsh M. 2010 Textbook of Pathology. 6th Edition. Published by Jitendar P Vij Jaypee Brothers Medical Publishers, India.

Hisham Tchelepi, Philip W. Ralls, Randall Radin and Edward Grant. 2002 . Sonography of Diffuse Liver Disease. American Institute of Ultrasound in Medicine. Journal of Ultrasound in Medicine, September 1, 2002 vol. 21 no. 9 1023-1032

Jan T, Radu B, Christoph F. 2013 Dietrich Student edition. EFSUMB – European Course Book. Ultrasound of the liver 04.10.201306:59

Jane A. Bates M. 2004. Abdominal Ultrasound How, Why and When. 2nd edition British Library Cataloguing in Publication Data . Kazuo, M., M. Utsu and P. E.

Kadah, Y., A. Farag, J. Zurada, A. Badawi and A.Youssef. 1996. Classification Algorithms for Quantitative Tissue Characterization of Diffuse liver Disease from Ultrasound Images. In: IEEE Transactions on Medical Imaging, Vol. 15, No. 4, August 1996

Kihaile. 1998. Quantification of sonographic echogenicity with grey-level histogram width: a clinical tissue characterization. In: Ultrasound in Medicine & Biology, Vol. 24, No. 2, pp. 225-234. Printed in the USA, 1998.

Kyung W, Harold M. Chung. 2012 Gross Anatomy 7th edition. Lippincott Williams & Wilkins, a Wolters Kluwer business. Philadelphia,

Lawrence S. Fried Man. Emmet B. Keeffe, Jules L. Dienstag. 2012 Handbook of liver disease 3rd edition. Saunders, an imprint of Elsevier Inc.

Leung , T. and J. Malik.2001. Representing and Recognizing the Visual Appearance of Materials using Three-dimensional Textons. In: International Journal of Computer Vision 43(1), pp. 29-44, 200.

Osawa, Hiroyuki, MD and Yassuaki Mori .1996. Sonographic diagnosis of fatty liver using a histogram technique that compares liver and renal cortical echo amplitudes. In: Journal of Clinical Ultrasound 24, pp. 25-29.

Giovanni Guido Cerri. 2011. Contribution of ultrasonography to the diagnosis of chronic hepatitis C histopathological changes, with emphasis on hepatic steatosis - Part I, Radiol Bras vol.44 no.3 São Paulo.

Maconi G. Bianchi P (Eds.) 2007 Ultrasound of the Gastrointestinal Tract. Springer Berlin Heidelberg New York.

Mojsilovic, A., M. Popovic, S. Markovic and M. Krstic. 1998. Characterization of Visually Similar Diffuse Diseases from B-Scan Liver Images Using Nonseparable Wavelet Transform. In: IEEE Transactions on Medica Imaging, Vol. 17, No. 4.

Murray L. Ian B. Wilkinson . Andrew B. Elizabeth W. 2014 Oxford Handbook Of Clinical Medicine 9th edition. Oxford University Press Inc., New York, United States.

Needleman L, Kurtz AB, Rifkin MD, Cooper HS, Pasto ME, Goldberg BB. 1986. Sonography of diffuse benign liver disease: accuracy of pattern recognition and grading. American Journal of Roentgenology > V146, Issue 5, PP 1011-1015.

Parker K.J. 1983. ''Ultrasonic Attenuation and Absorption in Liver Tissue,'' Ultrasound in Medicine and Biology, vol.9, pp. 363-369.

Peter H. Kevin M. Abigail T. 2010. Diagnostic Ultrasound Physics and Equipment 2nd edition. Cambridge University Press, New York.

Richard Alan, Kerry Thoirs and Maureen Philips 2010. Accuracy of ultrasound to identify chronic liver disease. World J Gastroenterol. Jul 28; V 16(28): 3510–3520.

Rickard L. Drake. 2015. Gray□s Anatomy for Students 3rd edition. Chruchill livingstone, an imprint of Elsevier inc. Printed in Canada.

Richard Snell. 2012. Clinical Anatomy By Regions 9th edition. Lippincott Williams & Wilkins, a Wolters Kluwer business.

Stephanie R. Michelle M . Stephen E. 2007 Anatomy for Diagnostic Imaging 2nd edition. British Library Cataloguing in Publication Data.

Stephen G. 2007. Clinical Physiology Made Ridiculously Simple. Publisher: Medmaster; 2007 edition.

Steven M. Penny. 2011. Examination Review For Ultrasound Abdomen & Obstetric And Gynecology. Lippincott Williams & Wilkins. Baltimore, Maryland, USA.

Sumeet B and Satish K B. 2013 Differential Diagnosis in Ultrasound. 2nd edition. Jaypee Brothers Medical Publishers.

Susan Standring. 2008 Gray's Anatomy 39th Edition. Elsevier Inc. Printed in Spain.

The European Federation of Societies for Ultrasound in Medicine and Biology (EFSUMB) guidelines (first version, dated January 2004)

Trish C. Basky T. 2004. Obstetric Ultrasound How, Why and When 3rd edition. Elsevier Limited.

Zakim and Boyers. 2006. Hepatology. A text book of liver disease 5th edition. Elsevier Inc. Printed in Canada.

Valckx, F. And J. M. Thijssen. 1997. Characterization of echographic image texture by cooccurrence matrix parameters. In: Ultrasound in Medicine & Biology, Vol. 23, No. 4, pp. 559-571. Printed in USA.

Yeh, Wen-Chun, Sheng-Wen Huang and Pai-Chi Li. 2003. Liver fibrosis grade classification with B-mode ultrasound. In: Ultrasound in Medicine and Biology, Vol. 29. No. 9, pp. 1229-1235. Printed in the USA.